Geological Society of America Field Trip No. 411
2008 GSA Annual Meeting
Houston, Texas
October 4, 2008

Geomorphic and Hydrochemcial History of the Edwards Aquifer at Inner Space Cavern

Led by: Jay Banner[1], George Veni[2], Brian Cowan[1], Elizabeth McGee[1]

1: Jackson School of Geosciences, The University of Texas at Austin, Austin, TX
2: National Cave and Karst Research Institute, Carlsbad, NM

Geomorphic and Hydrochemical History of the Edwards Aquifer at Inner Space Cavern

GSA Inner Space Field Trip Itinerary

0800 – 0815: Meet at University of Texas

- Bagels, doughnuts and coffee provided

0900 – 1015: Arrive at the cave.

- General orientation and description of day's schedule
- History of the cave's discovery and impact relative to Interstate Highway 35
- Hydrogeologic overview of the Edwards Aquifer system, Balcones Fault Zone, Edwards Limestone, application of speleothems to paleoclimate, etc.
- General safety briefing for on-trail and off-trail travel through cave; do's and don'ts
- Restroom break

1015-12:30: Tour trail

- Entrance room: overview of speleogenesis
- Soda straw balcony: overview of speleothem origin; diffuse vs. conduit flow paths through karst aquifers
- Discovery Room: 1) Bore hole: discovery of the cave and the role of geophysics in karst management; 2) Flowing Stone of Time: monitoring studies of modern speleothem growth, drip chemistry, and cave meteorology
- Discovery Room – Press Room transition: Scalloped ceiling
- Lake of the Moon: Description of specific speleothem, water chemistry, and cave meteorology results found in IS and other caves in the region
- Lunar Landscape: Sinkhole evolution and paleontological record

1230-1330: Off-trail

- Press Room: Preparation for off-trail
- Mud Room: Hydrological evolution of the conduit system
- Squid Room: Conservation of cave environments; off-trail caving
- Press Room: Synthesis

1330-1430: Return to surface for lunch. Time to shop in gift shop.

1500: Return to UT-Austin

Acknowledgements: We thank Taunya Vessels, the Staff of Inner Space Cavern and Thais Perkins for their assistance.

List of Attendees

Carlton Allen, NASA
carlton.c.allen@nasa.gov

Kelton Barr, Braun Intertec Corp.
kbarr@braunintertec.com

Marcus Buck, Karst Solutions
mbuck@karstsolutions.com

Laurence R. Davis, Univ. of New Haven
mailto:rldavis@newhaven.edu

Andrew Finnell, Texas Water Development Board

Michael Kuehlmuss

Dave Mattey, Royal Holloway University
mattey@gl.rhul.ac.uk

Isable Montanez, University of California - Davis
montanez@geology.ucdavis.edu

Francois Moussu, University Pierre et Marie Cur
francois.moussu@upmc.fr

Jessica Oster, University of California - Davis
oster@geology.ucdavis.edu

Valerie Plagnes, University Pierre et Marie Cur
valerie.plagnes@upmc.fr

E. Rasbury, SUNY at Stony Brook
troy.rasbury@sunysb.edu

Table of Contents

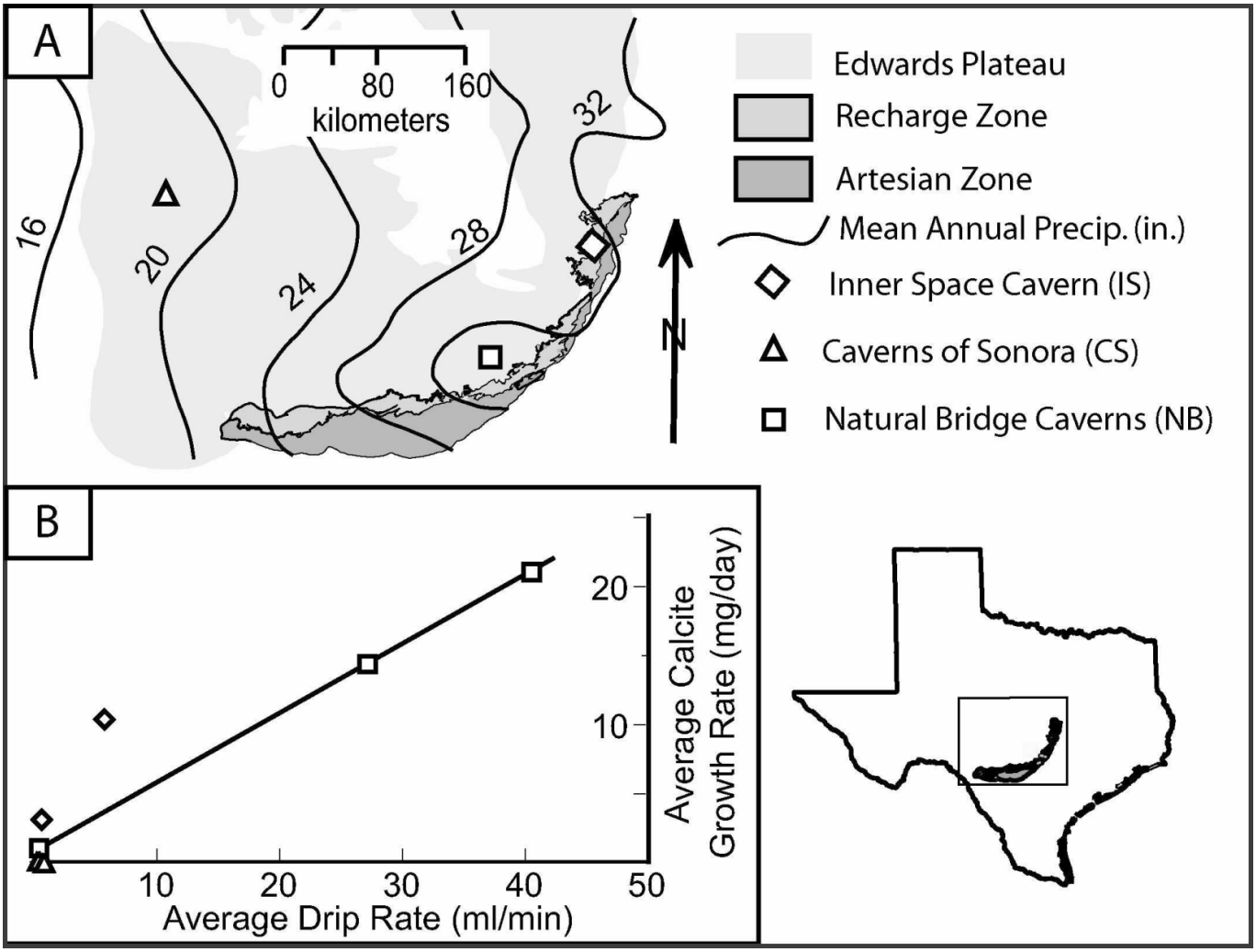

Figure 1: A) Maps of the Edwards Plateau and its location in central Texas, and locations of caves in which calcite growth rates were studied. The plateau comprises lower Cretaceous marine carbonate strata. Average annual precipitation in inches shown as contours (from Larkin and Bomar 1983). Different zones of the Edwards (Balcones Fault Zone) aquifer are indicated by shading. B) Average growth rate for speleothem plate calcite vs. average drip rate for eight drip sites in three caves (three sites at cave CS plot on top of each other). Regression for three sites at cave NB yields $r^2 = 0.99$. From Banner et al. (2007).

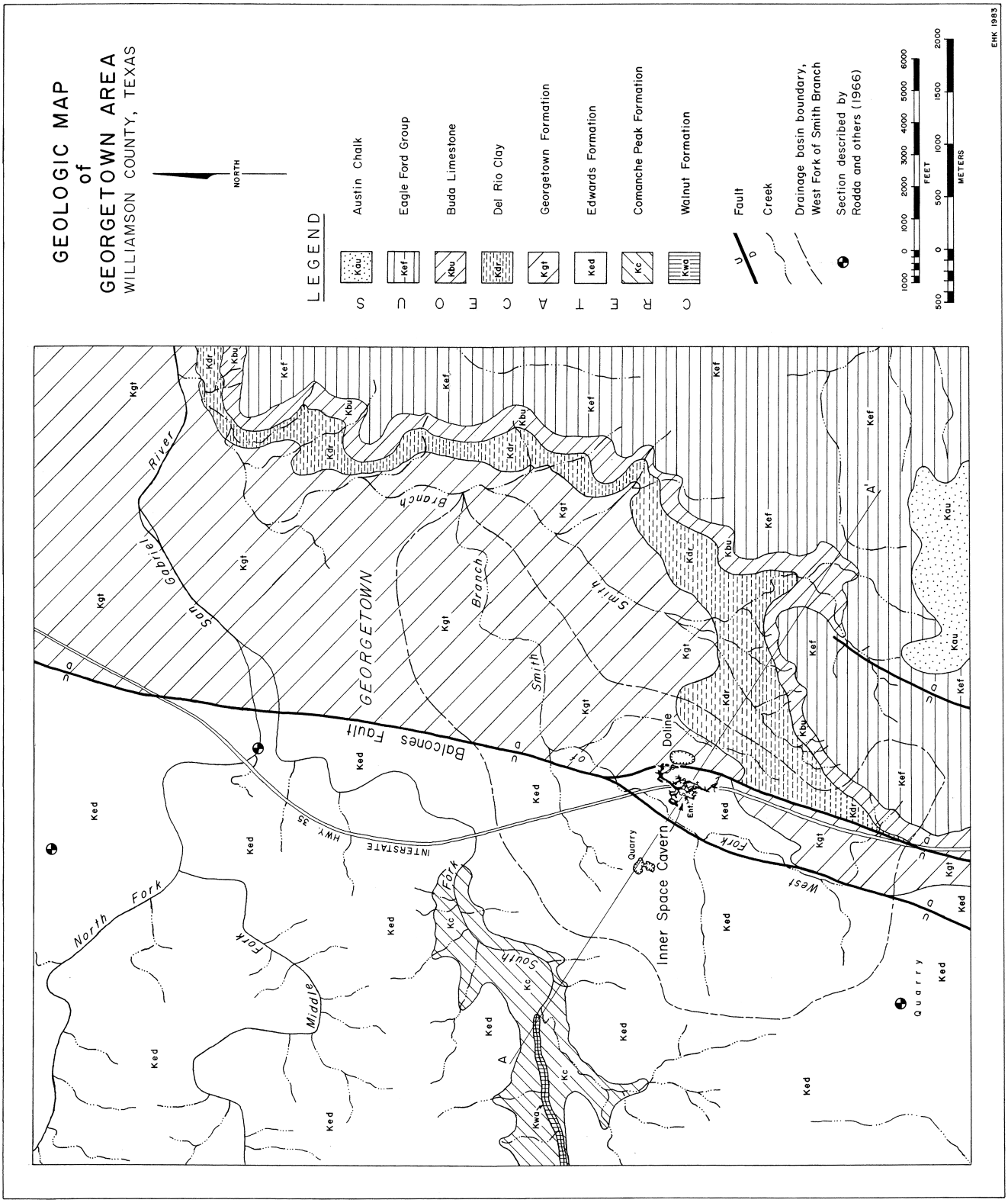

Figure 2: Geologic map of the Georgetown area. From Kastning (1983).

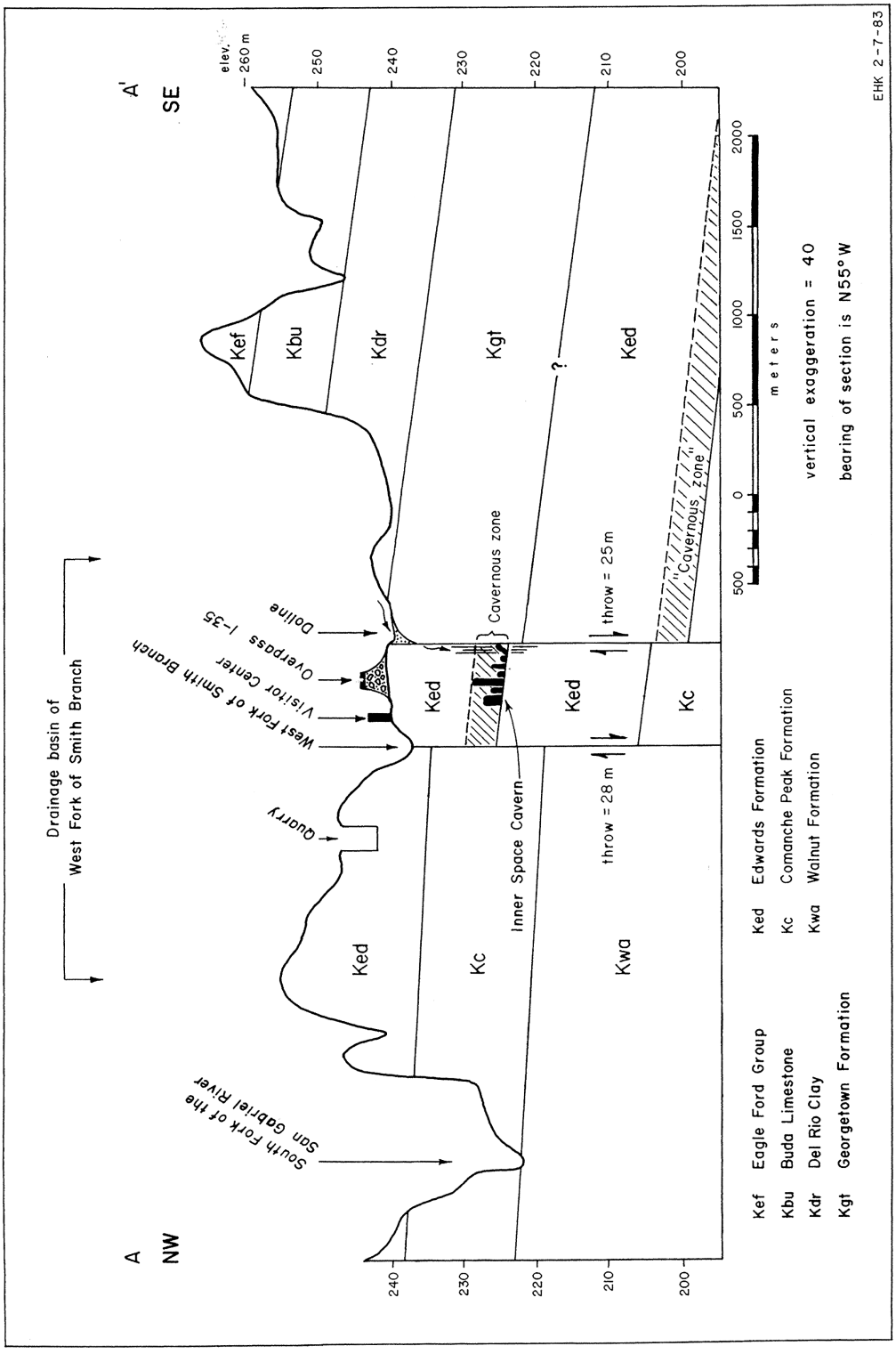

Figure 3: Geologic cross section A – A' from Figure 2, indicating location of Inner Space Cavern. From Kastning (1983).

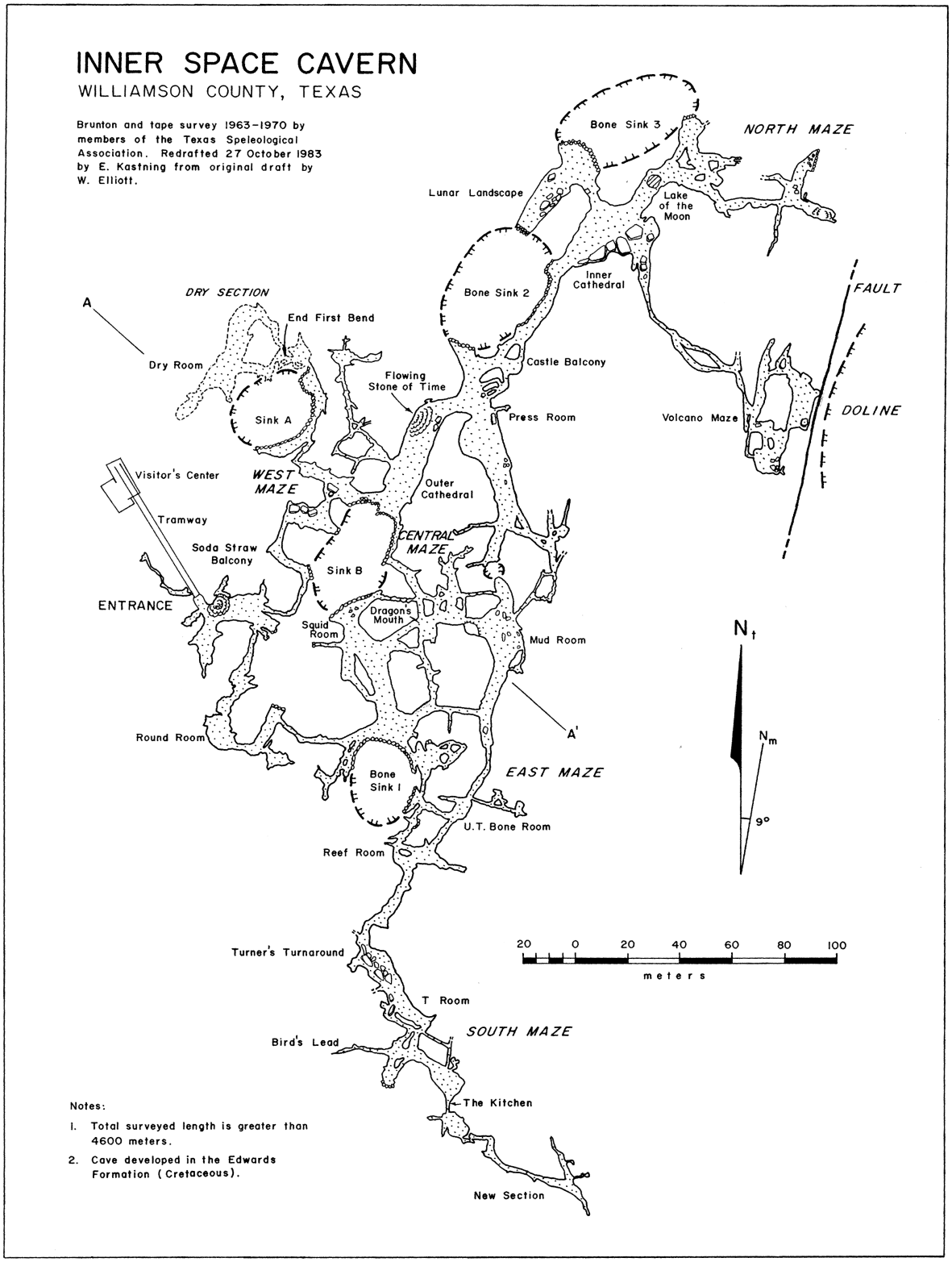

Figure 4: Map of Inner Space Cavern. From Kastning (1983).

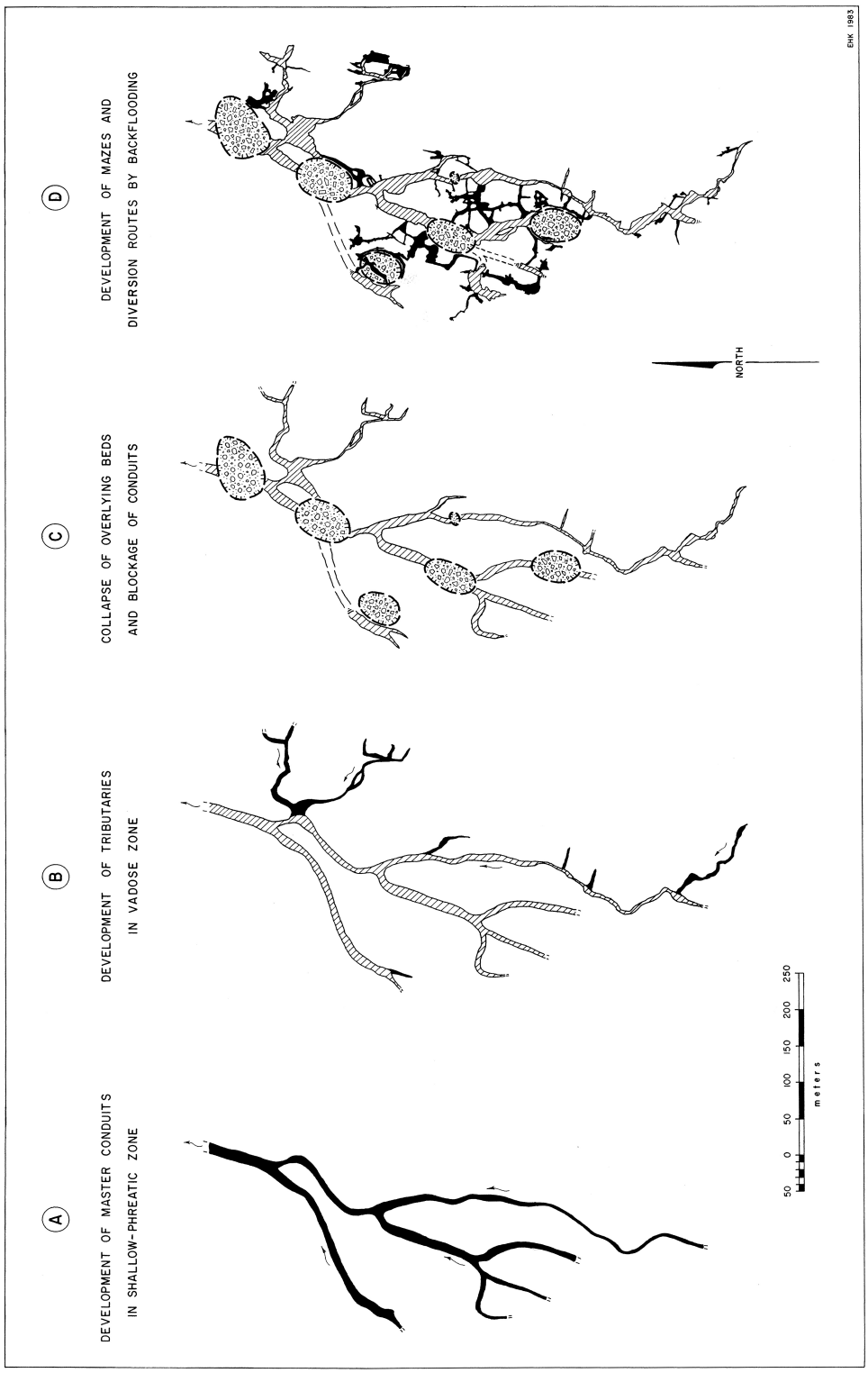

Figure 5: Stages of cave development. From Kastning (1983).

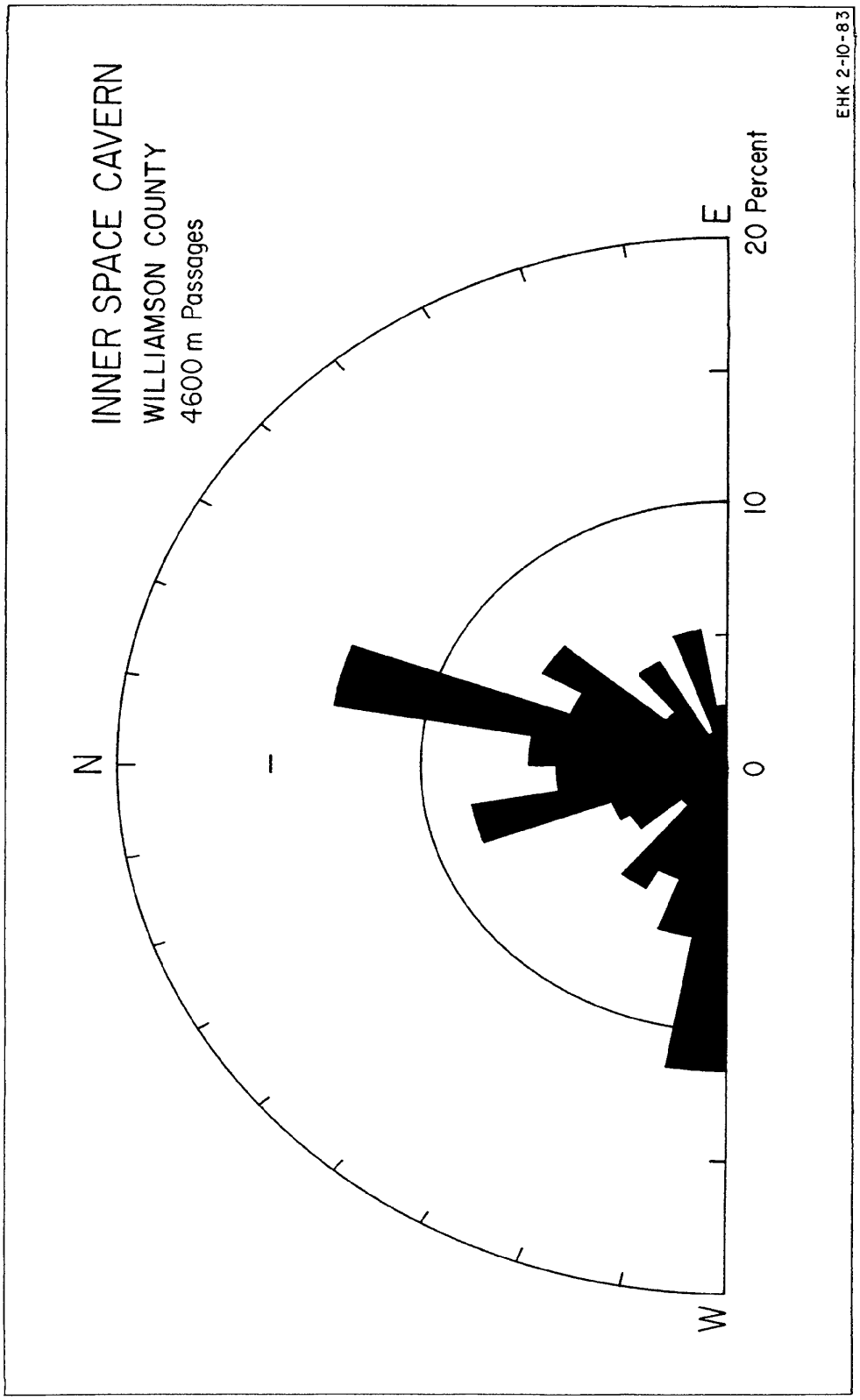

Figure 6: Rose-diagram showing orientations of linear segments of Innerspace Cavern. From Kastning (1983).

Figure 7: The Drapery Column, when active, is one of the fastest flowing formations in Inner Space Cavern.

Figure 8: In 1963 the Texas Department of Transportation drilled a series of test holes for Interstate Highway 35 that now passes over the cavern. These test holes eventually led to the discovery of the cavern.

Figure 9: At nearly three meters in diameter, the Flowing Stone of Time in the Discovery Room is the largest known formation in the cavern. Using uranium-series isotope methods, ages were determined on a core into the flowstone. The ages range from 13,210 ybp ±80 years at 3.9 cm into the formation, and 27,620 ybp ±200 years at 34.5 cm into the formation. From Musgrove (2000).

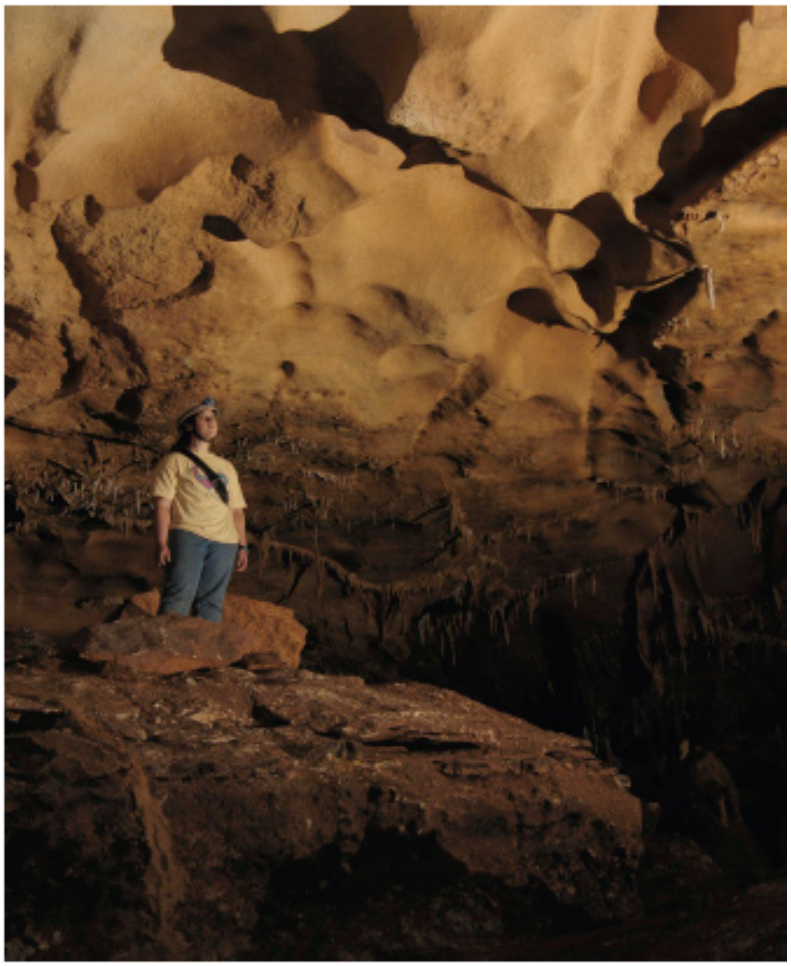

Figure 10: The scalloped ceiling near the Press Room is proposed to have been formed by the erosive power of flowing groundwater during a period of time when aquifer levels were much higher than at present.

Figure 11: High water marks (horizontal white lines) on the Castle Balcony formation leave behind a record of past flooding.

Figure 12: Lake of the Moon is one of the most ornate rooms in the cavern.

Excerpt from

*K*arst Hydrology:
Factors in Protecting and Restoring Caves and Their Hydrologic Systems

Published in: *Cave Conservation and Restoration*, 2006, Val Hildreth-Werker and Jim Werker, eds.,
National Speleological Society, pp. 121-132.

George Veni*
George Veni & Associates, 11304 Candle Park, San Antonio, Texas 78249-4421 USA
***now at National Cave and Karst Research Institute,**
1400 Commerce Dr., Carlsbad, New Mexico, 88220, USA

The Basics of Karst Hydrology

How Water Enters, Moves Through, and Exits Caves

The movement of water through caves is closely tied to the question of how caves form. Moore and Sullivan (1997) provide a good basic overview, while White (1988), Ford and Williams (1989), and Klimchouk et al. (2000) offer highly detailed information. Gillieson (1996) offers less detail but more emphasis on cave management.

Despite their wide variety of origins, caves or cave areas can be classified in one of three groups: carbonate, evaporite, and pseudokarst (see sidebar). Caves in carbonate rocks form primarily in limestone, but some also occur in dolomite and marble. Caves in evaporite rocks usually form in gypsum but also in halite in exceptionally arid climates. Caves in both carbonate and evaporite rocks form primarily by water dissolving away the bedrock. The landscapes where such solutional processes are dominant are called karst.

It is beyond the scope of this brief chapter to discuss all cave types in detail. Limestone caves will be emphasized since they are the most common.

The typical limestone cave begins to form where water enters the rock along a fracture or bedding plane and slowly flows downward and laterally until discharged from a spring at a lower elevation. While pure water has little ability to dissolve limestone, water entering the ground is charged with carbon dioxide from the atmosphere and soil to form carbonic acid. Over millennia, the weak acid enlarges fractures and bedding planes. As the openings become larger, water drains more efficiently. These increasing volumes of water then enlarge the openings at faster rates. This process self-accelerates. Eventually, one flow path toward the spring dominates the local drainage pattern and captures flows from smaller channels. When it becomes large enough for human exploration, we call that conduit a cave.

In the more common situation, a cave map looks like a branching surface stream. The tips of the hydrologic network typically include fractures, sinkholes, and swallets that capture surface water and route it underground. In the subsurface, each branch flows downstream to join other branches, eventually forming limbs and then the trunk of the underground drainage network which discharges from a spring (see "angular" and "curvilinear" passages in Figure 1). Geologic and hydrologic factors often prevent the development of such ideal flow systems, which usually occur in relatively flat-lying, highly-fractured rocks that sit atop relatively impermeable rocks.

Local geologic factors frequently affect cave development. Low fracture frequency and/or continuation of the limestone deep below spring levels result in cave networks that extend deep below the water table. Caves in dipping rocks may branch asymmetrically, capturing most water from the updip direction. Figure 1 shows some other examples of how hydrogeologic factors that create a cave relate to the cave's shape, such as:

- Braided or anastomotic passage patterns that indicate slow or ponded conditions.
- Rectilinear mazes that may suggest development by flooding or seepage through a caprock.
- Ramiform and spongework patterns, such as in Carlsbad Caverns, that did not form epigenically, by water flowing down from the surface, but hypogenically by rising hydrogen sulfide gas mixing with groundwater to form sulfuric acid, which in turn dissolved the limestone to create caves.

Beyond the Cave: Water in the Drainage Basin

For most of the 20th century, scientists argued whether caves form above, below, or at the water table, or even whether water tables actually exist in karst. We now know that caves form in all of those situations, and that karst water tables do exist. Caves are integral parts of karst aquifers and are a part of an interconnected series of voids that transmit water down through the

vadose zone (the area above the water table) and into the phreatic zone (the water-saturated area below the water table), and eventually out of the spring. Aquifers are reservoirs of water held underground in whatever voids exist in the rocks and soil. In karst, these voids make up complicated networks of fractures, bedding planes, some pore spaces, and of course, caves.

The area that feeds all water into a stream, spring, or cave is called the drainage basin. Valley ridgelines define the drainage basin boundaries for surface streams; all water that enters the basins must eventually flow through these streams. Groundwater drainage basins do not always conform to the boundaries of surface basins. Karst groundwater basins are notorious for crossing below surface basin boundaries, but they still function by similar principles. Rather than surface water flowing down a topographic surface, groundwater flows down from "ridges" to "valleys" or troughs in the water table where flow is concentrated. Significant cave streams often flow along these troughs.

Subsurface flow converges on large conduits because of their greater ability to transmit water. Even hypogenic caves, which form independently of water entering the ground from the surface, capture local flow paths from the surface to form drips, domes, pools, and streams. Figure 2 illustrates how water that seeps or floods into sinkholes, fractures, and sinking streams flows down troughs in the water table to merge into single large cave streams, and discharges from the same spring. It should therefore be clear that caves, plus the rate, volume, and quality of water that flows through them, and the materials carried in the water, directly reflect the conditions and activities on the surface in the cave's drainage basin.

Cave Chemistry and Speleothems

Some of the water which enters caves is responsible for creating speleothems. Hill and Forti (1997) provide the authoritative review of speleothems and cave minerals. While there are over 250 minerals and dozens of types and subtypes of speleothem forms, calcite and gypsum speleothems are by far the most common and are those discussed here.

As water moves through a rock, it dissolves minerals along the way and carries the ions in solution. At some point, the water may become supersaturated with respect to a particular mineral, meaning it is carrying more of the dissolved material than it can hold, and so it deposits the minerals. The amount of carbon dioxide (CO_2) in the water primarily determines how much dissolved calcite the water will hold, and where and at what rate the calcite will be released. The more CO_2 in the water, the more calcite it can keep in solution. Calcite is most commonly deposited where sufficient CO_2 is released from the water to result in calcite supersaturation. Typical locations include where water emerges from the limestone wall, releasing carbon dioxide into the cave atmosphere which has far less CO_2, or where turbulence releases CO_2 by splashing the water onto a stalagmite or running it over a flowstone slope or rimstone dam.

Evaporation also plays a part in the deposition of calcite but is far more important in the development of gypsum speleothems and is their usual cause of supersaturation. While calcite does not dissolve in pure water, gypsum is soluble in water and thus more chemically vulnerable to changes in cave environments. Consequently, gypsum speleothems form primarily in dry passages that no longer contain active streams.

The ages of speleothems are frequently misunderstood. Ages are often estimated based on an assumed constant growth rate, which is rarely the case. Each speleothem is different, reflecting the unique water chemistry and flow rate along each flow path, as well as soil and climatic factors on the surface. All of these factors change with time, and thus change the conditions of speleothem development. Generally, the larger speleothems are the oldest, but not always; they may just reflect rapid mineral deposition, while nearby small speleothems, which form by slower deposition rates, may in fact be much older. Under certain unusual conditions, speleothems can grow up to several centimeters within a year. Typically, several centimeters of growth requires hundreds to thousands of years. Thus, any impacts on speleothems are effectively permanent.

The Sensitivity of Karst Systems to Contamination and Modification

Among the various types of aquifers around the world, karst aquifers are the most sensitive to groundwater contamination and the most easily impacted by modification of the surface landscape. Drew and Hötzl (1999) describe these impacts in detail. Caves, solutionally enlarged fractures, and other voids create highly permeable features so that the volume of water discharged from karst wells and springs is the greatest on record. However, this same permeability also allows easy access for pollutants. Karst aquifers can respond so quickly to surface activities, that in many ways, they function as direct extensions of the surface landscapes. The conduit systems in karst allow for the rapid transmission of contaminants with effectively no filtration. Studies repeatedly show that when contaminants are present in karst areas, they invariably reach and adversely impact their aquifers.

The close hydrologic connection with the surface also makes karst aquifers sensitive to physical changes in the landscape. Increased flooding, decreased runoff, sedimentation, and erosion on the surface are often mirrored by changes in caves and the general behavior of the karst aquifer. Well pumping and artificial recharge of water can also dramatically change aquifer conditions on a scale and rate that is much greater than in other groundwater systems. Few effective engineering solutions have been developed to prevent many of the problems which are unique to karst. It is therefore vital that people living and working in karst areas avoid creating problems in the first place. Watson et al. (1997) and Veni and DuChene (2001) offer broad, yet concise guidelines for the protection and management of karst areas.

Bibliography

Ford DC, Williams PW. 1989. Karst geomorphology and hydrology. London: Unwin Hyman.

Gillieson D. 1996. Caves: processes, development, management. Cambridge: Blackwell Publishers.

Hill C, Forti P, editors. 1997. Cave Minerals of the World, second edition. Huntsville: National Speleological Society.

Klimchouk AB, Ford DC, Palmer AN, Dreybrodt W, editors. 2000. Speleogenesis: evolution of karst aquifers. Huntsville: National Speleological Society.

Moore GW, Sullivan N. 1997. Speleology: caves and the cave environment. St. Louis: Cave Books.

Palmer AN. 1991. Origin and morphology of limestone caves. Geological Society of America Bulletin, 103(1):1-21.

Quinlan, JF, Ewers RO. 1989. Subsurface drainage in the Mammoth Cave area. In: White WB, White EL, editors. Karst Hydrology: Concepts from the Mammoth Cave Area. New York: Van Nostrand Reinhold. p 65-103.

Veni G, DuChene H, editors. 2001. Living with karst: a fragile foundation. Environmental Awareness Series no. 4. Alexandria: American Geological Institute.

Watson J, Hamilton-Smith E, Gillieson D, Kiernan K, editors. 1997. Guidelines of cave and karst protection. Cambridge: International Union for Conservation of Nature and Natural Resources.

White WB. 1988. Geomorphology and hydrology of karst terrains. New York: Oxford University Press.

Excerpt from:
Kastning, Ernst H.
Geomorphology and hydrology of the Edwards Plateau karst, central Texas
Thesis (Ph.D.) – The University of Texas at Austin, 1983

CHAPTER TWELVE
GEORGETOWN AREA

Description of Area

The Georgetown area lies within the Balcones Fault Zone in west-central Williamson County in the northeastern part of the Edwards Plateau (Plate 1). It is bounded on the south and north along lines of 30<35'00" and 30<40'00" north latitude respectively and on the east and west along lines of 97<38'30" and 97<43'30" west latitude respectively. The area lies within the northwestern and southwestern 7.5-minute quadrants of the Round Rock 15-minute quadrangle (1:24,000-scale topographic maps have not been published at this writing), and is drained by the San Gabriel River, a major tributary of the Brazos River (Figure 150). The southeastern half of the area is principally drained by Smith Branch, a tributary of the San Gabriel River, whereas the northeastern half is drained by short creeks flowing directly into the North, Middle, and South Forks of the San Gabriel River. The city of Georgetown is located in the north-central part of the area, in the vicinity of the confluences of the three forks of the San Gabriel River.

The geology of the Georgetown area is shown on maps by Taff (1892, plate 10, scale 1:262,000), Wilson and Philpott (1949, figure 1, scale 1:195,000), Holcomb and Minton (1955, figure 1, scale 1:195,000), Ward (1950, plate 1, scale 1:21,120), Walls (1950, plate 1, scale 1:20,000), and Barnes (1974a, scale 1:250,000). Exposed rocks in the Georgetown area consist of the Edwards, Comanche Peak, and Walnut Formations (Lower Cretaceous) in the western half of the area and of the Georgetown Formation (Lower Cretaceous), Del Rio Clay, Buda Limestone, Eagle Ford Group, and Austin Chalk (Upper Cretaceous) in the eastern half (Figure 150). Geologic sections in the vicinity of the Georgetown area are described by Ward (1950), Walls (1950), Matthews (1951), Lozo (1959), Moore (1964), Rodda and others (1966), and Wilbert (1963, 1967).

The Edwards Formation consists of a sequence of beds of limestone, dolostone, and chert. Limestone is generally aphanitic to fine-grained, but some strata are medium- to coarse-grained. The limestone is massively to thinly bedded, hard, and brittle; in places it is nodular, cherty, or crystalline (Rodda and others, 1966; Ward, 1950; Barnes, 1974a). Fossiliferous zones contain abundant molluscs, including miliolids and rudists, generally within a biomicritic or biosparitic matrix. The abundance of rudistid corals and other fossils, composition, texture, and depositional and stratigraphic relations indicate that in the Georgetown vicinity and to the north the Edwards Formation may be largely reefal in origin (Matthews, 1951, 1956; Nelson, 1959, 1973; Rodda and others, 1966; Fisher and Rodda, 1967b, 1969; Rodda and Fisher, 1969). Dolostone of the Edwards Formation tends to be fine-grained, soft, massively to thinly bedded, moldic, and porous. Nodular chert and lenticular bedding is common. Chert as nodules and plates varies in amount among beds of limestone and dolostone. Weathered zones of the Edwards are considerably recrystallized and honeycombed, giving the rock a cavernous texture and locally high permeability as an aquifer. The thickness of the Edwards Formation in the vicinity of Georgetown is 18 to 50 m, thinning northwardly. The Walnut and Comanche Peak Formations crop out in the west-central part of the area. Here incision of the South Fork of the San Gabriel River has exposed these units which otherwise remain buried in the remainder of the area.

The Georgetown Formation, which covers most of the eastern half of the area (Figure 150), consists mostly of limestone, but it contains beds of marl and some shale. The limestone is generally soft, fine-grained, argillaceous, nodular, and moderately indurated. Some strata are relatively hard, brittle, and thinly bedded (Barnes, 1974a). Texturally, the beds of limestone are biomicritic. Because they are argillaceous, marly beds weather rapidly, causing slopes to recede quickly (Barnes, 1974a). Beds of limestone and some beds of marl of the Georgetown Formation contain burrows and casts of burrows. Irregular bedding in the Georgetown is in part the result of burrowing organisms. Abundant nodules of micrite occur in the burrowed and marly beds. Disseminated and nodular pyrite is common in the Georgetown, and most of the formation is also glauconitic. The Georgetown is approximately 32 m thick in the area, but it thins southwardly onto the San Marcos Arch in Travis County, generally in response to thinning of individual beds (Ward, 1950; Lozo, 1959; Wilbert, 1963, 1967).

The Del Rio Clay, Buda Limestone, Eagle Ford Group, and Austin Chalk are exposed in the southeastern part of the Georgetown area (Figure 150) and form an upland 15 to 45 m higher in elevation than the surface developed on the Edwards and Georgetown Formations to the north and west (Figure 151). These younger beds, which are described in Ward (1950), Walls

(1950), Tydlaska (1951), Atchison (1954), Barnes (1974a), and Appendix B, have little speleogenetic significance in the Georgetown area. However, the Buda and Austin are relatively resistant to erosion in comparison to the Del Rio Clay and Georgetown Formation. This is particularly true of the hard, massive, bioclastic Buda Limestone which upholds the escarpment along the southeastern margin of the drainage basin of the West Fork of Smith Branch (Figure 150).

Regional dip in the Georgetown area is approximately 0.1< to 1.0< to the southeast (Ward, 1950, p. 40 and plate 1; Walls, 1950, p. 42 and plate 1; see also Figure 151). Locally, especially in proximity to major faults, dips may be as great as 2< to 5< (Ward, 1950, p. 41).

Several major, *en echelon* faults of the Balcones Fault Zone pass through the area (Link, 1929; Barnes, 1974a; see also Figure 150). The largest of these, trending N 10<-20< E, forms the boundary between the Edwards Formation in the west and younger rocks to the east. It passes through Georgetown and 370 m east of the entrance to Inner Space Cavern (Figure 150). Displacement along the fault varies from 38 m where it crosses the South Fork of the San Gabriel River to possibly as much as 65 m near the southern boundary of the area (Ward, 1950, p. 40-41). In the southern part of the area the fault bifurcates into two significant and parallel branches that can be followed southwardly for at least 8 km (Barnes, 1974a). The western fault passes 210 m west of the entrance to Inner Space Cavern. Both branches are downthrown to the southeast and form a sizeable faulted block which encloses the cave (Figure 150).

Lesser faults are common throughout the area and many branch from the larger faults indicated on Figure 150. Minor, normal faults of small displacement, that are exposed along the banks of the San Gabriel River, are typically parallel to the Balcones trend of faults and in some places form grabens and horsts (Ward, 1950, p. 40; Walls, 1950, p. 42-43).

Rocks of the Georgetown area are well-jointed with most joints oriented vertically and spaced a few meters apart. In general, fractures are either parallel or orthogonal to major faults, especially where they lie close to them (Evans, 1965; Rogers, 1963). Away from large faults, the frequency of fractures decreases and orientations of fractures become less systematic.

Both lithology and geologic structure have controlled erosional development in the Georgetown area. Soft, marly units, such as the Georgetown Formation have eroded to gentle (0.1< to 0.5<) slopes east of the major fault; whereas hard, dense carbonate rocks, such as the Edwards Formation and Buda Limestone form steeper (1.0< to 6.0<) slopes west of the fault. This is particularly evident from topographic maps, where walls of valleys of streams are relatively steep in the Edwards Formation and Buda Limestone, but comparatively gentle in the outcrop of the Georgetown.

Faulting has modified the configuration of surficial drainage in the area. Streams have been deflected at or near faults and commonly follow traces of faults and associated fractures. This is apparent in segments of streams of the South Fork of the San Gabriel River and Smith Branch (Figure 150). Upstream tributaries of the West Fork of Smith Branch are either nearly coincident with major faults or are oriented parallel or perpendicular to them, suggesting structural control.

Distribution of Caves and Previous Investigations

Caves in Williamson County are principally distributed along the outcrop of the Edwards Formation, a 6 to 17 km-wide band extending north-south through the county just west of Georgetown. Most caves are within 17 km of Georgetown, including the 6 of more than 80 documented caves in the county known to exceed 300 m in length (Reddell and Finch, 1963). Caves of the area generally consist of wide (4 to 15 m) horizontal corridors that are confined to particular strata (see maps in Reddell and Finch, 1963, and Byrd, 1975). Several major caves have sizeable side-passages (e.g. The Bat Well, Beck Ranch Cave, Chinaberry Cave, Coffin Cave); others are large, singular conduits (e.g. Cobb Caverns) or have extensive, maze-like sections (e.g. Inner Space Cavern, Steam Cave).

Few caves were recorded in the Georgetown area prior to 1960 (Vinther, 1948; Widener, 1958). Cobb Caverns, 6.4 km north of the area, was opened commercially for a brief period beginning in 1962 (Reddell and Finch, 1963; Reddell, 1964b). However, Inner Space Cavern, the most significant cave in the area (more than 6 times longer than any other) and one of the longest in the state, was discovered in 1963 (Figure 152). At that time a crew from the Texas Highway Department drilled several coreholes to examine and test the foundation for a proposed overpass for Interstate Highway 35. At least four holes intersected cavities in the subsurface. Subsequently, one hole was enlarged to admit investigators from the Highway Department who quickly determined that a sizeable cave existed beneath the highway (Lindsley, 1963b; Kunath, 1965; Lehnhardt, 1970; Elliott, 1970b; Jasek, 1975c).

The Texas Speleological Association explored and mapped nearly 2 km of passages in the new cave from November 1963 to early 1964 (Lindsley, 1963b; anonymous, 1963b; Lehnhardt, 1970; Russell, 1975a). Originally called Laubach Cave, the well-decorated cave was developed and opened commercially as Inner Space Cavern in July, 1966 (Pinkard, 1966; Todd, 1966; Elliott, 1970b). Access thereafter has been through a tunnel excavated into the east side of the cave (Figure 152). Exploration, mapping, and study have continued sporadically since that time, with discovery of new passages (Jasek, 1975c; Russell, 1975a, 1980) and investigations of the cave's geology, internal environment, biota, and paleontological remains (Lundelius, 1975a,b).

Gravimetric traverses over the surface south of the new entrance (performed by A. Richard Smith and John Fish during the 1960's) indicate that at least two unentered passages may exist in that vicinity (Smith, 1966; Lehnhardt, 1970; Elliott, 1970b; Russell, 1975a, 1980). During the early visits explorers noted the variety of speleothems and mineral deposits. Reddell and Finch (1963) and Tart (1964) commented on sulfide minerals and calcitic boxwork in the northern part of the cave. Harmon (1969, 1970a,b) investigated the geochemistry of seeping water associated with active precipitation of calcite at the Flowing Stone of Time in the Outer Cathedral (Figure 152). He determined that precipitation of calcite from solution owing to loss of dissolved carbon dioxide to the atmosphere of the cave exceeds that resulting purely from evaporation by an order of magnitude. Speleothems taken from the cave were used in an investigation to verify that isotopic analysis of modern speleothems provides temperatures equivalent to those presently observed in the caves (Schwarcz and others, 1976). This method, which involves determination of deuterium/hydrogen ratios in fluid inclusions and $^{18}O/^{16}O$ ratios in calcite of speleothems and the calculation of paleotemperature, has been subsequently used in North America and elsewhere to help investigate paleoclimates (e.g. Harmon, 1975; Harmon and others, 1975, 1978).

Perhaps one of the most significant scientific finds in caves of the Edwards Plateau has been the discovery of considerable fossil remains of vertebrate fossils in Inner Space Cavern (Reddell and Finch, 1963; anonymous, 1963b; Frank, 1964; Slaughter, 1964, 1966a; Choate and Hall, 1967; Lehnhardt, 1970; Elliott, 1970b; Lundelius and Slaughter, 1971; Lundelius, 1975a,b). An annotated faunal list of fossils obtained from deposits in this cave has been compiled by Elliott (1970b, p. 204, 207).

Boyer (1979) investigated debris from talus-cones of Bone Sinks 2 and 3 in Inner Space Cavern which are known to contain remains of Pleistocene vertebrates. His analysis of clay minerals, in comparison with surficial and vugular deposits, indicated that the sediments may be relict soils from the late Pleistocene.

Few hydrogeologic investigations have been carried out in Williamson County. Cumley and others (1942) and Follett (1956e) have measured water-levels of wells and springs in the Georgetown vicinity. Cronin and others (1963, p. 70-73) present an overview of the water-bearing properties of the Edwards Formation, and Brune (1975) briefly describes several large springs in Williamson County. Water-quality and problems of land-use in carbonate terranes of the county have recently come under investigation (Hunt, 1973; Evans, 1974; Plamandon, 1975), indicating that an understanding of the hydrogeology of the local Edwards karstic aquifer is becoming increasingly important.

Development of Caves

I have chosen Inner Space Cavern as the focus of study for the Georgetown area. The cave exhibits characteristics that are typical of most caves along the outcrop of the Edwards Formation and Balcones Fault Zone in Williamson County: (1) Inner Space Cavern has developed along a favorable stratigraphic horizon, (2) it consists of main conduits of sizeable cross-section, tributary passages, and sections of mazes, and (3) linear segments of passages suggest structural control, particularly from regional faulting.

Description of Inner Space Cavern

The entrance to Inner Space Cavern is 2.9 km south-southwest of the center of the city of Georgetown and 180 m west of Interstate 35, approximately 2.1 km south of where it crosses the South Fork of the San Gabriel River (Figure 150). The cave has a mapped length of more than 4.6 km, an end-to-end extent of 644 m, and internal relief of approximately 25 m (Figure 52). Currently the cave is one of the longest mapped caves in Texas (Appendix C), and it is the longest cave of the northeastern part of the Balcones Fault Zone.

There are no natural entrances to the cave that have been open during historic times. Two artificial entrances provide access to the cave. The 13-m deep vertical borehole through which the cave was originally explored pierces the ceiling of the Inner Cathedral in the northern part of the cave. A 52 m-long included excavated tunnel enters the west-central part of the cave near the Soda Straw Balcony and presently serves and the entrance and exit for tours.

Inner Space Cavern is a complex maze-like cave in which both network and branchwork patterns are present (Figure 152; see Palmer [1975] for types of maze patterns). The overall maze-like character is produced through the integration of three primary types of passages: (1) trunk-passages, (2) linear segments of passages, and (3) collapsed sections (up to 20 m wide and 10 m high), and form the "backbone" of the cave. Linear segments of passages are generally shorter, linear in plan-view, small in cross-sectional area, and form angulate maze-patterns situated adjacent to trunk-passages. Collapsed passages are typically curved in plan-view, with one wall composed of collapsed material They commonly skirt the periphery of debris-cones within collapsed dolines and, in places, are blocked by breakdown. Examples of passages of each type are given in Table 11.

The larger passages form a somewhat dendritic pattern in which convergence occurs in a northerly direction (Figure 152). This is most pronounce in the trunk-passages; however, numerous linear segments of passages and some collapsed passages resemble "tributaries" to the system as well.

Most of Inner Space Cavern has developed along a single level positioned approximately 13 to 20 m below the surface. Strata of the Edwards Formation along this horizon are typically high (85 to 95 percent) in content of calcite (Rodda and others, 1966, p. 269-275) and exhibit moderate to honeycomb porosity. Some beds of the Edwards, both subjacent and superjacent to the horizon of the cave, are locally dolomitie and vary between 55 and 85 percent in content of calcite.

The northern half of the cave is relatively dry, with no perennial streams; however, the southern half of the cave often floods. During wet periods water inundates the trunk-passage extending from the Mud Room to the Chapel, tampering exploration for up to four months in some years (Elliott, 1970b; Russell, 1975a). This section is a few meters lower in elevation than the rest of the cave and ponds during wet seasons. The Volcano Maze also floods occasionally.

Locally, vertical seepage of surficial water into the cave is very pronounced. Deposits of dripstone and flowstone are profuse in some sections and several speleothems are massive (e.g. The Flowing Stone of Time in the Outer Cathedral; see Harmon [1969. 1970b] for description). Soda-straw stalactites are ubiquitous and some in the New Section southeast of the Kitchen are nearly 2 m long (Lehnhardt, 1970; Elliott, 1970b). Soda straws 0.5 to 1.0 m in length are relatively common throughout the cave (e.g. in the Soda Straw Balcony near the entrance). Helictites are also prevalent in many passages and soon attain lengths of 20 cm (Reddell and Finch, 1963, p. 55).

The cave is floored by a variety of sediments. Relatively thick deposits of fill of clay and silt occur in sections that flood. The passage between the Press Room and Mud Room has been completely filled at one point, blocking both exploration and flow of water. Other sections of the cave are floored with silt-to-sand-sized particles, and slabs of breakdown litter floors in the vicinity of collapsed dolines.

Considerable vertebrate fossils have been discovered in the debris-cones of the collapsed dolines and beneath sediments in the trunk-passages proximal to the doline-deposits. Many bones have been retrieved, dated by the C-14 method, and determined to be from mammals of the late Pleistocene (Choate and Hall, 1967; Frank, 1964; Lundelius, 1975a,b; Lundelius and Slaughter, 1971; Slaughter, 1964, 1966a). These finds suggest that the cave was open at various times during the Pleistocene, approximately 13 to 45 thousand years ago (Slaughter, 1966a; Elliott, 1970b; Lundelius, 1975a,b).

Deposits of sulfide minerals have been reported from the northern end of the cave, in the vicinity of the Inner Cathedral and Lake of the Moon. Reddell and Finch (1963) report crystals of galena, up to 5 m in size, along solutionally enlarged joints. Tart (1964) describes crystals of pyrite of similar size from the same locality and notes that many exposed crystals have weathered to limonite. Sulfide deposits are associated with crystals of calcite and calcitic boxwork similar in form to that found in Wind Cave, South Dakota, and described by White and Deike (1962) and Palmer (1981b).

Inner Space Cavern lies near the center of the drainage basin of the West Fork of Smith Branch where the surface of the land slopes gently (3.7 m/km) to the northeast. Fluvial dissection is moderate in the vicinity of the cave but increases northwardly to the San Gabriel River. Passages of the cave lie approximately 22 m above local baselevel at the San Gabriel River.

Further descriptive and historical information about the cave may be found in Lindsley (1963b), anonymous (1963b), Reddell and Finch (1963), Reddell (1964b), Pinkard (1966), Todd (1966), Lehnhardt (1970), Elliott (1970b), Jasek (21975c,d), Fieseler and others (1978), and Russell (1975a, 1980). Photographs of many features of the cave are included in Pinkard (1966), Todd (1966), Fieseler and others (1978), and in various issues of the *Texas Caver* (1963 to the present).

Speleogenesis

Superposition of three distinct types of passages has given Inner Space Cavern an inherent complexity that would not normally be expected in an area where stratigraphic, structural, and topographic settings are rather uniform and uncomplicated. This suggests that development of the cave has responded to some abrupt changes in the hydrogeologic environment, wherein more recent morphogenetic characteristics have been overprinted in older ones.

Lithologic Control

Inner Space Cavern has developed along a particular horizon that lies approximately in the middle of the Edwards Formation (Figure 151). The strata of this zone consist of medium- to thick-bedded, highly pure limestone with few chert beds. Most of the rock is aphanitic, crystalline, and honeycombed and some beds contain abundant molluscan fossils indicative of a biostromatal or reefal environment. These characteristics have given this horizon a considerable primary porosity which has apparently augmented later flow of groundwater under phreatic conditions.

Many passages in the cave have shelves or re-entrants along the wells where excavation has followed bedding-plane partings. These may represent burrowed zones in the original stratigraphic sequence that were later rendered vugular during diagenetic and dissolutional modification. In fact, most maze-like passages of low ceiling-height, which are products of ponding and flooding (see below), follow bedding-plane partings. In general, passages are conformable with the strata. Those to the west and slightly updip are slightly higher than those along the eastern side of the fault block (Figure 151).

The argillaceous Georgetown Formation has largely precluded excavation of caves east of the major faults at Inner Space Cavern. However, a large doline 460 m east of the entrance, and just east of the eastern-most major fault, has developed within the Georgetown Formation (Figures 150, 151, 152). Here, some of the runoff from the relatively impermeable uplands to the south has been diverted through fractures to the cave-system in the vicinity of the Volcano Maze. Dissolution and sapping in this area of infiltration have produced the doline adjacent to the fault-plane (Figure 151).

Structural Control

A preponderance of linear segments of passages on the map of Inner Space Cavern (Figure 152) suggests that development of the cave has been largely guided by structure. This is confirmed by comparison of trends of passages with the attitude of bedding and regional patterns of fractures.

Relationship to Attitude of Beds

Beds within the fault-block containing Inner Space Cavern dip about 0.2< to the southeast. Trunk-passages are typically aligned parallel or subparallel to the strike of the bedrock. In places, however, short segments are oriented otherwise, including parallel to the direction of dip. Horizontal development of trunk-passages along the strike and within relatively soluble strata is indicative of excavation in the shallow-phreatic zone where the piezometric surface is nearly horizontal. Inspection of the morphology of passages supports this interpretation. Trunk-passages are typically elliptical in cross-section where they have not been modified by collapse. Ceilings of trunk-passages are essentially horizontal except in areas of extensive modification by floodwater (see below). Where gradients of floors can be inferred, it is seen that they too are nearly horizontal.

Cross-sectional areas of trunk-passages are slightly larger in the northern part of the cave, particularly where two or more passages merge in this direction (Figure 153A). Northwardly confluent conduits and the northward surficial drainage of the area indicate that movement of groundwater within the evolving cave was to the north.

Trunk- and tributary-passages along the western flank of the cave are 0.5 to 3.0 m higher in elevation than those to the east. These locations correspond to equivalent stratigraphic positions within the cavernous horizon (Figure 151), a situation that does not preclude simultaneous development of the passages. For Inner Space Cavern this obviates the argument that passages of lower elevations are necessarily younger (owing to a progressive lowering of the piezometric surface, for example).
On the other hand, a few tributary-passages of high and narrow cross-section along the western flank of the cave are slightly higher in elevation than are the trunk-passages with which they communicate. This is true of passages in the North, Volcano, and South Mazes (Figure 152). Sections of these passages are discordant with strata, particularly avenues that trend across the strike of the bedrock. These passages have apparently served as collectors of water that has infiltrated through dolines and fractures in proximity to the large faults along the eastern margin of the cave. In this capacity these conduits may have evolved in the vadose

zone as dip-tubes. The passage connecting the Volcano Maze with the main cave is canyon-like, appearing as though its floor may have become entrenched and graded by free-surface streamflow.

Inclined, vadose, canyon-like passages aligned down the dip and horizontal, phreatic, tubular passages trending along the strike are common in gently dipping strata (Palmer, 1977, 1981a). The relationship of these two types of passages to one another in Inner Space Cavern is similar to that described in Longhorn Cavern, Burnet County (Chapter 9).

Relationship to Fractures

Nearly all passages in Inner Space Cavern consist of linear segments (Figures 152). Internal examination of passages shows that vertically oriented fractures are observable in ceilings and walls throughout the cave, and many are positioned longitudinally along passages. Horizontal extents of fractures are variable; most range between 2 and 90 m in length. Where vertical extents are observable, joints appear to extend completely through the cavernous zone; hence, lithologic differences in the rock have not significantly influenced fracturing within that horizon.

Orientations of segments of passages are shown in the rose-diagram of Figure 154. Because of the strong correspondence of passages with fractures, the rose-diagram can be viewed as a summary of the orientation of fractures. There are distinct concentrations of fractures (segments of passages) in the intervals N20< W to N 40 E and N 50<-90< W. However, closer examination shows there are two primary sets of fractures at N 10<-20< E (set I) and N 80<-90< W (set II) and corresponding conjugate sets at N 30<-40< E (set IIIA) and N 10<-20< W (set IIIB). A comparison of these orientations with those of major faults (Figure 150) shows that most segments of passages along fractures are generally either parallel or orthogonal to the faults, whereas most others are parallel to the conjugate directions.

Patterns of fractures are consistent with the tectonic history of the region (Figure 155). Balcones faulting during the early Miocene was primarily extensional in the northeastern Edwards Plateau; simultaneous uplift in the plateau to the west and subsidence in the Blacklands to the east created a series of *en echelon* step-faults (Foley, 1926; Jones, 1928; Link, 1929; Sellards, 1934; Perry, 1940: weeks, 1941, 1945b; Fowler, 1956, 1957). Orthogonal and conjugate sets of fractures such as those observed here are typical in rocks deformed under simple extension. Because tensionally produced joints tend to be fairly open (in comparison with those produced under compression) and thus augment circulation of groundwater, it is not surprising that nearly all avenues of excavation in Inner Space Cavern lie along them.

Small, subsidiary faults occur in various sections of the cave (Reddell and Finch, 1963). For the most part, they are of small displacement (0.5 m or less) and have merely behaved as open joints during speleogenesis. As such, small faults have operated "positively" in enlargement of conduits (Kastning, 1977c). A case in point is the Volcano Maze where small faults, striking parallel to the main Balcones fault and within 50 m of it, have guided development of at least two north-south trending passages (Figure 152). Seepage from the large doline created by solution-subsidence in the Georgetown Formation to the east may have moved downward along these faults during dissolutional excavation (Figure 151).

Elsewhere in the cave faulting has influenced excavation in a "negative" manner (Kastning, 1977c). The two large faults bordering the cave to the east and west have throws of approximately 25 m and 28 m respectively, bringing stratigraphic horizons favorable for development of caverns against others relatively resistant to excavation (Figure 151). Despite any openness in the faults incurred under tension, they behave as barriers to flow of groundwater normal to them. This is especially true along the eastern fault, where the Georgetown Formation is juxtaposed against the cavernous zone of the Edwards Formation. The overall effect is that groundwater is contained within the fault-block and restricted form moving eastwardly down the dip. Such compartmentalization is similar to that observed in the Bend, Burnet, New Braunfels, and Austin-San Marcos areas (Chapters 8, 9, 10, and 11 respectively).

Modification by Collapse

Passages of Inner Space Cavern are nowhere more than 25 m below the surface. Additionally, strata overlying the cave are thin- to medium-bedded, brittle, and intensely fractured. These conditions have made the cave highly susceptible to collapse. Ceilings have collapsed where trunk-passages have become too broad to support overlying expanses of limestone. In some places (e.g. the Inner Cathedral, Volcano Maze, and Turner's Turnaround) blocks and slabs of breakdown litter the floor, and cross-sections have been modified from elliptical to rectangular or trapezoidal. Elsewhere, especially where two or more trunk-or tributary-passages are close together or intersect, failure of the roof has been extensive, with some zones of collapse on the order of 40 to 70 m in diameter (Figure 152).

Faults and joints have significantly augmented collapse. Examination of the cave map (Figure 152) shows that major collapse dolines (Bone Sinks 1, 2, and 3; Sinks A and B) have formed in zones where fractures intersect. (In this visualization, extensions of linear segments of passages into collapsed areas are assumed to represent extensions of fractures.). Upward stoping of voids during collapse progressed to completion in some dolines, periodically opening the cave to the surface. Fossils of vertebrates from the late Pleistocene and Holocene found along walls of debris-cones and in sediments on the floor of the cave indicate that various entrances were open 13 to 45 thousand years ago (Slaughter, 1966a; Elliott, 1970b; Lundelius, 1975a,b). Difference in ages of debris-cones and entrances is suggested by differences in sediments within the cones an din the degree of cementation of these deposits (Lundelius, 1975b). Subsequent collapse, which may still be occurring today, has resealed these former entrances.

Collapse was aided by surficial processes as well as by subsurficial excavation. Denudation of the Edwards Formation and overlying strata progressed since the time of faulting, in response to changes in relief imposed by tectonism (see Chapter 2). Moreover, downward sapping of weathered limestone through open fractures, particularly in zones of high density of fractures, led to the development of dolines formed by solution-subsidence over the subsurficial cavernous zones. Concomitant solutional thinning of the overlying limestone from both above and below accelerated collapse.

Hydrogeological and Topographic Controls

Horizontal passage and their confinement along strike and within a favorable stratigraphic horizon imply that excavation occurred just below the piezometric surface. During enlargement of master conduits, groundwater flowed to the north-northeast, along a gentle hydraulic gradient roughly parallel to the evolving surface of the drainage basin of the West Fork of Smith Branch. Phreatic flow produced at least three major conduits which were confluent to the north (Figure 153A).

Discharge at baselevel probably occurred along the South Fork of the San Gabriel River at or near the point where it is crossed by the Balcones Fault (Figure (150). Although not established during this study, the conjectured northward route of the flow of groundwater lies adjacent to and west of the fault and largely follows fractures parallel to the trend of the fault and largely follows fractures parallel to the trend of the fault. Discharge along faults has been documented in the area. Brune (1975, p. 84) notes that Manske Branch Springs, 9.7 km east of Georgetown, flows at 65 liters per second.
Groundwater from the fault-block containing Inner Space Cavern presumably flowed northwardly within the Edwards Formation, although perhaps on a horizon lower than the cavernous zone in the vicinity of the cave. Today, lower beds probably conduct water northwardly from the locality of the cave.

The elevation of the piezometric surface at the cave remained in position long enough for master conduits to attain sufficient size and integration (Figure 153A). Originally water may have flowed along two or more parallel avenues. Upon solutional enlargement, hydraulic gradients between adjacent channels may have become steep in comparison to those to the north along strike. As a consequence, smaller channels may have been pirated and diverted along cross-fractures, integrating the system into a dendritic network (Figure 153B; see Palmer, 1975, p. 57-58, for an explanation of development of branchwork-patterns).

Piezometric levels are generally tied to incision by streams and to local baselevels. Waterlevels at Inner Space Cavern dropped in response to downward cutting of the San Gabriel River and denudation within the drainage basin of the West Fork of Smith Branch. Eventually the waterlevels dropped beneath the level of phreatically produced conduits. Based on data from wells published in Cumley and others (1942) and Follett (1956a), the present-day piezometric surface lies between 10 to 30 m below the level of the cave. In the ensuing vadose phase the cave became modified by collapse of some ceiling-beds, development of vadose feeder-passages carrying surface-derived recharge, periodic flooding, and deposition of sediments and speleothems.

Collapse of ceiling-beds was probably enhanced by removal of buoyant support. This initiated the stoping phenomena that would ultimately produce the large, collapsed dolines encountered in the cave (Figure 153C).

Surficial water entering open joints in the vicinity of the Balcones Fault easily percolated downward through the vadose zone to the piezometric surface. Some of this recharge was concentrated by intersecting systems of joints (Figure 153B) and transmitted to the trunk-passages at times when the latter were either still inundated or after they were drained. The best examples of vadose drainage are the easternmost passages of the cave which have collected water from the area of the fault and have transmitted it westwardly to the trunk-passages. Relatively high and narrow canyons along such routes typify vadose conditions, where floors of passages are lowered and incised by freely flowing streams.

Trunk-passages were severed by large-scale collapse of dolines (Figure 153C). Because the piezometric surface was still relatively

high, the cave was subjected to flooding during wet seasons. Flooding may also habve been enhanced by wetter and colder climates during the Pleistocene, at a time when many other caves on the Edwards Plateau are known to have flooded. Flood-pulses entered the cave from time to time, completely inundating all passages. Turbulent flood-waters, undersaturated with respect to calcite and under locally steep, hydraulic gradients, are known to be highly aggressive in the excavation of caves (Malott, 1937; Thrailkill, 1964, 1968; Palmer, 1971, 1972, 1975). In Inner Space Cavern, floodwaters impounded behind blockages at collapsed dolines rapidly excavated nearly fractures and produced numerous joint-spurs (short, dead-end side-passages along joints), enlargement of passages upstream from blockages, and routes of diversion around collapsed areas (Figures 152, 153D).

Flooding and vadose recharge may have transported much of the elastic sediment which now partially fills most conduits. Some fill is rich in vertebrate, skeletal material, indicating that its deposition may date from the late Pleistocene. This is supported to some extent by analyses of clay minerals from sediments of bone-deposits, which suggest that the sediments may, in part, be relict soils washed into the cave (Boyer, 1979).

Deposition of speleothems is actively occurring throughout the cave (Harmon, 1969, 1970a,b). The ubiquity of deposits of calcite, in particular rapidly forming soda-straw stalactites, and the steady availability of seepage suggest that infiltration is presently occurring along most fractures. Openness of fractures and an overall shallow depth of the cave undoubtedly contribute to high rates of percolation.

Soil in the vicinity of the cave may provide some explanation for present-day conditions of infiltration and deposition of speleothems. The Crawford stony clay and Denton stony-clay soil, which overlie the outcrop of the Edwards Formation within the fault-block and to the west, are typically shallow (5 to 90 cm) nonarable soils containing fragments of limestone and chert (Templin and others, 1938). The deeply developed, clay-rich zone over the Georgetown significantly impedes infiltration. In contrast, surficial runoff over the Edwards can more easily penetrate the shallow, stony soils overlying this fractured limestone. High rates of infiltration through the Edwards and its shallow mantle of soil may explain the wet character and profusion of speleothems in Inner Space Cavern. However, some water in the soil over the Edwards Formation may have been transmitted to the west from near-surficial, clayey soils overlying the Georgetown Formation. Percolation through deep. Organically rich, clayey soils will increase the content of carbon dioxide in such waters, making them more aggressive in dissolving limestone in the vicinity of the cave. Because these waters are then able to hold more dissolved calcite, they contribute more material for deposition of speleothems as seepage enters the atmosphere of the cave, where partial pressures of carbon dioxide are substantially reduced.

Chronology of Speleogenesis

The following chronological sequence is proposed for the origin of Inner Space Cavern:

1. Rocks of the Fredericksburg and Washita Divisions, including the Edwards, Georgetown, and later formations, were deposited during the Lower Cretaceous, and varied considerably in lithic character. During diagenesis, the Edwards Formation became a hard, brittle, highly porous, relatively pure limestone, in contrast to most of the overlying sediments which were considerably softer, less porous, marly, and dolomitic.

2. Rocks in the Georgetown area were faulted in the early Miocene. Tensional forces produced step-faults and fault-blocks striking generally north and a fault-scarp approximately 50 m in height in the present vicinity of Inner Space Cavern. Bedrock was extensively fractured during this time, forming joints of two primary orthogonal sets and two conjugate sets (Figures 154 and 155).

3. Erosion of the uplands west of the Balcones Fault Zone began in the late Tertiary and continued through the Pleistocene. During this interval the surface over Inner Space Cavern was gradually lowered in response to incision of the San Gabriel River and its tributaries. Hydraulic gradients in the subsurface steepened toward the river

4. As northward drainage evolved on the surface, so did northward paths of flow of groundwater. The piezometric surface within the Edwards Formation remained positioned above the present, cavernous zone for sufficient time to allow development of trunk-passages under shallow-phreatic flow (Figure 153A).

5. Infiltration entering carbonate units within the fault-block, near the upstream reaches within the drainage basin of the West Fork of Smith Branch, was transmitted northward through available fractures. This led to the development of a dendritic

network of conduits consisting of master conduits (trunk-passages) and tributaries (Figure 153B). Throughout its evolution the system of flow remained confined between the two faults of large displacement along the east and west boundaries of the fault-block. It is presumed that water leaving the northern end of the block was transmitted northward to the San Gabriel River, along fractures adjacent to the Balcones Fault and within the Edwards Limestone (Figure 150).

6. The piezometric surface gradually lowered during continual erosion of the surface, eventually dropping beneath the cavernous zone. Some minor collapse of ceiling-beds may have occurred at this time. Infiltration from the surface, entering along joints and faults in the vadose zone, became integrated along tributaries leading to the older cave (Figure 153B). Many of these avenues are canyon-like in cross-section, a characteristic of vadose development.

7. Further denudation of the landscape, coupled with stoping within larger passages, led to large-scale collapse (Figure 153C). This was augmented by the abundance of fractures and the close spacing of trunk- and tributary-passages.

8. Inner Space Cavern apparently underwent periodic flooding since (and perhaps during) the time of collapse. Flooding may have been induced by colder and wetter pluvial climates during the Pleistocene. Vadose waters coursing through segments of trunk-passages severed by collapse were impounded behind terminations of debris. Backflooding produced enlargements of passages upstream of blockages, excavations of spur-passages along joints, and propagations of diversion routes around zones of collapse. Joint-spurs and routes of diversion along fractures have made the cave maze-like (Figures 152, 153D).

9. Slumping of debris continued along the sides of collapsed dolines. At times entrances were opened to the surface, providing a means for animals and their remains to enter the cave. Sediments were deposited in the cave by three mechanisms: (1) washing through entrances in dolines, (2) transmission along open joints through solution--subsidence and sapping of dolines, and (3) transportation by surges of floodwater. In some cases these sediments form the matrix of deposits of vertebrate fossils. Deposition of speleothems began at about this time.

10. Further collapse eventually sealed all entrances. Deposition of calcite and small-scale flooding continued into the Holocene Epoch.

Summary

Development of caves in the Georgetown area has been largely confined to relatively porous and soluble beds within the highly fractured Edwards Formation. Large and complex caves have evolved in areas of intense faulting and jointing. Initially, caves developed as branching networks of conduits and consisted of tributary-channels which fed master-tubes (trunk-passages) that, in turn, conveyed water along strike under shallow-phreatic flow. Where fault-blocks were bordered by faults of large displacement, water had been guided to springs at base level along the axes of fault-blocks. Surficial degradation caused ceilings of large passages to collapse where they had been weakened by fractures or by enlargement of passages. Some major conduits had been blocked by collapse, and water ponded and flooded large sections of some caves, ramifying existing passages into extensive maze-like networks. The multigenetic development of caves in the Georgetown area is best exemplified by Inner Space Cavern. This mode of origin and extensive deposits of bones of Pleistocene animals and of speleothems make Inner Space Cavern one of the most geologically important caves of the Edwards Plateau.

Journal of Sedimentary Research

Journal of Sedimentary Research, 2007, v. 77, 615–622
Current Ripples
DOI: 10.2110/jsr.2007.065

SEASONAL VARIATIONS IN MODERN SPELEOTHEM CALCITE GROWTH IN CENTRAL TEXAS, U.S.A.

JAY L. BANNER, AMBER GUILFOYLE, ERIC W. JAMES, LIBBY A. STERN,* AND MARYLYNN MUSGROVE†
Jackson School of Geosciences and Environmental Science Institute, University of Texas at Austin, Austin, Texas 78712, U.S.A.
e-mail: banner@mail.utexas.edu

ABSTRACT: **Variations in growth rates of speleothem calcite have been hypothesized to reflect changes in a range of paleoenvironmental variables, including atmospheric temperature and precipitation, drip-water composition, and the rate of soil CO_2 delivery to the subsurface. To test these hypotheses, we quantified growth rates of modern speleothem calcite on artificial substrates and monitored concurrent environmental conditions in three caves across the Edwards Plateau in central Texas. Within each of two caves, different drip sites exhibit similar annual cycles in calcite growth rates, even though there are large differences between the mean growth rates at the sites. The growth-rate cycles inversely correlate to seasonal changes in regional air temperature outside the caves, with near-zero growth rates during the warmest summer months, and peak growth rates in fall through spring. Drip sites from caves 130 km apart exhibit similar temporal patterns in calcite growth rate, indicating a controlling mechanism on at least this distance. The seasonal variations in calcite growth rate can be accounted for by a primary control by regional temperature effects on ventilation of cave-air CO_2 concentrations and/or drip-water CO_2 contents. In contrast, site-to-site differences in the magnitude of calcite growth rates within an individual cave appear to be controlled principally by differences in drip rate. A secondary control by drip rate on the growth rate temporal variations is suggested by interannual variations. No calcite growth was observed in the third cave, which has relatively high values of and small seasonal changes in cave-air CO_2. These results indicate that growth-rate variations in ancient speleothems may serve as a paleoenvironmental proxy with seasonal resolution. By applying this approach of monitoring the modern system, speleothem growth rate and geochemical proxies for paleoenvironmental change may be evaluated and calibrated.**

INTRODUCTION

Use of the growth rate and geochemistry of cave calcite deposits, or speleothems, as paleoenvironmental proxies has grown rapidly in the past decade, reflecting the great potential of speleothems as high-resolution records for late Pleistocene and Holocene environmental change. These applications typically postulate a correlation between speleothem calcite growth rates and paleoclimate but cannot directly investigate the relationship between surface climate and subsurface speleothem growth (Musgrove et al. 2001). Radiometric chronologies cannot resolve seasonal or annual timescales of ancient speleothems. For the relatively uncommon cases where speleothems contain seasonal growth laminae (Shopov et al. 1994; Genty and Quinif 1996), meteorological data and water samples for the same time intervals are rare. Records of speleothem growth rate have the potential to address key paleoclimate questions during time intervals where other proxies have limitations (e.g., Smith et al. 2006). Of further interest, growth rates may control the extent to which geochemical proxies record equilibrium processes during speleothem growth (e.g., Huang and Fairchild 2001; Mickler et al. 2006).

We evaluate the application of the growth rate of speleothem calcite (referred to as "growth rate" hereafter) as a paleoenvironmental proxy by quantifying the growth rates of modern speleothem calcite. We placed artificial substrates under active drip-water sites in three caves across the Edwards Plateau of central Texas. Environmental measurements taken at the drip-water sites and at the surface allow direct comparison between growth rates on the substrates and the local and regional factors that may control the growth rates. Advancing the approach of Mickler et al. (2006), sampling intervals were designed to determine subseasonal variations in growth rates, meteorological parameters, and water chemistry. Our results over six years demonstrate consistent seasonal changes in growth rates between two caves 130 km apart. We examine the roles of temperature, rainfall, drip rates, drip-water composition, and cave-air composition in controlling speleothem growth.

HYDROGEOLOGIC SETTING AND CAVE DEVELOPMENT

The study sites span part of the Edwards Plateau (Fig. 1), which has a subhumid to semiarid subtropical climate. The plateau is a well-developed karst region built in lower Cretaceous marine carbonates, and contains caves with active speleothem deposition. It comprises parts of two regional aquifer systems, the Edwards–Trinity aquifer (Plateau aquifer) and the Trinity aquifer. The plateau also encompasses the contributing and recharge zones and is adjacent to the artesian zone of the Edwards aquifer (Balcones Fault Zone aquifer) along the plateau's southern and eastern margins. The geomorphology and hydrogeology of the plateau and the caves of this study are described by Eliot and Veni (1994), Musgrove et al. (2001), and Musgrove and Banner (2004). Caves of this study are formed below gentle slopes with thin, rocky soils supporting oak and juniper savannah. The drip waters of the caves are

* Present address: FBI Laboratory Division, Counterterrorism & Forensic Science Research Unit, Quantico Virginia 22135, U.S.A.

† Present address: USGS Texas Water Science Center, 8027 Exchange Drive, Austin, Texas 78754, U.S.A.

 1527-1404/07/077-615/$03.00

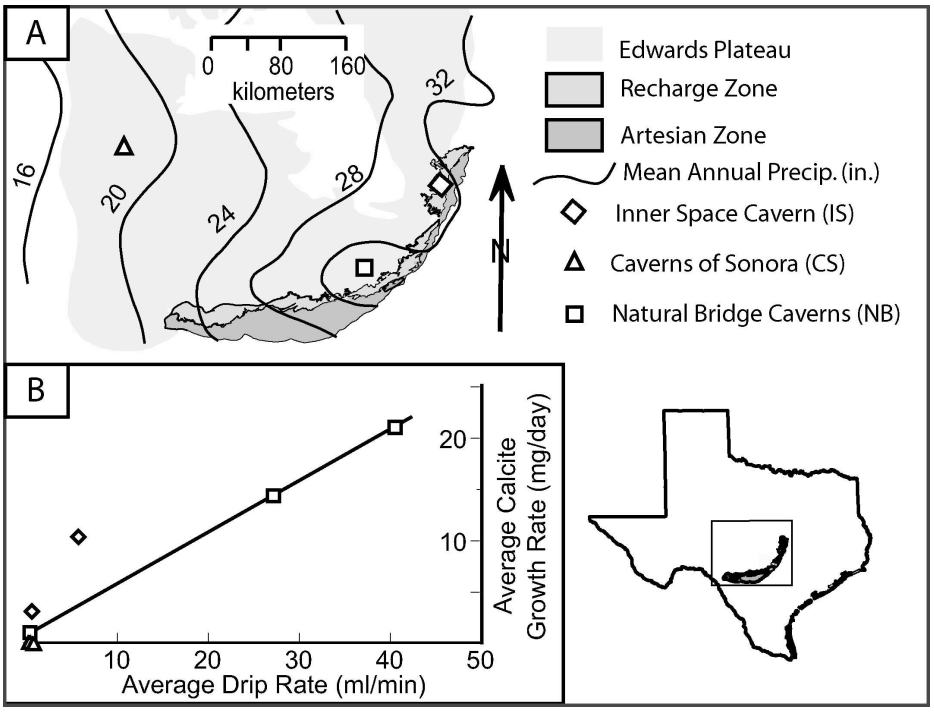

FIG. 1.—**A)** Maps of the Edwards Plateau and its location in central Texas, and locations of caves in which calcite growth rates were studied. The plateau comprises lower Cretaceous marine carbonate strata. Average annual precipitation in inches shown as contours (from Larkin and Bomar 1983). Different zones of the Edwards (Balcones Fault Zone) aquifer are indicated by shading. **B)** Average growth rate for speleothem plate calcite vs. average drip rate for eight drip sites in three caves (three sites at cave CS plot on top of each other). Regression for three sites at cave NB yields $r^2 > 0.99$.

$Ca\text{-}HCO_3$ waters, and were sampled at depths of 17–45 m. Inner Space Cavern (IS) is formed within the Edwards Limestone, which contains minor dolostone. Natural Bridge Caverns was divided by collapse into two caverns known as the North and South Caverns (NB North and NB South), which are formed in the interbedded limestone, marly limestone, and dolostone of the upper Glen Rose Formation and lower Walnut Formation. The Caverns of Sonora (CS) are formed in the Segovia Member of the Edwards Limestone. Land use change has occurred above each cave, most extensively above cave IS via urban development in the 1960s and establishment of a visitors center, and above NB North via a visitors center. At IS, a man-made tunnel entrance remains open to air exchange, whereas at both NB North and CS, the natural entrances are no longer open and visitors enter and exit through glass doors, normally kept closed to limit air exchange. During development of each cave, several conduits were constructed from the surface into the cave for various purposes, including running electrical cables, controlling air exchange, and surveying. Some of these conduits remained open during the course of the present study. Relative to the natural setting prior to cave development, the total cross sectional area of openings to the surface increased at caves IS and NB South, decreased at cave CS, and remained approximately the same at cave NB North.

METHODS

Modern speleothem calcite was collected by placing 10 cm × 10 cm glass plates horizontally under active drip sites in the three caves. Sites chosen were previously characterized for drip-rate and geochemical variability (Musgrove and Banner 2004). Plates were retrieved at 4–8 week intervals, except at CS, where they were retrieved at 5–16 week intervals. The amount of calcite growth during a given time interval was determined by weighing each plate before and after its deployment. Precise weights are obtained using multiple calibrations. Glass plates were sandblasted, cleaned, weighed, and mounted horizontally on a clay or plastic support placed on cave formations, which are protected with a polyethylene bag. The weights of plates, before and after calcite growth, were determined using a Sartorius MC1 RC 210P electronic balance. The balance is calibrated internally prior to each use and externally on a periodic basis. An active ionized air generator is used to control static charging during weighing. Repeated measurements of the weight of an in-house standard glass plate are interspersed with measurements of the glass sample collection plates and are used to adjust sample weights for drift in the balance. Prior to the use of the ionized air generator, reproducibility of the weight of the standard plate yielded a standard deviation of 0.0165 g. Use of the ionizing system starting in January of 2003 improved reproducibility substantially, yielding a standard deviation of 0.0003 g, with an average standard deviation for a given day's measurements of the standard plate of 0.00007 g.

Drip-water pH, conductivity, and temperature were measured in the field. *In situ* pH measurements on small-volume water films on plates and natural speleothems were made using an IQ solid-state pH probe. Ion concentrations were measured by ICP–MS, ion chromatography, and titration. Cave-air relative humidity, temperature, and CO_2 concentration were measured during each cave visit with portable meters. Relative humidity was measured using a Vaisala HM34 and an Omega RH85 (+/− 5% above 90% RH), and CO_2 concentrations and temperature were measured using a Telaire 7001 meter. CO_2 data are reported as concentrations (Table 1). Discussions in the text refer to cave-air P_{CO2} for comparison with drip-water P_{CO2}. Conversion from concentration to P_{CO2} requires measurements of barometric pressure, which are not available, but the conversion would result in differences of less than the measurement uncertainty of +/− 5%. Surface meteorological data are from NOAA's National Climatic Data Center database.

RESULTS

Results for calcite growth rates, drip-water chemistry, and cave meteorology are given in Table 1. Eight drip sites were monitored from 2001 through 2006, during which time calcite growth rates ranged from 0 to 107 mg/day (within measurement uncertainty, see Table 1), with mean growth rates at each site ranging from 0 to 21 mg/day (Table 1, Fig. 1B). Calcite grown on the plates occurs mainly as isolated to intergrown crystals of low-Mg calcite, 10 to 500 microns in length. Calcite

TABLE 1.—*Ranges of cave drip site physical and chemical parameters.*

Site	Depth (m)	Water Temp (°C)	Drip rate (ml/min)	pH	S.I.$_{calcite}$	Calcite growth rate (mg/day)	Ca (mg/L)	Cave-air CO_2 (ppm)	RH (%)
Inner Space Cavern									
ISST	17	18.6–22.5	0.12–16.5	7.29–8.52	−0.33–1.06	0–36.5	62–92	450–7780	89–96
ISLM	20	20.7–23.4	0.13–0.94	6.75–8.42	−0.10–1.17	0–13	87–101	500–7670	90–98
Natural Bridge Caverns North Cavern									
NBCT	42	17.5–24.2	1.07–200	6.82–8.27	−0.04–1.02	0–107	52–99	380–7890	90–98
Natural Bridge Caverns South Cavern									
NBOP	45	ND	0–0.23	ND	ND	0–4.36	57–67	610–31,000	86–95
NBWS	45	17.5–24.2	2.4–300	6.77–8.15	−0.19–1.11	0–63.1	85–137	920–30,000	89–97
Caverns of Sonora									
CSDP	30	19.8–25.1	0.21–1.77	7.39–8.15	0.15–0.61	0	68–74	3290–5640	85–93
CSDC	35	19.5–24.6	0.26–0.37	7.16–7.99	0.20–0.30	0	69–73	4530–6500	85–95
CSHL	30	19.3–23.7	0.50–0.78	6.95–7.84	0.20–0.40	0	74–89	5330–6610	88–95

S.I.$_{calcite}$ = log [IAP/K_{sp}], where IAP = ion activity product [Ca^{2+}]*[CO_3^{2-}]; K_{sp} = solubility product constant of calcite at measured water temperature. S.I. values calculated using PHREEQC (Parkhurst and Appelo 1999). RH = relative humidity. ND, not determined due to slow drip rates. Calcite growth rates reported as zero are those below the detection limit of 0.37 mg/day prior to January 2003, and below 0.007 mg/day after this date, as described in the Methods section. Ranges given for the time period shown in Figures 3 and 4, except for Ca and S.I. $_{calcite}$, for which ranges are for time period up to January 2006 for IS and NB sites, and up to October 2003 for CS sites.

morphology ranges from equant rhombohedra to complexly faceted crystals. Mean calcite growth rates over the study period at different drip sites correlate directly to mean drip rate (Fig. 1B). Within and between caves NB and IS, 130 km apart, different drip sites exhibit similar temporal cycles in growth rates, despite these sites having large differences in their mean growth rate (Figs. 2, 3). These cycles correspond to seasonal changes above the caves, with the lowest growth rates occurring during the summer, and peak growth rates occurring in fall through spring (Figs. 2, 3). In contrast, growth rates at all three drip sites at CS are within analytical uncertainty of zero year-round. Annual rainfall and effective precipitation are much lower, and cave-air P_{CO2} is more constant at CS compared with NB and IS (Fig. 1; Table 1). Results for the five NB and IS drip sites, which exhibit significant temporal changes in growth rates, are described herein.

Temporal changes in growth rate are inversely correlated to outside air temperature at all five NB and IS sites (highly significant at $p < 0.01$), and also inversely correlated to changes in cave-air P_{CO2} at all five sites (significant at $p < 0.05$; Table 2; Figs. 2, 3). Temporal growth rate changes are also inversely correlated to drip-water P_{CO2} at three of four sites ($p < 0.05$). A weaker correspondence is found between temporal growth rate changes and both drip rate and effective precipitation, with three of five sites having a significant correlation (Table 2; Figs. 2, 3).

Near-zero growth rates occur at essentially the same time each year, in July–August at sites ISLM, ISST, and NBWS, and in June–August for sites NBOP and NBCT, coinciding with peak outside-air temperatures (~ 29°C; Figs. 2, 3). Within the uncertainty interval of the 4–8 week sampling periods of calcite growth, the slowest calcite growth rates each year coincide with the warmest outside air temperatures each year (vertical dashed lines in Figs. 2, 3). During all of the periods of near-zero calcite growth, drip rates do not fall to zero at any site (Figs. 2, 3). The rise in growth rates at site ISLM, which is located deeper in cave IS, consistently lags the growth rate rise at site ISST by one to four months each year (Fig. 3). Drip waters range from slightly undersaturated to supersaturated with respect to calcite, as indicated by saturation indices from −0.33 to 1.17, with the highest values typically occurring from November to March (Table 1; Guilfoyle 2006). In contrast, drip water Ca concentrations at a given site show limited variability (Table 1). During the fall–winter of 2005–2006, relatively low effective precipitation occurred above both caves, low drip rates occurred at all five IS and NB sites, and low calcite growth rates relative to other years occurred at three of the five sites (Figs. 2, 3).

Cave-air P_{CO2} varies seasonally in caves IS and NB, with low, near-atmospheric levels in the winter, and higher values measured during summer months, coinciding with the periods of lowest growth rate (Figs. 2B, C, 3B, C). Similarly, high cave-air P_{CO2} in summer and low cave-air P_{CO2} in winter are found in caves from a variety of locations (e.g., Buecher 1999; Carrasco et al. 2002). Carbon dioxide levels in most caves are controlled by the balance between CO_2 transport into the cave from overlying soil and removal of CO_2 via cave ventilation. Ventilation is often seasonally driven by temperature and density contrasts between outside and cave air (Wigley and Brown 1976).

Spatial measurements of the pH of water films on the plates and natural substrates at site ISST in March and July 2005 reflect chemical evolution during water flow. For each time period, pH increased radially outward from the point of drip impact to the plate edge. In March, pH increased outward from 7.78 to 7.99, whereas in July pH increased outward from 7.59 to 7.61. Similar downstream pH gradients were observed in water films on a flowstone at this site. The higher pH and larger pH gradient occurred at this site in March, when cave-air P_{CO2} was low (550 vs. 4800 ppm in March vs. July) and calcite growth rate was high (22.5 vs. 4.2 mg/day in March vs. July).

DISCUSSION

General Controls on Growth of Speleothem Calcite

Deposition of speleothem calcite is driven by the degassing of CO_2 from water entering a cave, which engenders, or increases, calcite supersaturation in the water (Holland et al. 1964). The controls on speleothem growth have been analyzed empirically in Pleistocene and Holocene speleothems, and by theoretical consideration of a range of physical and chemical controlling factors (Baker et al. 1993; Dreybrodt 1988). Modeled speleothem calcite precipitation is dependent on the interplay of a number of factors, including rainfall and amount of infiltration, drip rate, drip-water calcium concentration, water-film thickness, cave-air CO_2 concentration, soil and bedrock thickness, and temperature (Dreybrodt 1988). Temperature affects multiple factors that influence growth rate, including calcite solubility, soil CO_2 production, solubility of CO_2, and effective precipitation, leading to both growth-

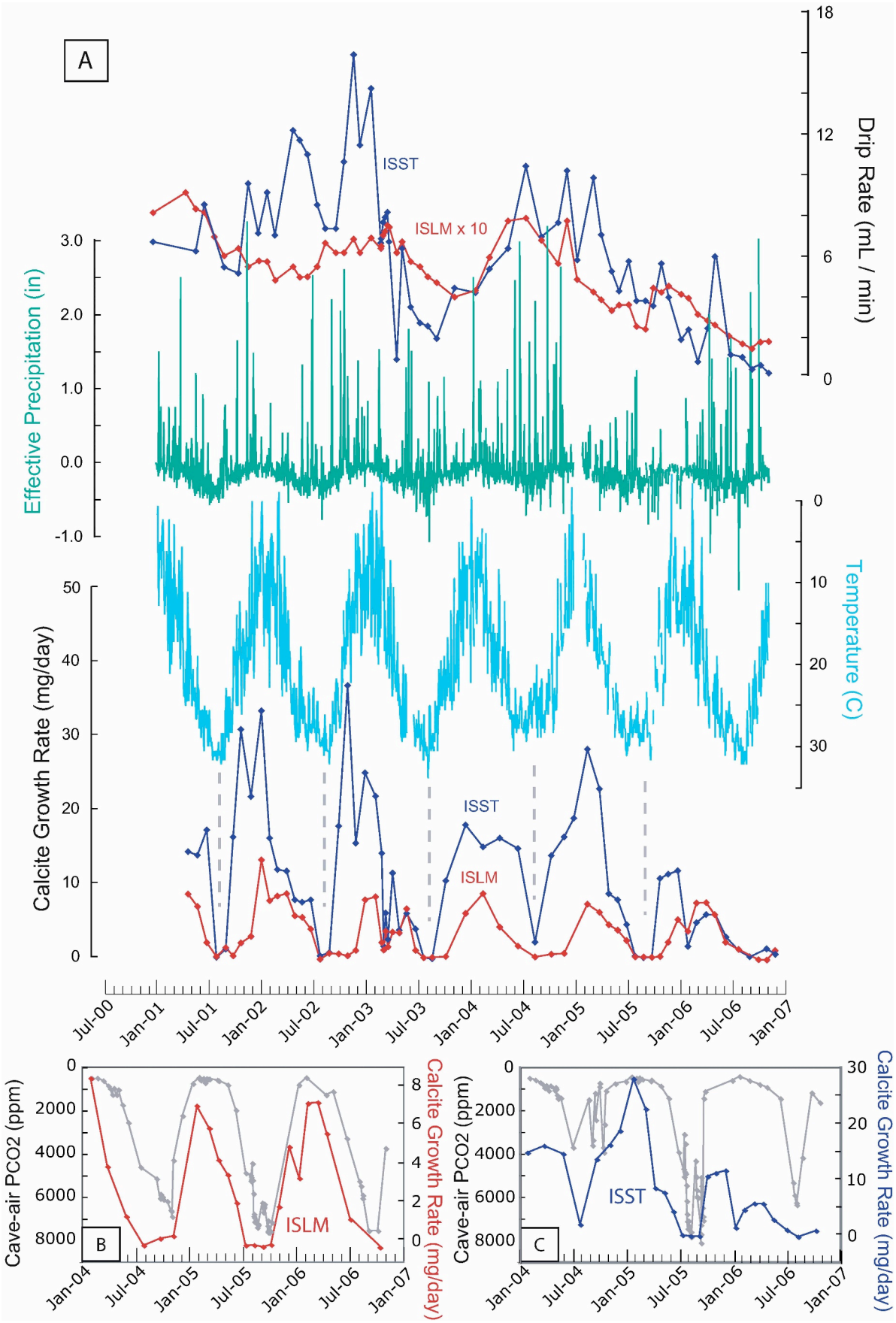
A
ISST
ISLM x 10
Drip Rate (mL / min)
Effective Precipitation (in)
Temperature (C)
Calcite Growth Rate (mg/day)
ISST
ISLM
Jul-00
Jan-01
Jul-01
Jan-02
Jul-02
Jan-03
Jul-03
Jan-04
Jul-04
Jan-05
Jul-05
Jan-06
Jul-06
Jan-07
B
Cave-air PCO2 (ppm)
Calcite Growth Rate (mg/day)
ISLM
C
ISST

enhancing and growth-retarding effects (Dreybrodt 1988). Models also predict that drip-water Ca concentration and drip rate will positively correlate with speleothem growth, and studies of some Holocene speleothem growth rates support this prediction (Genty et al. 2001).

The specific relationship between speleothem growth rate and these factors, however, is complex and influenced by local differences. For example, a direct relationship between temperature and growth rate is attributed to the controls of surface temperature and soil moisture on soil CO_2 production, yet this relationship may break down for sites with little soil cover (Genty et al. 2001). Soil CO_2 production is correlated with soil temperature both geographically and temporally at specific locations, but soil moisture availability also affects soil respiration rates (Reichstein et al. 2003). While numerous factors may influence speleothem growth, two basic conditions must be met for speleothem growth to occur: (1) high CO_2 levels in the soil zone, which contribute to elevated P_{CO2} of the infiltrating water, calcite dissolution, and subsequent CO_2 degassing in the cave, and (2) an availability of water for recharge (Baker et al. 1993).

Controls on Central Texas Speleothem Growth Rates

We summarize here several key observations (from Figs. 1–3, and Tables 1 and 2) that constrain the mechanisms that control growth rates of calcite on glass plates at caves IS and NB: (1) the pronounced seasonal changes in growth rate; (2) the significant inverse correlation between growth rate and surface air temperature at all sites; (3) the similar temporal changes in growth rate from site-to-site within and between caves, including sites that differ by two orders of magnitude in their average growth rates; (4) the near-zero growth rates at each site during the warmest months of each year; (5) the positive correlation between average drip rate and average growth rate from site to site; and (6) the limited variability in drip-water Ca concentrations.

The consistent site-to-site and cave-to-cave seasonality in growth rate (observation 3) precludes mechanisms controlling growth rates that involve the particular evolution of flow paths or water chemistry at an individual drip site. The mechanism must operate on at least the 130-km distance between caves IS and NB. Temporal variations in growth rate in a given cave might be influenced by the changing delivery rate of supersaturated water, which would in turn be a function of effective precipitation, soil CO_2 output, and variations in water residence time in the vadose zone. Positive calcite saturation indices and non-zero drip rates throughout most of the year at caves IS and NB leads to the prediction that some deposition of calcite will take place during most of the year. A drip-rate control is also consistent with the site-to-site variability in growth rate (Fig. 1B), and some interannual variation in growth rate appears to correspond to changes in drip rate (e.g., low drip rate and growth rates during fall–winter of 2005–2006; see Results). However, the near-zero growth rates at all sites each summer, when drip rates are not zero, indicates a mechanism other than drip rate as the main control on the seasonal changes in growth rate. A process that can control growth rates in this manner is changes in P_{CO2} of the cave air.

The seasonal changes in cave-air CO_2 (Figs. 2B, C, 3B, C) is the likely mechanism controlling the low speleothem growth rate during summer months. The low cave-air CO_2 levels during the winter cause a large contrast in CO_2 concentration between cave air and drip water (''air-water CO_2 contrast'' hereafter), which drives CO_2 degassing from the drip water (Spötl et al. 2005). This in turn would yield high levels of calcite supersaturation in the drips, and increase calcite precipitation rates. Elevated summertime cave-air P_{CO2} levels, on the other hand, would lower the air-water CO_2 contrast, which would inhibit degassing and reduce the rate of calcite growth. The lack of calcite growth at cave CS during any season is consistent with its relatively invariant and high levels of cave-air CO_2 (Table 1).

Two possible mechanisms can explain the observed seasonal variations in cave-air P_{CO2}. (1) First, many caves exhibit seasonal variations in cave-air P_{CO2} that are a function of the temperature difference between cave air and outside air. During the winter, caves are often well ventilated as a consequence of relatively cold and dense outside air (with low, atmospheric CO_2 levels) displacing warmer, high-CO_2 cave air. This lowers cave-air P_{CO2} and increases the air-water CO_2 contrast. During the summer, relatively warm outside air and relatively stable high-pressure weather systems create the opposite effect, leading to stagnant cave air with high P_{CO2} (e.g., Kartchner Caverns, Arizona; Obir Cave, Austria; Buecher 1999; Spötl et al. 2005). The ventilation process will vary within a cave depending on location, and between caves and regions, depending on cave geomorphology, temperature seasonality, and water flow, among other factors. The decrease in cave-air P_{CO2} at the onset of the cool season in Texas is closely followed each year by the increase in growth rate at site ISST, which in turn precedes the same changes at site ISLM. Because ISLM is deeper in cave IS, this cool-season sequence is consistent with the ventilation mechanism. (2) Alternatively, seasonal changes in cave-air CO_2 at caves IS and NB may be driven by drip-water delivery of higher levels of dissolved CO_2 to the cave in the summer. Low wintertime drip-water P_{CO2} likely results from temperature control on soil respiration. Central Texas soil respiration rates are high during the spring through late summer, with a peak in late summer, and low during the fall and winter (Litvak et al., unpublished data). High summer temperatures, coupled with the plateau's thin soils, make soil moisture availability during the summer low except following intermittent, large rain events common to this region. Re-wetting of warm soils in such environments can induce rapid and large increases in soil respiration (Huxman et al. 2004), and recharge is also associated with these events. While a soil CO_2 production model can account for seasonal cave-air CO_2 changes, ventilation is also required to provide the air-water CO_2 contrast needed for driving seasonal changes in growth rate. The lack of both calcite growth and pronounced seasonal CO_2 changes at cave CS suggest that relatively little ventilation occurs at this cave.

Cave-air CO_2 levels may also be affected by visitors, in as much as their respiration adds to CO_2 levels (Ek and Gewelt 1985; Baker and Genty 1998; Baldini et al. 2006). This effect may be significant in show caves (Carrasco et al. 2002) such as IS, NB, and CS. Visitation at caves IS and NB reaches a maximum in the summer each year, suggesting an alternative mechanism to the outside air temperature or soil respiration control on the seasonal cave-air CO_2 changes observed. Several observations, however, indicate that the contribution from visitor respiration is not the primary control on the seasonal cave-air CO_2 variations: (1) visitation rates peak in March and July each year at each cave, but cave-air CO_2 increases or maintains a relatively high level throughout the summer and through September at most sites each year (Figs. 2B, C, 3B, C); and (2) the highest CO_2 levels occur in the least visited cave (NB South, Fig. 3B). Regardless of the mechanism causing low cave-air CO_2 levels during the fall–winter, it is the larger fall and winter air-water CO_2 contrast that likely drives greater degassing, resulting in higher calcite supersaturation and more growth.

←

FIG. 2.—**A)** Time series of modern speleothem plate calcite growth rate and drip rate for sites ISST and ISLM in cave IS, and outside air temperature (plotted inverse) and effective precipitation (= rainfall − evaporation). Vertical dashed gray lines indicate average midpoint of slowest growth period for the two sites each year. ISLM drip rates are multiplied by 10 for comparative purposes. **B**, **C)** Time series of cave-air P_{CO2} (plotted inverse) and modern speleothem plate calcite growth rates for the same IS sites.

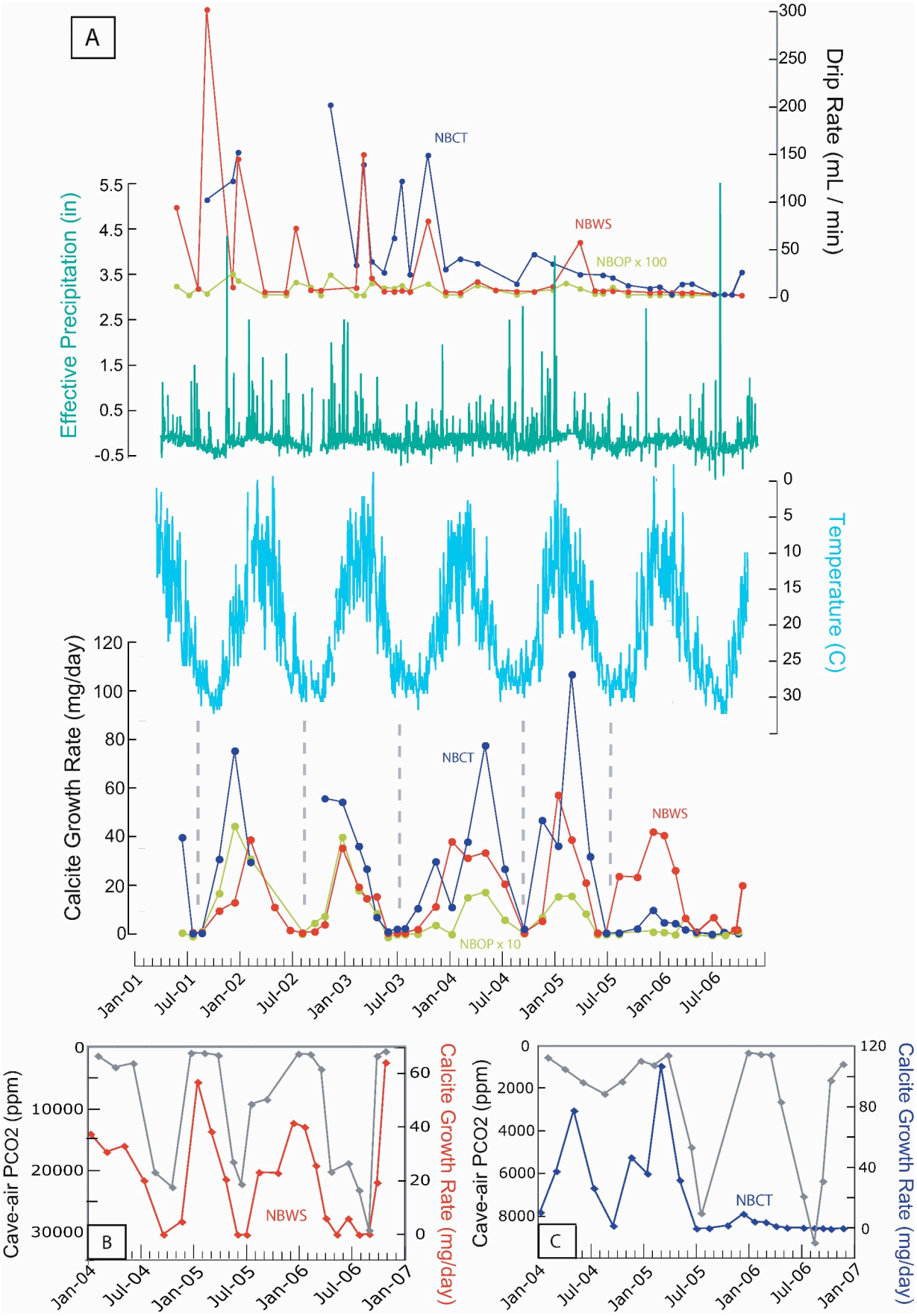
A
Effective Precipitation (in)
Drip Rate (mL / min)
NBCT
NBWS
NBOP x 100
Temperature (C)
Calcite Growth Rate (mg/day)
NBOP x 10
Jan-01
Jul-01
Jan-02
Jul-02
Jan-03
Jul-03
Jan-04
Jul-04
Jan-05
Jul-05
Jan-06
Jul-06
B
Cave-air PCO2 (ppm)
Calcite Growth Rate (mg/day)
Jan-07
C

TABLE 2.—*Significance of correlation between calcite growth rate and environmental characteristics at five NB and IS drip sites.*

p value	Drip-water P_{CO2}	Cave-air P_{CO2}	Drip Rate	Effective Precip.	Surface Temp
NS	1	0	2	2	0
S	1	2	1	0	0
HS	2	3	2	3	5

Number of drip sites categorized as having non-significant (NS: $p > 0.05$), significant (S: $p < 0.05$), highly significant (HS: $p < 0.01$) correlations are indicated for temporal variations at drip sites. Only four sites reported for drip-water P_{CO2} due to slow drip rate at site NBOP. N ranges from 20–25 for cave-air P_{CO2} and from 28–70 for all other parameters at a given drip site.

The higher pH and larger pH gradients in water films at site ISST during the cool season (see Results) are likely driven by higher extents of CO_2 degassing as water flows towards the edges of the plate and across the speleothems. Higher calcite growth across the glass plates at site ISST during the same time period is also consistent with more CO_2 degassing from these water films during cool seasons driving more calcite precipitation. Whereas the seasonal growth-rate cycles at a given site can be accounted for by temporal changes in the size of the air-water CO_2 contrast, site-to-site changes in the magnitude of growth rate are controlled principally by drip-rate variations (Fig. 1).

Application to Ancient Speleothem Records

Pleistocene to Holocene growth rates of central Texas stalagmites have been interpreted as a function of century- to millennial-scale changes in effective precipitation (Musgrove et al. 2001). Growth rates of these stalagmites drop by nearly two orders of magnitude from the late Pleistocene to the Holocene. We consider here an alternative model for variations in stalagmite growth rate involving changes in both the air-water CO_2 contrast and moisture availability during these time periods. Long-term increases in the seasonality of temperature would likely enhance seasonality of cave-air CO_2 levels both by promotion of seasonal cave ventilation and by enhancement of the seasonality of soil respiration. Such changes would affect the magnitude of the air-water CO_2 contrast. In addition, changes in the seasonal distribution of rainfall may affect the magnitude of drip rates during seasons when the air-water CO_2 contrast is favorable for speleothem growth. By this reasoning, time periods of high seasonality of temperature and rainfall, such as that inferred for the Holocene relative to the Pleistocene on the Edwards Plateau (Cooke et al. 2003), would lead to larger variability of Holocene growth rates. This seasonality model is inconsistent with the higher and more variable late Pleistocene stalagmite growth rates (Musgrove et al. 2001). This model does not take into account, however, the longer-term higher rainfall and cooler temperatures inferred for central Texas during the late Pleistocene relative to the Holocene, which would lead to higher effective precipitation during the late Pleistocene. A control on variations in ancient stalagmite growth rate by long-term changes in effective precipitation and, in turn, drip rate (Musgrove et al. 2001) is also consistent with the site-to-site correlation between drip rate and growth rate in the modern system (Fig. 1).

Uncertainties in applying our results from the modern to ancient speleothem records from this region include: (1) differences in the nature of the glass plate substrate relative to stalagmites; (2) human development of the caves studied, which in other settings has changed ventilation patterns (Spötl et al. 2005); (3) lower temporal resolution in the ancient speleothem records, (4) evidence that central Texas soils were thicker and sinkholes more open at some times in the past (Cooke et al. 2003; Sansom and Lundelius 2005), which may have changed CO_2 production and ventilation, and water infiltration paths relative to today; and (5) the hysteresis in drip rates common to karst systems (Baker et al. 1997). These uncertainties may be addressed through studies using: (1) automated, high-frequency drip-rate measurements, (2) other proxies with seasonal resolution, (3) different substrate materials, (4) soil CO_2 and respiration monitors, and (5) measurements in caves that (a) have been subject to minimal human impact, (b) underlie relatively thick soils, and (c) have a range of ventilation characteristics. The similarity in seasonal growth patterns at caves NB and IS and the lack of calcite growth at cave CS likely portray differences in geomorphology and human development between these caves. This suggests caution in generalizing conclusions regarding ventilation mechanisms across a region.

IMPLICATIONS

These results indicate that growth-rate variations in ancient speleothems may serve as a paleoenvironmental proxy with seasonal resolution. Using the monitoring approach outlined in this study, speleothem growth rate and, moreover, geochemical proxies may be evaluated and calibrated. If growth rate variations driven by seasonal changes can be understood as a function of environmental change in modern settings, then the controls on such variations in ancient speleothems can be more rigorously interpreted. The effects of growth rate on isotopic and elemental variations in speleothems may be directly assessed using this framework (e.g., Mickler et al. 2006; Guilfoyle et al. 2006; Stern et al. 2005). We also note that such proxies will only record environmental conditions for the times of the year during which calcite growth occurs, and that temperature and seasonality effects on cave-air CO_2 should be explicitly included in models of speleothem growth.

ACKNOWLEDGMENTS

We thank the owners, managers, and staff at Natural Bridge Caverns, Inner Space Cavern, and the Caverns of Sonora for their assistance with this project. Scientific input and assistance in the field were ably provided by Brian Vauter, Bill Sawyer, Pat Mickler, Lance Christian, Larry Mack, George Veni, Brian Cowan, Mike Osborne, Sarah Pierson, Molly Purcell, Laura DeMott, Lauren Greene, January Ruddy, and Mike Jaffre. JSR reviewers made useful suggestions for improving the manuscript. Support was provided by NSF (EAR 0233584), and the Geology Foundation and Environmental Science Institute of the University of Texas.

REFERENCES

BAKER, A., AND GENTY, D., 1998, Environmental pressures on conserving cave speleothems: effects of changing surface land use and increased cave tourism: Journal of Environmental Management, v. 53, p. 165–175.

BAKER, A., SMART, P.L., AND FORD, D.C., 1993, Northwest European palaeoclimate as indicated by growth frequency variations of secondary calcite deposits: Palaeogeography, Palaeoclimatology, Palaeoecology, v. 100, p. 291–301.

BAKER, A., BARNES, W.L., AND SMART, P.L., 1997, Variations in the discharge and organic matter content of stalagmite drip waters in Lower Cave, Bristol: Hydrological Processes, v. 11, p. 1541–1555.

←

FIG. 3.—**A)** Time series of modern speleothem plate calcite growth rate and drip rate for sites NBWS and NBOP in cave NB South, and NBCT in cave NB North, and outside air temperature (plotted inverse) and effective precipitation. Vertical dashed gray lines indicate average midpoint of slowest growth period for the three sites. NBOP drip rates are multiplied by 100 and growth rates are multiplied by 10 for comparative purposes. Missing growth-rate data for site NBCT in part of 2002 are due to flooding at this site. **B**, **C)** Time series of cave-air P_{CO2} (plotted inverse) and modern speleothem plate calcite growth rates for the same NB sites.

Baldini, J.U.L., Baldini, L.M., McDermott, F., and Clipson, N., 2006, Carbon dioxide sources, sinks, and spatial variability in shallow temperate zone caves: evidence from Ballynamintra Cave, Ireland: Journal of Cave and Karst Studies, v. 68, p. 4–11.

Buecher, R.H., 1999, Microclimate study of Kartchner Caverns, Arizona: Journal of Cave and Karst Studies, v. 61, p. 108–120.

Carrasco, F., Vadillo, I., Liñán, C., Andreo, B., and Durán, J., 2002, Control of environmental parameters for management and conservation of Nerja Cave (Malaga, Spain): Acta Carsologica, v. 9, p. 105–122.

Cooke, M.J., Stern, L.A., Banner, J.B., Mack, L.E., Stafford, T., and Toomey, R.S., 2003, Precise timing and rate of massive late Quaternary soil denudation: Geology, v. 31, p. 853–856.

Dreybrodt, W., 1988. Processes in Karst Systems: Physics, Chemistry and Geology: Springer Series in Physical Environments 4, Berlin, Springer-Verlag, 288 p.

Ek, C., and Gewelt, M., 1985, Carbon dioxide in cave atmospheres: new results in Belgium and comparison with some other countries: Earth Surface Processes and Landforms, v. 10, p. 173–187.

Eliot, W.R., and Veni, G., 1994. The Caves and Karst of Texas: Huntsville, National Speleological Society, Convention Guidebook 342 p.

Genty, D., and Quinif, Y., 1996, Annually laminated sequences in the internal structure of some Belgian stalagmites—importance for paleoclimatology: Journal of Sedimentary Research, v. 66, p. 275–288.

Genty, D., Baker, A., and Vokal, B., 2001, Intra- and inter-annual growth rate of modern stalagmites: Chemical Geology, v. 176, p. 191–212.

Guilfoyle, A.L., 2006. Temporal and spatial controls on cave water and speleothem calcite isotopic and elemental chemistry, central Texas [M.S. Thesis]: Austin, University of Texas, 337 p.

Guilfoyle, A.L., Banner, J.L., and Stern, L.A., 2006, Spatial and temporal controls on the geochemical evolution of cave dripwaters and modern speleothem calcite (abstract): Geological Society of America, Annual Meeting, Abstracts with Programs, v. 38, 24 p.

Holland, H.D., Kirsipu, T.W., Huebner, J.S., and Oxburgh, U.M., 1964, On some aspects of the chemical evolution of cave waters: Journal of Geology, v. 72, p. 36–67.

Huang, Y., and Fairchild, I.J., 2001, Partitioning of Sr^{2+} and Mg^{2+} into calcite under karst-analogue experimental conditions: Geochimica et Cosmochimica Acta, v. 65, p. 47–62.

Huxman, T.E., Cable, J.M., Ignace, D.D., Eilts, J.A., English, N.B., Weltzin, J., and Williams, D.G., 2004, Response of net ecosystem gas exchange to a simulated precipitation pulse in a semi-arid grassland: the role of native versus non-native grasses and soil texture: Oecologia, v. 141, p. 295–305.

Larkin, T.J., and Bomar, G.W., 1983. Climatic Atlas of Texas: Austin, Texas Department of Water Resources.

Mickler, P., Stern, L.A., and Banner, J.L., 2006, Large kinetic isotope effects in modern speleothems: Geological Society of America, Bulletin, v. 118, p. 65–81.

Musgrove, M., and Banner, J.L., 2004, Controls on the spatial and temporal variability of vadose dripwater geochemistry; Edwards aquifer, central Texas: Geochimica et Cosmochimica Acta, v. 68, p. 1007–1020.

Musgrove, M., Banner, J.L., Mack, L.E., Combs, D.M., James, E.W., Cheng, H., and Edwards, R.L., 2001, Geochronology of late Pleistocene to Holocene speleothems from central Texas: implications for regional paleoclimate: Geological Society of America, Bulletin, v. 113, p. 1532–1543.

Parkhurst, D.L., and Appelo, C.A.J., 1999, User's guide to PHREEQC (Version 2)—a computer program for speciation, batch-reaction, one-dimensional transport, and inverse geochemical calculations U.S. Geological Survey, Water Investigations Report 99-4259, 312 p.

Reichstein, M., and 26 others, 2003, Modeling temporal and large-scale spatial variability of soil respiration from soil water availability, temperature and vegetation productivity indices: Global Biogeochemical Cycles, v. 17, 1104 p.

Sansom, J.W, Jr., and Lundelius, E., Jr., 2005, Inner Space Cave: Discovery and geological and paleontological investigations: Austin Geological Society, Bulletin, v. 1, p. 53–69.

Shopov, Y.Y., Ford, D.C., and Schwarcz, H.P., 1994, Luminescent microbanding in speleothems: high-resolution chronology and paleoclimate: Geology, v. 22, p. 407–410.

Smith, C.L., Baker, A., Fairchild, I.J., Frisia, S., and Borsato, A., 2006, Reconstructing hemispheric-scale climates from multiple stalagmite records: International Journal of Climatology, v. 26, p. 1417–1424.

Spötl, C., Fairchild, I.J., and Tooth, A.F., 2005, Cave air control on dripwater geochemistry, Obir Caves (Austria): implications for speleothem deposition in dynamically ventilated caves: Geochimica et Cosmochimica Acta, v. 69, p. 2451–2468.

Stern, L.A., Banner, J.L., Cowan, B., Copeland, E.A., Mickler, P.J., James, E., Guilfoyle, A., Musgrove, M., and Mack, L.E., 2005, Trace element variations in speleothem calcite: influence of non-environmental factors [abstract]: Geological Society of America, Annual Meeting, Abstracts with Programs, v. 37, 435 p.

Wigley, T.M.L., and Brown, M.C., 1976, The physics of caves, *in* Ford, T.D., and Cullingford, C.H.D., eds., The Science of Speleology: London, Academic Press, p. 329–345.

Received 26 July 2006; accepted 9 November 2006.

Pergamon

Geochimica et Cosmochimica Acta, Vol. 68, No. 5, pp. 1007–1020, 2004

0016-7037/04 $30.00 + .00

doi:10.1016/j.gca.2003.08.014

Controls on the spatial and temporal variability of vadose dripwater geochemistry: Edwards Aquifer, central Texas

MARYLYNN MUSGROVE[1,*] and JAY L. BANNER[2]

[1]Department of Earth and Planetary Sciences, Harvard University, 20 Oxford Street, Cambridge, MA 01238, USA
[2]Department of Geological Sciences, The University of Texas at Austin, Austin, TX 78712, USA

(*Received February* 21, 2003; *accepted in revised form August* 12, 2003)

Abstract—A 4-yr study of spatial and temporal variability in the geochemistry of vadose groundwaters from caves within the Edwards aquifer region of central Texas offers new insights into controls on vadose groundwater evolution, the relationship between vadose and phreatic groundwaters, and the fundamental influence of soil composition on groundwater geochemistry. Variations in Sr isotopes and trace elements (Mg/Ca and Sr/Ca ratios) of dripwaters and soils from different caves, as well as phreatic groundwaters, provide the potential to distinguish between local variability and regional processes controlling fluid geochemistry, and a framework for understanding the links between climatic and hydrologic processes.

The Sr isotope compositions of vadose cave dripwaters (mean $^{87}Sr/^{86}Sr = 0.7087$) and phreatic groundwaters (mean $^{87}Sr/^{86}Sr = 0.7079$) generally fall between values for host carbonates (mean $^{87}Sr/^{86}Sr = 0.7076$) and exchangeable Sr in overlying soils (mean $^{87}Sr/^{86}Sr = 0.7088$). Dripwaters have lower Mg/Ca and Sr/Ca ratios, and higher $^{87}Sr/^{86}Sr$ values than phreatic groundwaters. Dripwater $^{87}Sr/^{86}Sr$ values also inversely correlate with both Mg/Ca and Sr/Ca ratios. Mass-balance modeling combined with these geochemical relationships suggest that variations in fluid compositions are predominantly controlled by groundwater residence times, and water-rock interaction with overlying soils and host aquifer carbonate rocks. Consistent differences in dripwater geochemistry (i.e., $^{87}Sr/^{86}Sr$, Mg/Ca, and Sr/Ca) between individual caves are similar to compositional differences in soils above the caves. While these differences appear to exert significant control on local fluid evolution, geochemical and isotopic variations suggest that the controlling processes are regionally extensive. Temporal variations in $^{87}Sr/^{86}Sr$ values and Mg/Ca ratios of dripwaters from some sites over the 4-yr interval correspond with changes in both aquifer and climatic parameters. These results have important implications for the interpretation of trace element and isotopic variations in speleothems as paleoclimate records, as well as the understanding of controls on water chemistry for both present-day and ancient carbonate aquifers.

1. INTRODUCTION

Relatively little is known regarding how groundwaters evolve temporally (e.g., annual to decadal to millennial time scales), yet this knowledge provides a framework for assessing the controls of factors such as climatic variations on aquifer and karst development, long-term patterns of recharge, sources of dissolved constituents, and local vs. regional scale influences on groundwater. Although climate variability must play a fundamental role in hydrology (e.g., Barron et al., 1989; Gascoyne, 1992; Blum and Erel, 1995), the specific mechanistic interdependence of climatic, hydrologic, and geochemical processes is not well understood. Such links are particularly relevant for karst systems, which may respond rapidly to environmental and climatic conditions.

It has been previously demonstrated that soil water geochemistry may vary depending on fluid flow-routes through a soil zone (Trudgill et al., 1983). There has, however, been limited consideration of the role of soil compositions in controlling groundwater geochemistry. The influence of soils may be of particular relevance in karst aquifers due to the rapid and sensitive response of many karst groundwater systems to fluctuations in rainfall and recharge.

* Author to whom correspondence should be addressed (mlm@eps.harvard.edu).

Many studies have investigated the major element chemistry of karst groundwater systems. In recent years there has been a growing interest in understanding controls on the geochemical evolution and spatial variability of fluids in the vadose zone of karst systems, such as cave dripwaters (e.g., Tooth and Fairchild, 2003). Previous work in the Edwards aquifer of central Texas (e.g., Oetting 1995) has investigated phreatic groundwater geochemistry and provides an understanding of regional scale controlling processes on groundwater evolution. That understanding provides an ideal framework within which to examine both spatial and temporal controls on vadose processes. This study integrates variations in trace elements (Mg/Ca and Sr/Ca ratios) and Sr isotopes in central Texas soils, vadose waters (i.e., cave dripwaters) and phreatic groundwaters to constrain hydrologic variables such as water-rock interaction, groundwater residence time, recharge, vadose flow-routes, the influence of soils on fluid geochemistry, and local vs. regional scale controls on cave dripwater evolution. We focus specifically on water samples collected from Natural Bridge Caverns in Comal County, Texas, and, to a lesser extent, Inner Space Cavern in Williamson County, Texas (Figs. 1 and 2).

Studies of fracture fill and cave calcite deposits (speleothems) using trace element and isotope geochemistry have yielded insight into Quaternary climate change (e.g., Harmon et al., 1978; Dorale et al., 1992; Winograd et al., 1992; Banner et al., 1996; Roberts et al., 1998; Musgrove et al., 2001). An

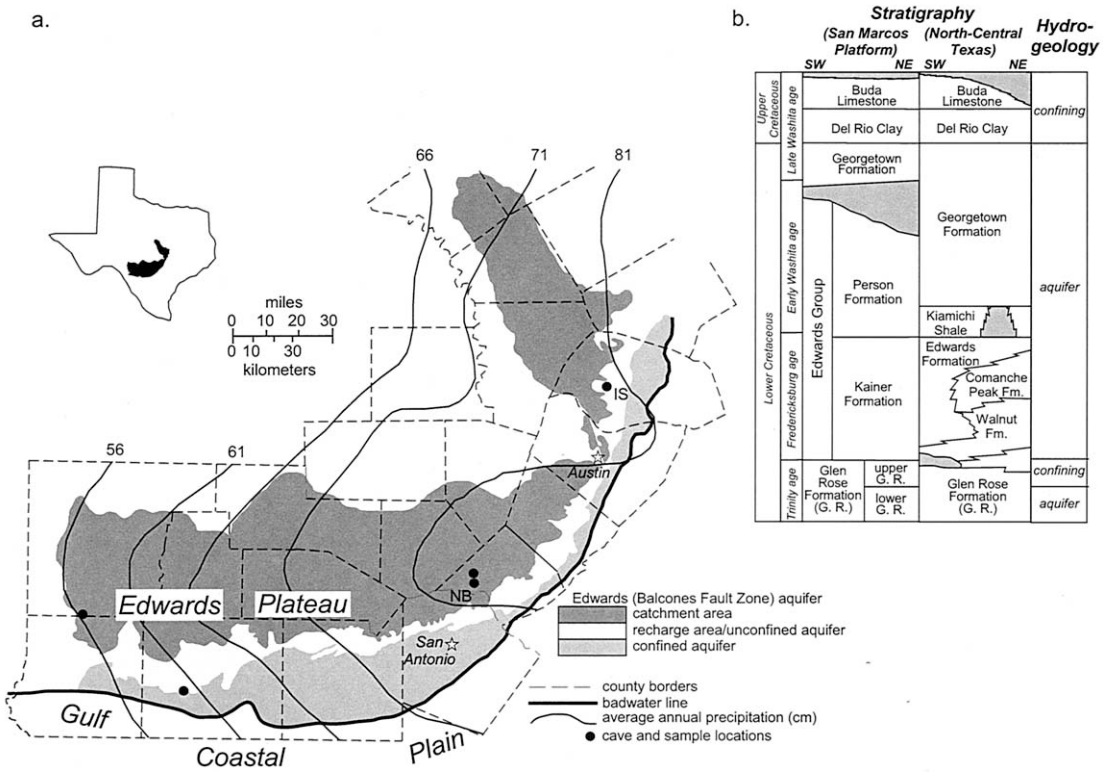

Fig. 1. (a) Hydrologic zones of the Edwards aquifer of central Texas, and cave locations. The badwater line defines the down-dip limit of potable water in the aquifer. Precipitation contours from Larkin and Bomar (1983). Temporal sequences of water samples were collected from Natural Bridge Caverns (NB) and Inner Space Cavern (IS). Caves are described in Figure 2, and in detail by Kastning (1983) and Elliott and Veni (1994). Samples from other cave locations (filled circles; detailed in Musgrove, 2000) are considered in evaluation of regional trends. Regional aquifer map after Burchett et al. (1986) and Brown et al. (1992). (b) Correlation of regional stratigraphic and hydrologic units from Rose (1972) and Maclay (1989). Natural Bridge Caverns is located in the upper member of the Glen Rose Formation (San Marcos Platform and North-Central Texas columns). Inner Space is developed within the Edwards Formation (North-Central Texas column). Note that although the upper member of the Glen Rose Formation is the regional basal confining unit of the Edwards aquifer, a cavernous lens (comprising the Upper Trinity Aquifer) exists in its upper 130 ft in Comal and Bexar counties in the San Antonio area. Shaded areas are locally absent. The Del Rio Clay, a gypsiferous and pyritic clay, is the upper confining unit of the Edwards aquifer, but is eroded over the Edwards Plateau aquifer catchment area and recharge area. The Kiamichi Shale is not present in the stratigraphic section near IS.

understanding of the sources and transport of geochemical constituents in modern aquifer systems is necessary to assess speleothem records that may preserve longer-term changes in water chemistry, sources of dissolved ions in groundwater, regional and local scale karst groundwater processes, and the links between hydrology and climate. The results of this study have implications for the interpretation of speleothem records, as well as the study of present-day and ancient carbonate aquifers, and provide insight into the fundamental role of soils in karst terrains.

2. HYDROGEOLOGIC SETTING

The Edwards aquifer region of central Texas is developed in Cretaceous limestone that is extensively karstified with many sinkholes and caves. The study area encompasses the Edwards (Balcones Fault Zone) aquifer, and includes portions of two other regional aquifer systems, the Edwards-Trinity (Plateau) aquifer, and the Trinity aquifer (Fig. 1). Late Cenozoic faulting of the predominantly flat-lying region along the Balcones Fault Zone formed a series of high-angle normal en echelon faults, which display a-down-to-the-coast displacement (Clement and Sharp, 1988; Sharp, 1990). This faulting resulted in a series of blocks of Edwards aquifer rocks that are partially to completely offset, dividing the confined and unconfined portions of the aquifer (Maclay and Small, 1983). The Edwards Limestone is exposed on the Edwards Plateau, ranging between 350 to 500 ft in thickness (Burchett et al., 1986). Along the Fault Zone, the Edwards Limestone dips steeply to the south and southeast. Streams flowing south and east toward the Gulf of Mexico drain the Edwards Plateau and recharge the aquifer across the Balcones Fault Zone. Many studies have investigated the aquifer's development, fluid hydrodynamics, and groundwater geochemistry (e.g., Clement and Sharp, 1988; Sharp, 1990; Oetting et al., 1996; Sharp and Banner, 1997). Although the phreatic groundwater system is well characterized, only a few studies have addressed vadose zone geochemistry (Harmon, 1970; Oetting, 1995; Veni, 1997).

Climatic and hydrologic extremes are common in this region

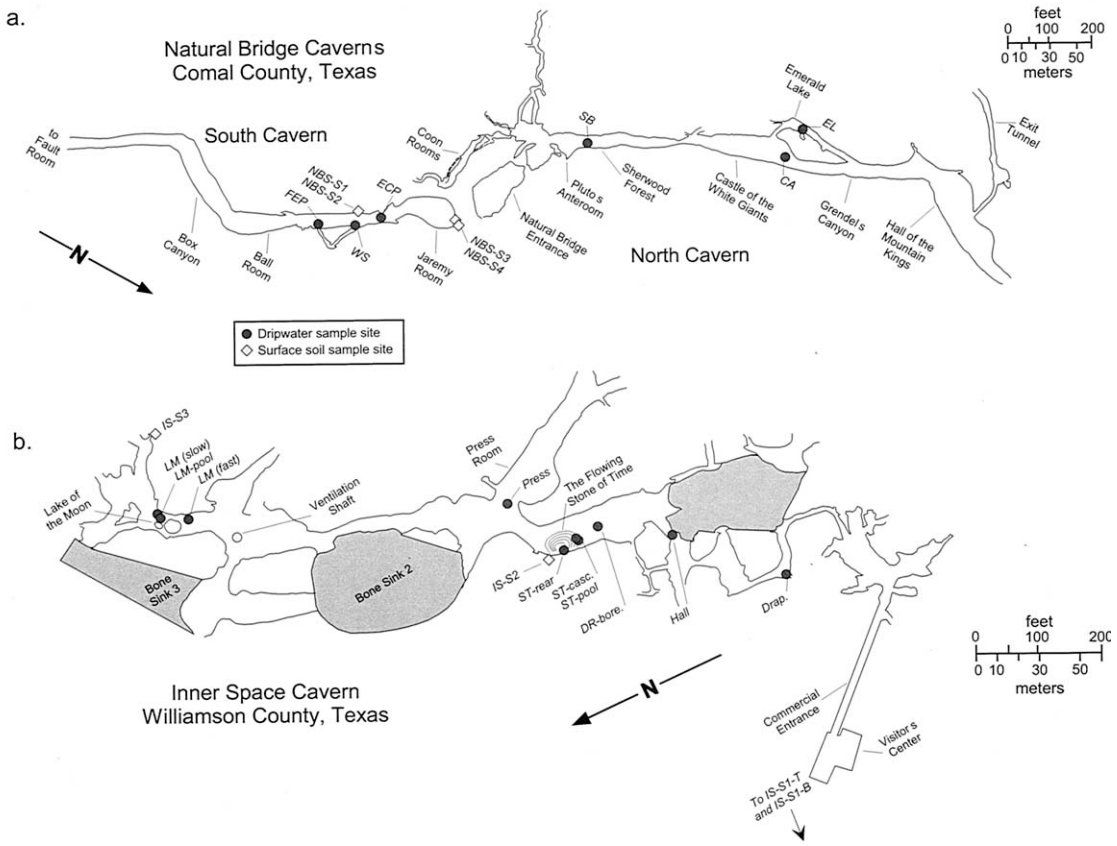

Fig. 2. Maps of Natural Bridge Caverns (a; NB) and Inner Space Cavern (b; IS) showing locations of cave dripwater samples and projections for surface soil sample sites. Soil samples IS-S1 (T and B) in (b) are located off the scale of the map to the west. Maps simplified from Elliott and Veni (1994). See text for lithologic description and geologic setting of caves.

(Griffiths and Strauss, 1985; Jones, 1991). Annual recharge to the Edwards aquifer varies markedly in response to regional precipitation. Effective moisture (i.e., precipitation less evaporation estimates) is strongly linked to precipitation (Musgrove, 2000). Approximately 85 to 90% of regional precipitation is lost through evapotranspiration (Maclay, 1995). Edwards Plateau soils, which are regionally characterized as mollisols, support grasses and live oak savanna vegetation with some mesquite and juniper (Godfrey et al., 1973; McMahan et al., 1984; Riskind and Diamond, 1986). Soils across the region as well as within the vicinity of the study areas are generally thin and stony. Soils are regionally characterized as dominantly calcareous, clayey, and loamy materials over indurated limestone, interbedded limestone and marls, and calcareous clayey outwash (Godfrey et al., 1973). Within this regional context, the gradual east-west decrease of moisture across the Plateau (Fig. 1) may contribute to local changes in soils and vegetation. A number of other factors, such as variations in the regional stratigraphy, as well as land use and development, may also contribute to differences in the soils. For example IS is located in a more urban area than NB, and a major highway crosses over IS. Assessing the impact of land use changes on soil compositions is complex, even in areas that appear undisturbed. Although the extent to which variations in soil geochemistry are due to natural vs. anthropogenic factors is not certain, our results demonstrate that the soils vary compositionally.

The two caves that are the focus of this study, Inner Space Cavern (IS) and Natural Bridge Caverns (NB) are separated geographically by ~130 km, and stratigraphically by part of the Edwards Group limestones (Figs. 1 and 2). The local climate of the areas above the caves, however, is similar with respect to climatic conditions such as temperature and rainfall. Annual rainfall distribution is characterized by dry winters, and in particular, summers, and relatively wet conditions in the spring and fall. Descriptions of the geology and stratigraphy of the caves that follow are based on Kastning (1983). Both caves are overlain by relatively low or subdued topography. Although the exposed surface rocks above NB are the limestone Kainer Formation, the cave is largely formed within the upper member of the Glen Rose Formation, which contains interbedded limestone, marl, dolomite, and clay. Dripwater sites at NB are in a depth range of ~40 to 50 m below land surface.

IS is formed within a relatively pure horizon of the Edwards Limestone, although there are locally dolomitic and chert-rich units both above and below the cave. Dripwater sites are within the main level of the cave, between 12 and 18 m below land surface. Seepage of water into IS is locally pronounced, which is consistent with the fractured nature of the Edwards Forma-

Table 1. Mean groundwater and cave dripwater geochemistry.

	Cave dripwaters		
	Natural Bridge Caverns; NB	Inner Space Cavern; IS	Groundwaters
	Mean (*n*)	Mean (*n*)	Mean (*n*)
Geochemical parameter	*Range (standard deviation)*	*Range (standard deviation)*	*Range (standard deviation)*
$^{87}Sr/^{86}Sr$	0.7088 *(61)*	0.7083 *(22)*	0.7079 *(49)*
	0.7083–0.7091 (0.0002)	*0.7080–0.7086 (0.0002)*	*0.7076–0.7086 (0.0002)*
Mg/Ca	0.118 *(81)*	0.141 *(48)*	0.326 *(27)*
	0.015–0.359 (0.071)	*0.057–0.268 (0.062)*	*0.119–0.752 (0.163)*
Sr/Ca	0.26×10^{-3} *(82)*	0.63×10^{-3} *(48)*	2.07×10^{-3} *(27)*
	[0.08–0.57 (0.08)] × 10^{-3}	*[0.24–0.84 (0.09)] × 10^{-3}*	*[0.58–5.8 (1.1)] × 10^{-3}*
HCO_3	261 *(42)*	241 *(36)*	230 *(27)*
	152–413 (66)	*129–328 (53)*	*110–377 (50)*
Ca	91 *(84)*	90 *(49)*	80 *(27)*
	38–320 (35)	*60–125 (15)*	*54–150 (23)*
Mg	5.7 *(81)*	7.6 *(48)*	17.5 *(27)*
	1.1–10.0 (2.0)	*2.6–12.9 (3.1)*	*7.2–54 (9.7)*
Sr	0.05 *(82)*	0.12 *(48)*	1.43 *(27)*
	0.03–0.07 (0.01)	*0.05–0.16 (0.02)*	*0.09–3.2 (0.57)*
Ba	0.03 *(82)*	0.04 *(47)*	0.04 *(27)*
	0.02–0.05 (0.007)	*0.03–0.07 (0.010)*	*0.03–0.15 (0.02)*
Na	5.25 *(82)*	6.26 *(47)*	11.73 *(27)*
	3.0–19.9 (2.1)	*3.1–15.8 (3.5)*	*4.5–96.0 (17.5)*
K	0.44 *(71)*	5.53 *(48)*	1.36 *(27)*
	0.08–3.3 (0.44)	*0.20–48.0 (9.1)*	*0.70–3.4 (0.64)*
Si	4.5 *(69)*	4.1 *(48)*	12.41 *(27)*
	3.7–5.8 (0.4)	*2.3–5.1 (0.6)*	*10.0–22.0 (2.1)*
U	0.44 *(35)*	0.79 *(48)*	1.4 *(1)*
	0.29–0.61 (0.08)	*0.43–1.14 (0.19)*	
Th	0.28 *(13)*	0.40 *(21)*	NA
	0.10–0.59 (0.17)	*0.10–0.87 (0.22)*	
Rb	0.48 *(35)*	1.95 *(47)*	NA
	0.26–1.82 (0.29)	*0.39–20.1 (3.7)*	

NB = Natural Bridge Caverns. IS = Inner Space Cavern. Units for all concentrations, except U, Th, and Rb, are in mg/L. U, Th, and Rb concentrations are in μg/L. Number in parentheses (n) following mean value = number of samples in mean calculation. Numbers in parantheses below mean value = range of values used in mean calculation and standard deviation. NA = not analyzed. Element ratios are molar concentrations. Detailed data for cave dripwaters available in Musgrove (2000) or from the authors. Groundwater data, excluding Sr and $^{87}Sr/^{86}Sr$, from Gandara and Barbie (1998). Groundwaters, collected by the Austin branch of the U.S. Geological Survey (NAWQA program), were analyzed for $^{87}Sr/^{86}Sr$ at the University of Texas at Austin, and for Sr concentration by ICP-AES at the University of California, Riverside, as detailed in Musgrove (2000).

tion. The Edwards Limestone is ~30 to 40 m thick in the vicinity of IS and is exposed at the surface above the cave. IS is wholly contained within a fault block of the Balcones Fault Zone. The Edwards Formation is also exposed in the adjacent block several hundred feet to the west of IS. The Georgetown Formation and Del Rio Clay are exposed in the adjacent block several hundred feet to the east. The Georgetown Formation is predominantly composed of limestone, but contains some beds of marl and shale.

3. METHODS AND RESULTS

Dripwater samples were collected periodically at NB from 1995 to 1999, and at IS during 1998 and 1999. Sampling procedures, sample locations and analytical methods are discussed in detail in Musgrove (2000). Table 1 summarizes the dripwater data by comparing mean elemental and isotopic values with regional phreatic groundwaters. The majority of elemental analyses for waters and soil leachates were determined by ICP-MS (Perkin Elmer/Sciex Elan 5000) at The University of Minnesota. Analytical uncertainties are generally $< 5\%$ for Ca, Mg, Sr, Ba, and Na analyses, and $< 10\%$ for other elemental analyses. Replicate analyses on water samples are within analytical uncertainty.

Soil samples collected from above the caves were leached with 1 mol/L NH_4Ac to determine the composition of the exchangeable fraction (Suarez, 1996). Soil leachate analyses are summarized in Table 2. Reproducibility of soil leachates for Sr isotope values and trace element ratios (Mg/Ca and Sr/Ca) is generally within analytical uncertainty. Leachate elemental concentrations, however, for an equivalent weight of initial soil are more variable (by up to ~30%). These differences may result from heterogeneities in soil subsamples. The better reproducibility of isotopic values and trace element ratios in soil leachates, however, suggests that concentration differences may reflect differences in the net amount of material leached from the soils. X-ray diffraction analyses indicate that the soils are predominantly composed of variable mixtures of calcite, clay, and quartz (Table 3; Musgrove, 2000).

All strontium isotope values for dripwaters, groundwaters, and soils were measured at The University of Texas at Austin on a Finnigan-MAT 261 thermal ionization mass spectrometer using both static and auto-dynamic techniques. Results were

Table 2. Comparison of soil leachate geochemistry.

Geochemical parameter	Natural Bridge Caverns (NB) Mean (n = 4) *Range (standard deviation)*	Inner Space Cavern (IS) Mean (n = 4) *Range (standard deviation)*
$^{87}Sr/^{86}Sr$	0.7089 *0.7086–0.7093 (0.0003)*	0.7086 *0.7084–0.7089 (0.0002)*
Mg/Ca	0.037 *0.017–0.080 (0.030)*	0.086 *0.053–0.123 (0.033)*
Sr/Ca	0.21×10^{-3} *[0.11–0.28 (0.07)] × 10^{-3}*	0.56×10^{-3} *[0.40–0.91 (0.24)] × 10^{-3}*
Ca	265 *114–459 (172)*	235 *215–266 (22)*
Mg	7.6 *1.4–21.0 (9.0)*	12.1 *8.5–16.1 (3.9)*
Sr	0.153 *0.027–0.262 (0.112)*	0.296 *0.201–0.526 (0.155)*
Ba	0.670 *0.110–1.72 (0.726)*	0.740 *0.583–1.02 (0.201)*
Fe	0.139 *0.016–0.370 (0.167)*	0.198 *0.172–0.222 (0.021)*
Mn	0.029 *0.004–0.090 (0.041)*	0.010 *0.0005–0.026 (0.011)*
Na	0.897 *0.090–2.75 (1.249)*	0.378 *0.149–0.555 (0.175)*
K	11.54 *1.32–31.6 (13.8)*	11.97 *3.77–26.6 (10.1)*
Si	5.22 *2.28–8.16 (4.16)*	1.83 *0.97–2.78 (0.74)*
Rb	0.066 *0.059–0.072 (0.009)*	0.038 *0.012–0.059 (0.019)*
P	0.151 *0.098–0.204 (0.074)*	0.087 *0.072–0.102 (0.013)*

Units for all concentrations are mg/L. Element ratios are molar concentrations. Approximately 1.5 g of representative soil subsamples were leached with 10 mL of 1 molar NH_4Ac, buffered to a pH of between 7 and 8, for 1 h at 25°C. Samples were centrifuged and the supernatant collected and split for elemental and isotopic analysis. Detailed data available in Musgrove (2000) or from the authors.

normalized for fractionation to $^{86}Sr/^{88}Sr = 0.1194$ using an exponential fractionation law. A mean value of 0.710264 was determined for standard analyses of NIST-SRM 987 (external $2\sigma = \pm 0.000026$ for auto-dynamic runs, $n = 79$, and external $2\sigma = \pm 0.000025$ for static runs, $n = 44$). Replicate analyses yielded a mean deviation of 0.000018 ($n = 26$). Blank values (3–40 pg) are negligible with respect to sample size (~200 ng Sr). $^{87}Sr/^{86}Sr$ values for Cretaceous

Table 3. Soil x-ray diffraction analyses.

Sample	Location	% Clay	% Quartz	% Potassium feldspar	% Plagioclase feldspar	% Calcite	Other (trace)
Natural Bridge Caverns; NB							
NBS-S1	Upper horizon, organic rich, 18 cm depth	61	20	Trace	Trace	19	
NBS-S2	Lower horizon, altered limestone at base, 29 cm depth	4	1	Trace	0	94	Goethite
NBS-S3	~0.6 m above base of South Cave entrance pit; lower karst fill	76	21	1	0	2	Goethite
NBS-S3	Replicate	71	22	2	0	4	Goethite
Inner Space Cavern; IS							
IS-S1-T[a]	Small thicket to west of visitor's center, upper horizon, 2.5 cm depth	36	61	2	1	0	—
IS-S1-B[a]	Small thicket to west of visitor's center, lower horizon, 18 cm depth	38	60	2	1	0	—
IS-S2	~40 ft N of I-35 overpass; halfway down slope of overpass, 7–10 cm depth	55	41	3	0	0	—
IS-S3	East of I-35, in thicket adjacent to parking lot north of IS wellshaft housing, upper horizon, 2.5 cm depth	57	30	3	1	9	—

Analyses are on whole soil fractions. Analytical methods are detailed in Lynch (1997). Locations shown on Fig. 2, excluding IS-S1.
[a] IS-S1 latitude and longitude coordinates are 30.61005°N and 97.68947°W.

carbonate rocks discussed in the text are from Koepnick et al. (1985) and Oetting (1995) and have been adjusted to a value for NIST-SRM 987 of 0.710264.

Total alkalinity was determined by titration for only a small number of samples due to sampling constraints. Correspondingly, saturation states for carbonate minerals were not determined on the majority of the dripwaters. The samples with complete data necessary to calculate saturation states are from widely spaced caves across the Edwards Plateau and are supersaturated with respect to calcite and undersaturated with respect to dolomite (Musgrove, 2000). A comparison of these limited saturation state values with previous studies of Edwards aquifer groundwaters shows no clear evolution in carbonate equilibrium relationships from dripwaters to groundwaters (Oetting, 1995). Similar to the phreatic groundwaters and cave waters from previous work in central Texas caves, the dripwaters of this study are dilute Ca-HCO_3 waters of meteoric origin (Harmon, 1970; Oetting, 1995; Veni, 1997). However, a comparison of dripwaters from specific caves and phreatic groundwaters reveals distinct differences (Table 1). For example, the mean Sr/Ca ratio of IS dripwaters is greater than NB dripwaters (Sr/Ca = 0.63×10^{-3} and 0.26×10^{-3}, respectively). Mean Mg/Ca ratios for NB and IS dripwaters (0.12 and 0.14, respectively) are less than values for phreatic groundwaters (0.33). Strontium isotope values of all dripwaters range from 0.7080 to 0.7091. The mean $^{87}Sr/^{86}Sr$ value for NB dripwaters (0.7088) is higher than that for IS dripwaters (0.7083). Dripwater $^{87}Sr/^{86}Sr$ values for both caves are offset to lower $^{87}Sr/^{86}Sr$ values than the range for soil leachates corresponding to the individual caves. Both temporal and spatial differences are present in the dripwater data.

4. DISCUSSION

4.1. Strontium Isotope Variations

Applications of Sr isotopes to natural waters have demonstrated their utility as a tracer for fluid evolution, weathering processes, and sources of dissolved constituents to fluids (e.g., Miller et al., 1993; Banner et al., 1994). Previous studies in the Edwards aquifer have applied Sr isotopes to constrain sources of dissolved constituents to phreatic groundwaters (Oetting, 1995; Oetting et al., 1996; Sharp and Banner, 1997). Strontium isotope values of Edwards cave dripwaters (0.7080–0.7091) are bracketed between (1) values for carbonate host rocks (0.7074–0.7081) and (2) values for soil leachates (0.7084–0.7093; Fig. 3). Values for fresh phreatic groundwaters of the Edwards aquifer range to more radiogenic $^{87}Sr/^{86}Sr$ than the aquifer host rocks (Fig. 3). The most likely source of Sr to the waters is the Cretaceous carbonate rocks that constitute the aquifer. The influence of the host carbonate rocks on regional groundwater geochemistry is well documented (Clement, 1989; Oetting, 1995; Oetting et al., 1996). Elevated $^{87}Sr/^{86}Sr$ values for both vadose and phreatic groundwaters relative to the host aquifer rocks are indicative of a source of more radiogenic $^{87}Sr/^{86}Sr$ to the waters. The migration of fluids from aquifer rocks located down-dip of the badwater line along faults and/or fractures has been demonstrated to be a source of radiogenic Sr to specific geochemical facies of Edwards phreatic groundwaters (Oetting et al., 1996). This is not a possible source of Sr to vadose dripwaters, however, and cannot account for the regional trends in Sr isotope variations. Soil leachate $^{87}Sr/^{86}Sr$ values point to the overlying soils as this source.

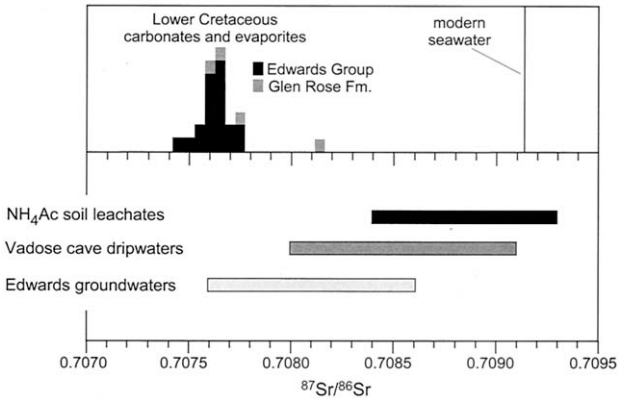

Fig. 3. Strontium isotope variations in regional Edwards aquifer system components. Histogram in the upper portion of the diagram represents twenty whole rock $^{87}Sr/^{86}Sr$ values determined for Lower Cretaceous carbonates and evaporites (18 from Koepnick et al., 1985, and 2 from Oetting, 1995). In the lower portion of the diagram are $^{87}Sr/^{86}Sr$ variations measured in different aquifer components. Data for soil leachates ($n = 12$) and dripwaters ($n = 100$) are from caves across the Edwards Plateau as shown in Fig. 1. Groundwater data are from Edwards aquifer wells across the region ($n = 49$). Soil leachates represent exchangeable Sr in soils near cave recharge zones. Modern seawater value ($^{87}Sr/^{86}Sr = 0.709173$) from Capo and DePaolo (1990).

The $^{87}Sr/^{86}Sr$ of soil leachates range to higher values than the ranges for host limestones, vadose dripwaters, and phreatic groundwaters. The exchangeable silicate/clay components of the soils are a likely source of radiogenic Sr. Airborne dust across the region, largely composed of mica and quartz (Rabenhorst et al., 1984), may also contribute a radiogenic component to the soils. One possible airborne source with high $^{87}Sr/^{86}Sr$ that may contribute to Texas soils is North African dust (Borg and Banner, 1996; Perry et al., 1997).

Several analyses of rainwaters in the Austin area have yielded $^{87}Sr/^{86}Sr$ values of 0.7088 to 0.7091 (Oetting, 1995). These values approach that of modern seawater. Limited analyses of central Texas rainwater suggest that Sr concentrations are generally not a significant source of Sr to the aquifer system (0.5–17 ppb; mean = 5.6 ± 8 ppb ; $n = 4$; Oetting, 1995). However, the highest value of this range approaches 20% of the Sr concentration for the most dilute dripwaters and precludes dismissing rainwater as a potential source of Sr to soils and/or dripwaters. Rainwater $^{87}Sr/^{86}Sr$ values are higher than values for the regionally extensive Cretaceous carbonates, and lie within the range of soil leachates. A lack of correlation between Na concentration and $^{87}Sr/^{86}Sr$ values for dripwaters (Musgrove, 2000), coupled with the distance of the region from the Gulf of Mexico, suggests that rainwater Sr is derived from airborne dust, rather than from sea salts.

The radiogenic/silicate component of the soils is likely derived from some combination of the insoluble residue of weathered underlying carbonate rocks and airborne dust. Regardless of the specific source of radiogenic strontium to the soils, regional strontium isotope values record a progression toward lower $^{87}Sr/^{86}Sr$ values from (1) soil leachates to (2) vadose cave dripwaters to (3) fresh phreatic groundwaters to (4) host

limestones (Fig. 3). This trend indicates that both dripwaters and groundwaters acquire Sr from two principal isotopically-distinct endmember sources: the soils and carbonate host rocks. As waters migrate through the aquifer system (e.g., from vadose to phreatic groundwaters), they acquire a larger component of Sr from interaction with the carbonate host rocks. This progression is consistent with the evolution of Sr isotope values of aquifer fluids toward limestone values with increased residence time, which allows for greater potential extents of water-rock interaction with the carbonate host rocks.

Within this regional context, spatial variability in $^{87}Sr/^{86}Sr$ values from different caves indicates that variations in the composition of host limestones and overlying soils exert a strong control on local scale fluid evolution. For example, both dripwaters and soil leachates at NB have more radiogenic $^{87}Sr/^{86}Sr$ values relative to IS. Yet, within each cave, soil leachates have more radiogenic $^{87}Sr/^{86}Sr$ values than corresponding dripwaters. These differences between NB and IS may reflect the caves' settings and the lithology of the local carbonate rocks. NB is primarily within the Glen Rose Formation. The argillaceous nature of this formation suggests the presence of a greater detrital, and therefore radiogenic Sr-rich component, in comparison with the Edwards Formation, which houses IS. In contrast, the Edwards Formation in the vicinity of IS is relatively pure limestone (Rodda et al., 1966). As proposed above, if dripwater $^{87}Sr/^{86}Sr$ values evolve from interaction with soils and limestones, then the higher $^{87}Sr/^{86}Sr$ range for NB dripwaters, relative to IS dripwaters, would be expected. It is, however, not clear from existing measurements that Glen Rose carbonates exhibit more radiogenic $^{87}Sr/^{86}Sr$ values (Fig. 3; Koepnick et al., 1985). These measurements were made for reconstruction of the paleoseawater Sr isotope curve and thus the data set is biased toward relatively pure samples. A more comprehensive study of cave host rocks would help clarify differences in whole rock strontium isotope compositions between the cave locations. As will be discussed below, the local control of soil and host rock geochemistry on dripwater $^{87}Sr/^{86}Sr$ values appears to be superimposed on broader regional controls.

4.2. Mg/Ca and Sr/Ca Variations

A fundamental influence of residence time on Mg/Ca ratios of carbonate groundwaters was illustrated in the Floridan aquifer where residence times may be thousands to tens of thousands of years (Plummer, 1977). Similarly, important controls on Mg/Ca ratios have since been demonstrated in carbonate groundwater systems with much shorter residence times (Langmuir, 1971; Cowell and Ford, 1980; Trudgill et al., 1980; Fairchild and Killawee, 1995; Fairchild et al., 1996). Proposed mechanisms for observed increases in groundwater Mg/Ca ratios with increasing residence time include progressive water-rock interaction processes such as the incongruent dissolution of dolomite, and calcite recrystallization (Wigley, 1973; Plummer, 1977; Lohmann, 1988). If these processes are also occurring in the vadose zone, then dripwater Mg/Ca ratios should also be strongly dependent on water residence time and the composition of the host aquifer rocks (Fairchild et al., 1996). The partitioning of trace elements such as Mg and Sr into a fluid during the recrystallization of either calcite or dolomite is largely controlled by the trace element's distribution coefficient (K_D value; e.g., $K_D^{Sr\text{-}Ca} = [Sr/Ca]_{mineral}/[Sr/Ca]_{solution}$) and the host rock composition (Banner and Hanson, 1990). For K_D values < 1, the trace element will generally be preferentially excluded from the mineral phase, and partition into the interacting fluid. Both Mg and Sr generally have K_D values < 1 and will therefore increase relative to Ca in a fluid progressively recrystallizing calcite or dolomite (Oomori et al., 1987; Banner and Hanson, 1990; Banner, 1995).

The observed variability in dripwater Mg/Ca and Sr/Ca ratios in this study indicates that water-rock interaction processes are neither spatially nor temporally constant, and that processes of water-rock interaction that control the evolution of phreatic groundwaters with long residence times also control vadose dripwater compositions. The range of Mg/Ca and Sr/Ca values for Edwards phreatic groundwaters overlaps with values for cave dripwaters, but extends to much higher values (Fig. 4). A correlation between Mg/Ca and Sr/Ca ratios is evident for different dripwater sites within a cave, as well for at different caves (Fig. 4). At NB there is a single positively correlated trend exhibited by the dataset, whereas at IS there are multiple positively correlated trends, each delineated by more than one dripwater site. Although each dripwater site has its own trend, the groupings of sites from the two caves are geochemically distinct. The spread in the data from site to site and cave to cave likely results from local variations in host limestone compositions, overlying soils, vadose flow-routes, and residence times.

Similar to the relationship of Mg/Ca and Sr/Ca ratios in the dripwaters, leachate values for soils from the two caves also overlap with respect to Mg/Ca, but exhibit distinct ranges for Sr/Ca (Fig. 4). This points to the importance of constituents derived from the soils in determining the "starting point" of dripwater geochemical evolution. The ranges of Mg/Ca and Sr/Ca values for individual dripwater sites also vary (Fig. 4). Dripwaters from IS appear to exhibit greater variability in their starting point than NB dripwaters. This may reflect the greater range of soil leachate geochemistry at IS relative to NB (Fig. 4). The relationship between Mg/Ca-Sr/Ca values for the soils and dripwaters at these two caves suggests that the spread in the dripwaters reflects variations in the soils. Soil differences, in turn, may reflect differences in the composition of underlying carbonate rocks. In spite of these local variations, the ranges of Mg/Ca and Sr/Ca values for all cave dripwaters are bracketed by regional values for soil leachates at their low end, and phreatic groundwaters at their high end (Fig. 4). These relationships suggest that the major controls on dripwater geochemistry are operating regionally across the Edwards Plateau.

4.3. Trace Element and Isotope Covariations

Mg/Ca and Sr/Ca ratios of central Texas vadose dripwaters and phreatic groundwaters covary inversely with Sr isotopes (Fig. 5). Low $^{87}Sr/^{86}Sr$ values, indicative of a large component of Sr derived from the limestones relative to the soils, correspond with high Mg/Ca and Sr/Ca ratios. High Mg/Ca and Sr/Ca ratios are indicative of greater extents of water-rock interaction that likely result from increased residence time in the limestone. Water-rock interaction processes, including both dissolution and progressive recrystallization of host limestones can be modeled based on mass-balance relationships, distribu-

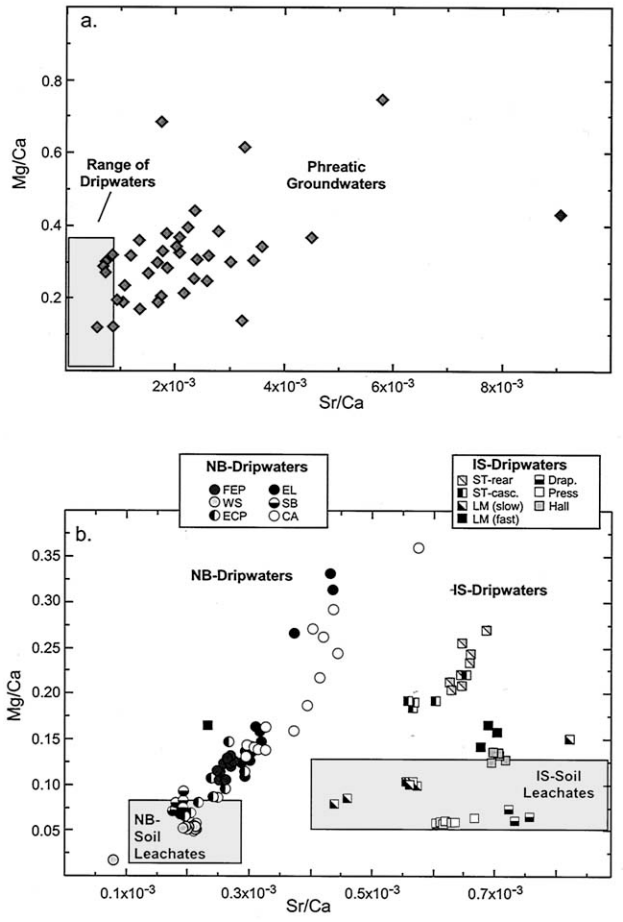

Fig. 4. Mg/Ca vs. Sr/Ca ratios for Edwards aquifer system components: (a) phreatic groundwaters (diamonds), and (b) dripwaters and soil leachates from Natural Bridge Caverns (NB) and Inner Space Cavern (IS). Note scale differences between (a) and (b). Shaded box in (a) marks area expanded in (b). Shaded boxes in (b) denote the range of Mg/Ca and Sr/Ca in soil leachates from the two caves. Soil leachates represent exchangeable Sr in soils near cave recharge zones. Symbols for NB (circles) and IS (squares) represent different dripwater sites within the caves (shown in Fig. 2), which were sampled periodically over the course of the study. Regional phreatic groundwaters (a) exhibit a similar trend as the dripwaters of increasing Mg/Ca with increasing Sr/Ca, but range to markedly higher values. Phreatic groundwater data from Oetting (1995), Gandara and Barbie (1998), and Musgrove (2000).

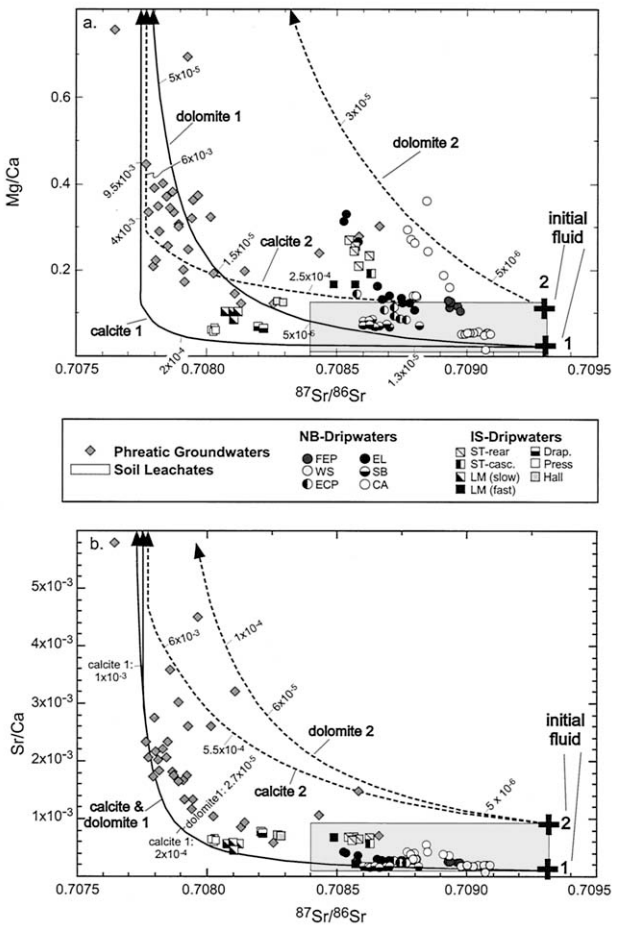

Fig. 5. $87Sr/^{86}Sr$ vs. Mg/Ca (a) and Sr/Ca (b) ratios and carbonate mineral recrystallization models for regional phreatic groundwaters (triangles), and dripwaters and soil leachates from Natural Bridge Caverns (NB) and Inner Space Cavern (IS). Symbols for NB (circles) and IS (squares) represent different dripwater sites within the caves (shown in Fig. 2), which were sampled periodically over the course of the study. Shaded box in (a) and (b) represents range of values for exchangeable components of soils (combined NB and IS soils range). Average $^{87}Sr/^{86}Sr$ value for regional Cretaceous carbonate rocks = 0.7077 (Koepnick et al., 1985, and Oetting, 1995; n = 20). Phreatic groundwater data from Oetting (1995), Gandara and Barbie (1998), and Musgrove (2000). Model curves illustrate the evolution of $^{87}Sr/^{86}Sr$ and Mg/Ca (a), and $^{87}Sr/^{86}Sr$ and Sr/Ca (b) for a fluid that progressively recrystallizes either calcite or dolomite. Model curves labeled "calcite 1" and "dolomite 1" represent evolving composition of initial fluid 1 as it recrystallizes calcite or dolomite; model curves labeled "calcite 2" and "dolomite 2" represent evolving composition of initial fluid 2. Initial fluid compositions are based on range of values measured for soil leachates. Model calculations follow Banner et al. (1989) and Banner and Hanson (1990). Fluid 1 composition: Mg = 2 ppm, Sr = 0.04 ppm, Ca = 180 ppm, Mg/Ca = 0.02, Sr/Ca = 0.0001, $^{87}Sr/^{86}Sr$ = 0.7093. Fluid 2 composition: Mg = 10 ppm, Sr = 0.3 ppm, Ca = 150 ppm, Mg/Ca = 0.1, Sr/Ca = 0.0009, $^{87}Sr/^{86}Sr$ = 0.7093. Element ratios are molar concentrations. Initial composition of calcite (Sr = 250 ppm, Mg = 3000 ppm, $^{87}Sr/^{86}Sr$ = 0.7077) and stoichiometric dolomite (Sr = 1000 ppm, $^{87}Sr/^{86}Sr$ = 0.7077) is based on diagenetic studies and analyses of Edwards Group limestones (Fisher and Rodda, 1969; Rose, 1972; Petta, 1977; Ellis, 1985). Fluid-rock ratios (N = molar rock/water ratio) are given along the curves. Arrows indicate direction of increasing N values.

tion coefficients (K_D), porosity, and the composition of the interacting fluid and rock (Banner et al., 1989; Banner and Hanson, 1990). In this model a fluid (with an initial composition of that measured for the soil leachates) infiltrates into a limestone aquifer (with a constant composition and characteristics approximating central Texas carbonates). The fluid repeatedly dissolves and reprecipitates calcite or dolomite. An iterative calculation is used to simulate isotopic and trace-element exchange. Modeling results for the ongoing geochemical evolution ($^{87}Sr/^{86}Sr$, Mg/Ca and Sr/Ca) of two representative soil waters (with compositions similar to leachates from NB) that progressively recrystallize calcite or dolomite are shown in Figure 5. These results encompass the vadose and phreatic groundwater data, and demonstrate a clear progression

toward lower $^{87}Sr/^{86}Sr$ values and higher Mg/Ca and Sr/Ca ratios with increasing water-rock interaction. This progression is evident regionally, as well as at individual drip sites. Higher rock/water ratios, and therefore greater extents of water-rock interaction, are required to account for phreatic groundwater data (Fig. 5). This would be expected based on the longer residence and greater water-rock interaction potential of phreatic groundwaters relative to dripwaters. Dissolution of calcite and dolomite may also play a role in controlling water compositions. Dissolution reactions alone, however, cannot account for the range or pathway of data observed. For example, dissolution pathways in Sr/Ca vs. $^{87}Sr/^{86}Sr$ space would result in relatively flat horizontal trends from the initial fluid composition toward lower $^{87}Sr/^{86}Sr$ values.

It should be noted that for a given fluid and host rock composition (i.e., Mg, Sr, and Ca concentrations, and $^{87}Sr/^{86}Sr$ values) variations in the K_D value used in the model (for typical values < 1) will not affect the shape of the water-rock interaction pathway shown in Figure 5 (Banner, 1995). The relative rock/water ratio along the pathway, however, will vary in response to K_D values. Thus, although the absolute values of the rock/water ratios may not be quantitatively pertinent, the model approach allows us to evaluate the diagnostic trends of fluid evolution. Experimental determinations of $K_D^{Mg\text{-}Ca}$ have shown a temperature dependence wherein K_D values, and correspondingly, Mg concentrations, increase with increasing temperature (Katz, 1973; Oomori et al., 1987; Mucci and Morse, 1990). While temperature may be a possible consideration for Mg/Ca changes in speleothems precipitated over thousands of years (e.g., the last glacial period in central Texas is proposed to have been on the order of 2 to 6°C cooler; Stute et al., 1992; Toomey et al., 1993), a more likely control is hydrologic variability (that is, variations in the chemical composition of the fluid precipitating the speleothems). Dripwater sites are within cave interiors where temperatures are relatively stable year-round. Thus, temperature variations at dripwater sites cannot account for Mg/Ca variations exhibited by the dripwaters in the modern aquifer system. Although little temperature dependence has been demonstrated for $K_D^{Sr\text{-}Ca}$, temperature may play a role in calcite precipitation rates and, thus, indirectly affect Sr partitioning into speleothem calcite (Katz et al., 1972; Baker et al., 1982; Banner, 1995). Experimental studies have demonstrated that mineral precipitation rates may have an important control on K_D values (Lorens, 1981; Banner, 1995).

In a discussion of controlling processes on dripwater geochemistry at two geographically separate European caves, Fairchild et al. (2000) call upon several potential factors that may contribute to elevated and covarying Mg/Ca and Sr/Ca ratios: (1) incongruent dolomite dissolution, (2) the initial faster dissolution of calcite over dolomite, which may lead to elevated Mg/Ca during drier conditions (i.e., increasing proportion of dolomite dissolution associated with longer residence times); and (3) the precipitation of calcite by vadose waters along a flow path, which will concentrate Mg and Sr in the fluid relative to Ca. Studies of Mg/Ca and Sr/Ca variations in speleothem calcite also support the importance of residence time in controlling vadose water geochemistry (Roberts et al., 1998; Musgrove, 2000). Precipitation of calcite along flow-routes within the Edwards aquifer has been called upon by previous workers investigating phreatic groundwaters and discharging springwaters of the Edwards aquifer (Ogden and Collar, 1990).

The geochemistry of central Texas dripwaters suggests that multiple controls contribute to spatial geochemical variability; regionally, locally, and at individual dripwater sites. Mass-balance modeling and correlations between $^{87}Sr/^{86}Sr$, Mg/Ca, and Sr/Ca suggest that water-rock interaction with overlying soils and host limestones governs a regionally extensive fluid evolution pathway from soil waters, to vadose dripwaters, to phreatic groundwaters. Within this regionally extensive system, however, local variability in the soil composition accounts for the starting point of the evolution pathway. Although some component of fluid evolution occurs in the soil zone, the dripwater and groundwater data require subsequent modification by water-rock interaction with host limestones.

4.4. Temporal Variations in Dripwater Geochemistry

Regional monitoring of total dissolved solids concentrations in recharge and fresh groundwater wells in the Edwards aquifer indicates that small annual fluctuations may occur (Bader et al., 1993). These fluctuations are proposed to result from the response of the aquifer system to above- or below-average recharge conditions (Bader et al., 1993). Saturation states in spring discharge for central Texas springs also appear to change in response to aquifer recharge events (Ogden and Collar, 1990). For a suite of dripwaters collected from a central Texas cave (Cave Without a Name) over a 28-month period, Veni (1997) recognized seasonal geochemical variability, which may result from recharge variations. These studies collectively suggest that processes controlling spatial variations in dripwater geochemistry, such as water-rock interaction and evaporation, may also operate temporally to affect dripwater geochemistry. That is to say, if variations in these processes contribute to differences in dripwater geochemistry across the region, then changes in these process at a single site over time will also affect dripwater geochemistry. Such temporal changes may result from climatic and hydrologic variables (e.g., rainfall, recharge) that may affect the extent of these processes.

Dripwaters at NB that were sampled multiple times over a 4-yr period exhibit different amounts of variability in geochemical parameters such as $^{87}Sr/^{86}Sr$ values and Mg/Ca ratios. While some dripwater localities exhibit little geochemical variation, others change markedly (Fig. 6). For the latter group, changes in dripwater $^{87}Sr/^{86}Sr$ values and Mg/Ca ratios, which inversely correlate, appear to also correlate with variations in rainfall, effective moisture, and spring discharge at Comal Springs over the same time period (Fig. 7). Comal Springs is one of the major regional discharge points for the Edwards aquifer. Based on the short response time of the aquifer to precipitation variations, Comal Springs discharge is broadly indicative of the regional state of the aquifer. Most notably, a large drop in springflow occurred during the summer of 1996 in response to a regional drought. The temporal record of vadose dripwater geochemistry shows a corresponding decrease in $^{87}Sr/^{86}Sr$ values and increase in Mg/Ca ratios (Fig. 7) with the 1996 drop in springflow. The dripwater variations observed in $^{87}Sr/^{86}Sr$ values and Mg/Ca ratios at this time are in the direction that would be predicted (i.e., lower $^{87}Sr/^{86}Sr$ higher Mg/Ca) based on the potential increase in residence time and

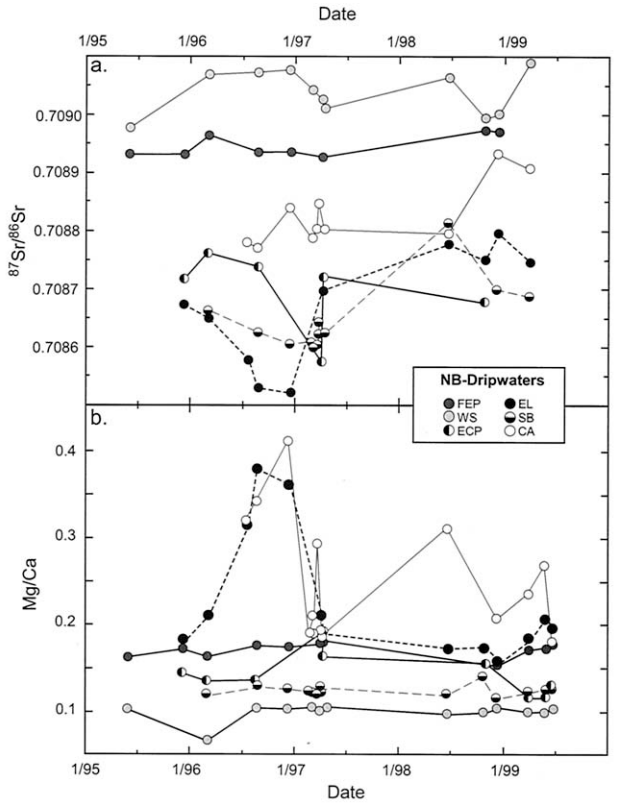

Fig. 6. Temporal variations in $^{87}Sr/^{86}Sr$ values (a) and Mg/Ca ratios (b) for vadose cave dripwaters sampled from Natural Bridge Caverns between 1995 and 1999. Locations indicated by sample abbreviations are shown in Fig. 2.

water-rock interaction accompanying drier conditions. Effective moisture trends for the period of 1995 to 2000 are similar to rainfall trends for this period, but also incorporate other factors (such as temperature and evapotranspiration) that may affect drip rates and the transport of water in the vadose zone.

Changes in dripwater geochemistry at some sites seem to lag temporally behind changes in rainfall, effective moisture, and spring discharge (Fig. 7). This lag time is not synchronous for different dripwater sites and may reflect residence time of dripwaters for different flow-routes in the vadose zone and different responses to antecedent conditions. This discussion focuses on samples from NB, because the temporal record for dripwaters sampled from IS is shorter. However, similar to the dripwaters from NB, only some of the sites sampled at IS exhibit temporal variability in $^{87}Sr/^{86}Sr$ values and Mg/Ca ratios. Nonetheless, the timing and direction of geochemical variability in IS dripwater geochemistry is similar to that observed for dripwater sites at NB (Musgrove, 2000). Although this discussion focuses on Mg/Ca ratios, data for Sr/Ca ratios exhibits similar temporal trends.

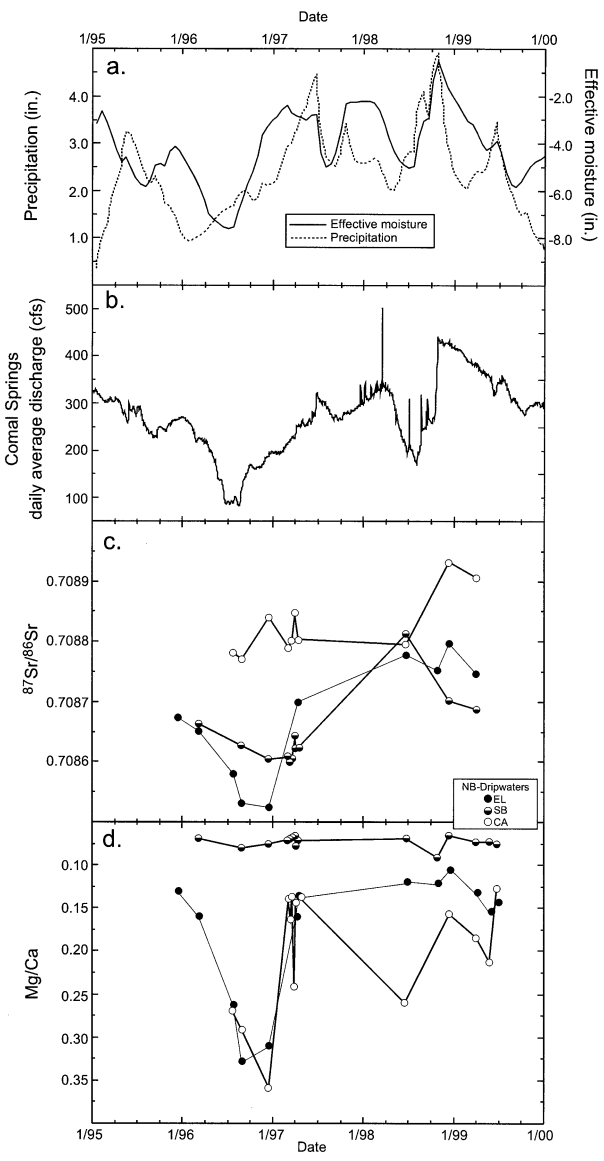

Fig. 7. Temporal variability between 1995 and 1999 in (a) central Texas precipitation and effective moisture, (b) springflow at Comal Springs, which is broadly representative of regional aquifer conditions (c) $^{87}Sr/^{86}Sr$ values for NB dripwaters, and (d) Mg/Ca ratios for NB dripwaters. Note inverted scale for Mg/Ca in (d). Effective moisture is the difference between monthly precipitation and evaporation data. Rainfall and evaporation data from the National Climatic Data Center (http://www.ncdc.noaa.gov) archive for San Antonio, TX—Seaworld (National Weather Service Cooperative Station Network—COOP ID # 418169). Note that effective moisture values are negative. This may reflect pan evaporation values that do not represent actual ground evapotranspiration values. In spite of the negative values, during a 5-yr observation period (1995–2000), drips in caves in the region remained active to varying degrees. Curves for rainfall and effective moisture are smoothed. Historical records for Comal Springs daily average discharge (cfs = cubic feet/s) from U. S. Geological Survey archives (station number #08168710; http://txwww.cr.usgs.gov/).

4.5. Mechanism for Spatial and Temporal Dripwater Geochemical Variations

Carbonate aquifers can be characterized as a mix of different permeability networks along a continuum from low-permeability diffuse flow pathways to high-permeability conduit flow pathways (Atkinson, 1977). Migration of fluid dominantly along high-permeability conduit pathways will limit both the residence time and reactivity (due to lower mineral-surface/

fluid-volume ratios) of that fluid with the limestone. Quantitative tracer studies in the Mendip Hills karst terrain of Great Britain support a model involving changes in the routes of vadose groundwater movement as a function of rainfall and resultant aquifer recharge (Smart and Friederich, 1987). In this model, groundwater migration is predominantly along low-permeability, diffuse flow-routes during periods of low rainfall and correspondingly, low recharge. As rainfall and recharge increase, the capacity of low-permeability diffuse flow-routes is exceeded and groundwater migration along pathways of high-permeability conduit flow-routes increases. Thus, during periods of high rainfall-recharge, the increase in high-permeability conduit flow will result in less interaction between vadose groundwaters and host limestones. Consequently, fluid $^{87}Sr/^{86}Sr$ values will reflect a soil signature (i.e., for the Edwards aquifer, high $^{87}Sr/^{86}Sr$) and Mg/Ca ratios will be low due to shorter residence times. Conversely, during periods of low rainfall-recharge both residence time and interaction between the groundwaters and host limestones will increase. As a result, $^{87}Sr/^{86}Sr$ values will shift toward limestone values (i.e., low $^{87}Sr/^{86}Sr$) and Mg/Ca ratios will increase as a result of increased residence time.

This rainfall/flow-route model has been applied to the karst groundwater system of Barbados in conjunction with Sr isotopes to demonstrate a climatic (i.e., rainfall-recharge) control on the temporal fluctuations between contrasting soil and limestone contributions to groundwater (Banner et al., 1996). Similar to the central Texas Edwards aquifer system, the soils and limestones in the Barbados Pleistocene aquifer exhibit contrasting Sr isotope signatures (Banner et al., 1994, 1996; Borg and Banner, 1996). The similarities in the behavior of Sr isotopes in response to changes in rainfall-recharge in both of these aquifer systems indicate that the application of this model may be valid in other karst aquifer systems. However, geochemical characterization of different aquifer components is necessary. For example, although Sr isotopes variations in both aquifer systems are controlled by fluxes from different reservoirs (e.g., soils vs. limestones) the age and purity of the limestones and the parent materials of the soils result in isotopically-distinct and aquifer-specific relationships. Central Texas limestones are less radiogenic than the overlying soils, whereas Barbados Pleistocene limestones are more radiogenic than overlying Barbados soils. Central Texas limestones and, correspondingly, groundwaters, exhibit a larger range of variation in $^{87}Sr/^{86}Sr$ values than Barbados limestones and groundwaters (Banner et al., 1994, 1996). In some groundwater systems other constituents in addition to soils and host carbonates, such as sea salts and dust, may contribute an important component of Sr and affect $^{87}Sr/^{86}Sr$ values (Bar-Matthews et al., 1999). Geochemical reservoirs or components that may influence fluid geochemistry must be delineated for specific aquifer systems.

As noted earlier, temporal variability in geochemical parameters is not observed at all locations (Fig. 6). This is consistent with dripwaters at these sites having a relatively long residence time. A study of the timing of vadose transport based on dripwater tritium ages and geochemistry in an arid karst system in Israel indicates that waters may be held in the vadose zone for long periods of time (e.g., decades; Ayalon et al., 1998). Tritium variations in Edwards aquifer groundwaters are consistent with residence times of 30 yr or less near the aquifer's recharge zone (Pearson et al., 1975). Mean phreatic groundwater ages in the Edwards aquifer have been estimated to range from 16 to $>$ 130 yr based on a mixing-cell model and tritium analyses of rainwaters and groundwaters (Campana and Mahin, 1985). The behavior of cave dripwater sites with respect to both discharge and geochemistry is a reflection of the permeability network(s) contributing to that flow. An examination of cave inlets from the Mendip Hills indicates that dripwaters span a broad continuum from diffuse flow seepage, characterized by low flow volume of little variation, to conduit or shaft flow with a maximum higher flow volume but greater variability (Smart and Friederich, 1987). Based on these observations, central Texas dripwaters that exhibit little to no geochemical variability (Fig. 6) likely reflect cave inlets that are dominated by diffuse flow over the 4-yr study period. Similarly, the marked geochemical variability measured in some of the dripwaters may reflect a mixture of diffuse and conduit flow-routes that are responding to changes in flow-routing over the study period.

Dripwater geochemistry over the period of this study does not consistently vary with drip rate. Drip rates have been demonstrated to both increase and decrease non-linearly with increased precipitation and recharge, and both drip rate and dripwater chemistry are influenced by antecedent hydrologic conditions (Baker et al., 1997; Doctor and Alexander, 1998). We note that higher frequency sampling of dripwater sites, a focus of ongoing research in central Texas caves, may reveal more detailed information and/or important features of dripsite hydrology and geochemistry. The results of this study suggest that temporal variability in dripwater geochemistry may have multiple scales of variation. Discharge rates are influenced by many parameters including precipitation, evaporation, temperature, soil moisture, vadose storage, flow-routing, and limestone characteristics (Friederich and Smart, 1982; Smart and Friederich, 1987). The ultimate mix of these parameters affects recharge, and subsequently, the extent of processes such as water-rock interaction and residence time. Thus, dripwater sites that exhibit little to no geochemical variability over the study period may respond over longer periods of time and/or in response to more severe fluctuations in both the hydrologic system and climate. An understanding of these processes over seasonal, annual, and decadal timescales provides insight into the paleogroundwater system.

5. SUMMARY

Geochemical and isotopic variations in vadose groundwaters of the Edwards aquifer reflect interaction with overlying soils and host carbonate aquifer rocks along different geochemical evolution pathways. Small-scale spatial variability in soils, vadose flow-routes, recharge characteristics, and aquifer rocks contribute to geochemical differences between dripwaters from different sites within a single cave. On a larger scale these factors contribute to the geochemical disparity in dripwaters between different caves. Soil compositions exert a fundamental control on the starting point of fluid-rock evolution pathways. Despite the wide range of geochemical values for soils, limestones, and dripwaters both at the small-scale and aquifer-scale, geochemical and isotopic variations in $^{87}Sr/^{86}Sr$, Mg/Ca, and Sr/Ca suggest that controlling processes on fluid evolution are regionally extensive. Water-rock interaction modeling indi-

cates that shifts to lower $^{87}Sr/^{86}Sr$ values and higher Mg/Ca and Sr/Ca values are enhanced during periods of increased residence time, such as those associated with drier climatic periods. Changes in vadose flow-routes as a function of rainfall-recharge is a mechanism by which these parameters in groundwater geochemistry may vary temporally by receiving varying fluxes of dissolved constituents from geochemically distinct sources (i.e., soils vs. host limestones), changes in residence time, and different water-rock interaction pathways. High frequency sampling of dripwaters and continuous monitoring of drip rates will provide more detailed information regarding these processes in karst systems.

Acknowledgments—We thank the management and owners of Inner Space Cavern and Natural Bridge Caverns, especially Brian Vauter and George Norsworthy, for cave access and generous logistical and sampling assistance. We are grateful to F. Leo Lynch for performing X-ray diffraction analyses and to the numerous colleagues who helped with sampling. We thank Larry Mack for contributing analytical expertise. Lynne Fahlquist of the U.S.G.S. provided phreatic groundwater samples for Sr isotope analyses, groundwater elemental data, and helpful discussions. The manuscript benefited from the constructive comments and suggestions of several anonymous reviews. This research was supported by the Department of Energy (DE-FG03-97ER14812), the Environmental Protection Agency (915135-01), the National Science Foundation (EAR-9526714), the Cave Conservancy Foundation, and the Geology Foundation of the University of Texas at Austin.

Associate editor: L. M. Walter

REFERENCES

Atkinson T. C. (1977) Diffuse and conduit flow in limestone terrain in the Mendip Hills, Somerset (Great Britain). *J. Hydrol.* **35,** 93–110.

Ayalon A., Bar-Matthews M., and Sass E. (1998) Rainfall-recharge relationships within a karstic terrain in the Eastern Mediterranean semi-arid region, Israel: $\delta^{18}O$ and δD characteristics. *J. Hydrol.* **207,** 18–31.

Bader R. W., Walthour S. D. and Waugh J. R. (1993) *Edwards Aquifer Hydrogeologic Status Report for 1992*. Edwards Underground Water District.

Baker P. A., Gieskes J. M., and Elderfield H. (1982) Diagenesis of carbonates in deep-sea sediments—Evidence from Sr/Ca ratios and interstitial dissolved Sr^{2+} data. *J. Sed. Petrology.* **52,** 71–82.

Baker A., Barnes W. L., and Smart P. L. (1997) Variations in the discharge and organic matter content of stalagmite drip waters in Lower Cave, Bristol. *Hydrol. Proc.* **11,** 1541–1555.

Banner J. L. (1995) Application of the trace element and isotope geochemistry of strontium to studies of carbonate diagenesis. *Sedimentology* **42,** 805–824.

Banner J. L. and Hanson G. H. (1990) Calculation of simultaneous isotopic and trace-element variations during water-rock interactions with applications to carbonate diagenesis. *Geochim. Cosmochim. Acta* **54,** 3123–3137.

Banner J. L., Wasserburg G. J., Dobson P. F., Carpenter A. B., and Moore C. H. (1989) Isotopic and trace-element constraints on the origin and evolution of saline groundwaters from central Missouri. *Geochim. Cosmochim. Acta* **53,** 383–398.

Banner J. L., Musgrove M., and Capo R. C. (1994) Tracing groundwater evolution in a limestone aquifer using Sr isotopes: Effects of multiple sources of dissolved ions and mineral-solution reactions. *Geology* **22,** 687–690.

Banner J. L., Musgrove M., Asmeron Y., Edwards R. L., and Hoff J. A. (1996) High-resolution temporal record of Holocene ground-water chemistry: Tracing links between climate and hydrology. *Geology* **24,** 1049–1053.

Bar-Matthews M., Ayalon, A., Kaufman A., and Wasserburg G. J. (1999) The Eastern Mediterranean paleoclimate as a reflection of regional events: Soreq cave, Israel. *Earth Planet. Sci. Lett.* **166,** 85–95.

Barron E. J., Hay W. W., and Thompson S. (1989) The hydrologic cycle: A major variable during earth history. *Palaeogeogr. Palaeoclim. Palaeoecol.* **75,** 157–174.

Blum J. D. and Erel Y. (1995) A silicate weathering mechanism linking increases in marine $^{87}Sr/^{86}Sr$ with global glaciation. *Nature* **373,** 415–418.

Borg L. E. and Banner J. L. (1996) Nd and Sr isotopic constraints on weathering processes and soil sources in Barbados, West Indies. *Geochim. Cosmochim. Acta* **60,** 4193–4206.

Brown D. S., Petri B. L. and Nalley G. M. (1992) Compilation of hydrologic data for the Edwards Aquifer, San Antonio area, Texas, 1991, with 1934-91 summary. *Edwards Underground Water District Bulletin* **51**.

Burchett C. R., Rettman P. L. and Boning C. W. (1986) *The Edwards Aquifer—Extremely Productive, But. . .A Sole-Source Water Supply for San Antonio and Surrounding Counties in South-Central Texas*. U. S. Geological Survey and Edwards Underground Water District, San Antonio, TX.

Campana M. E. and Mahin D. A. (1985) Model-derived estimates of groundwater mean ages, recharge rates, effective porosities and storage in a limestone aquifer. *J. Hydrol.* **76,** 247–264.

Capo R. C. and DePaolo D. J. (1990) Seawater strontium isotopic variations from 2.5 million years ago to the present. *Science* **249,** 51–55.

Clement T. J. (1989) *Hydrochemical Facies of the Badwater Zone of the Edwards Aquifer, Central Texas*. M.A. thesis, University of Texas at Austin.

Clement T. J. and Sharp J. M., Jr. (1988) Hydrogeochemical facies in the bad-water zone of the Edwards aquifer, Central Texas. In *Proceedings of the Ground Water Geochemistry Conference*, pp. 127–149. National Water Well Association, Dublin, OH.

Cowell D. W. and Ford D. C. (1980) Hydrochemistry of a dolomite karst: The Bruce Peninsula of Ontario. *Can. J. Earth Sci.* **17,** 520–526.

Doctor D. H. and Alexander E. C., Jr. (1998) Discharge, chemistry and stable isotope measurements of drip waters in Mystery Cave, Minn.: Records of hydrologic processes in the vadose zone. *SEPM Research Conference, Fluid Flow in Carbonates: Interdisciplinary Approaches*, September 20-24, 1998, Door County, Wisconsin, Program with Abstracts.

Dorale J. A., Gonzalez L. A., Reagan M. K., Pickett D. A., Murrell M. T., and Baker R. G. (1992) A high-resolution record of Holocene climate change in speleothem calcite from Cold Water Cave, northeast Iowa. *Science* **258,** 1626–1630.

Elliott W. R. and Veni G. (1994) *The Caves and Karst of Texas—1994 NSS Convention Guidebook*. National Speleological Society, Huntsville, AL.

Ellis P. M. (1985) *Diagenesis of the Lower Cretaceous Edwards Group in the Balcones Fault Zone Area, South-Central Texas*. Ph.D. dissertation, University of Texas at Austin.

Fairchild I. J. and Killawee J. A. (1995) Selective leaching in glacierized terrains and implications for retention of primary chemical signals in carbonate rocks. In *Water-Rock Interaction—Proceedings of the 8th International Symposium on Water-Rock Interaction, WRI-8* (eds. Y. K. Kharaka and O. V. Chudaev), pp. 79–82. A. A. Balkema, Rotterdam, the Netherlands.

Fairchild I. J., Tooth A. F., Huang Y., Borsato A., Frisia S., and McDermott F. (1996) Spatial and temporal variations in water and stalactite chemistry in currently active caves: A precursor to interpretations of past climate. In *Proceedings of the Fourth International Symposium on the Geochemistry of the Earth's Surface* (ed. S. H. Bottrell), pp. 229–233. University of Leeds, Ilkley, England.

Fairchild I. J., Borsato A., Tooth A. F., Frisia S., Hawkesworth C. J., Huang H., McDermott F., and Spiro B. (2000) Controls on trace element (Sr-Mg) compositions of carbonate cave waters: Implications for speleothem climatic records. *Chem. Geol.* **166,** 255–269.

Fisher W. L. and Rodda P. U. (1969) Edwards Formation (Lower Cretaceous), Texas: Dolomitization in a carbonate platform system. *Am. Assoc. Petrol. Geol. Bull.* **53,** 55–72.

Friederich H. and Smart P. L. (1982) The classification of autogenic percolation waters in karst aquifers; a study in G.B. Cave, Mendip Hills, England. *Proceedings–Univ. of Bristol Spelaeological Soc.* **16,** pp. 143–159.

Gandara S. C. and Barbie D. L. (1998) U.S. Geological Survey Ann. Data Report: Water Data Report TX-98-4: Water Resources Data, Texas, Water Year 1998 **4,** Groundwater.

Gascoyne M. (1992) Palaeoclimate determination from cave calcite deposits. *Quat. Sci. Rev.* **11,** 609–632.

Godfrey C. L., McKee G. S., and Oakes H (1973) *General Soil Map of Texas*. Texas Agricultural Experimental Station, Texas A & M University, in cooperation with the Soil Conservation Service, U. S. Department of Agriculture.

Griffiths J. F. and Strauss R. F. (1985) The variety of Texas weather. *Weatherwise* **38,** 137–141.

Harmon R. S. (1970) The chemical evolution of cave waters, Inner Space Cavern, Texas. *Caves Karst* **12,** 1–8.

Harmon R. S., Thompson P., Schwarcz H. P., and Ford D. C. (1978) Late Pleistocene climates of North America as inferred from stable isotope studies of speleothems. *Quat. Res.* **9,** 54–70.

Jones B. D. (1991) Texas; floods and droughts. In *National Water Summary 1988-89, Hydrologic Events and Floods and Droughts*, U. S. Geological Survey Water-Supply Paper 2375 (comps. R. W. Paulson, E. B. Chase, R. S. Roberts and D. W. Moody), pp. 513–520.

Kastning E. H., Jr. (1983) *Geomorphology and Hydrogeology of the Edwards Plateau Karst, Central Texas, Vols. 1 and 2*. Ph.D. dissertation, University of Texas at Austin.

Katz A. (1973) The interaction of magnesium with calcite during crystal growth at 25-95° C and one atmosphere. *Geochim. Cosmochim. Acta* **37,** 1563–1568.

Katz A., Sass E., Starinsky A., and Holland H. D. (1972) Strontium behavior in the aragonite-calcite transformation: An experimental study at 40-98° C. *Geochim. Cosmochim. Acta* **36,** 481–496.

Koepnick R. B., Burke W. H., Denison R. E., Hetherington E. A., Nelson H. F., Otto J. B., and Waite L. E. (1985) Construction of the seawater $^{87}Sr/^{86}Sr$ curve for the Cenozoic and Cretaceous: Supporting data. *Chem. Geol.* **58,** 55–81.

Langmuir D. (1971) The geochemistry of some carbonate ground waters in central Pennsylvania. *Geochim. Cosmochim. Acta* **35,** 1023–1045.

Larkin T. J. and Bomar G. W. (1983) *Climatic Atlas of Texas*. Texas Department of Water Resources, Austin.

Lohmann K. C. (1988) Geochemical patterns of meteoric diagenetic systems and their application to studies of paleokarst. In *Paleokarst* (eds. J. P. James and P. W. Choquette), pp. 58–80. Springer-Verlag, New York.

Lorens R. N. (1981) Sr, Cd, Mn, and Co distribution coefficients in calcite as a function of calcite precipitation rate. *Geochim. Cosmochim. Acta* **45,** 553–561.

Lynch F. L. (1997) Frio shale mineralogy and the stoichiometry of the smectite-to-illite reaction: The most important reaction in clastic sedimentary diagenesis. *Clays Clay Miner.* **45,** 618–631.

Maclay R. W. (1989) Edwards Aquifer in the San Antonio region: Its hydrogeology and management. *Bull. South Texas Geol. Soc.* **30,** 11–28.

Maclay R. W. (1995) *Geology and Hydrology of the Edwards Aquifer in the San Antonio Area, Texas*. U. S. Geological Survey Water-Resources Investigations Report 95-4186.

Maclay R. W. and Small T. A. (1983) Hydrostratigraphic subdivisions and fault barriers of the Edwards aquifer, south-central Texas, U.S.A. *J. Hydrol.* **61,** 127–146.

McMahan C. A., Frye R. G., and Brown K. L. (1984) *The Vegetation Types of Texas Including Cropland*. Texas Parks and Wildlife Department, Wildlife Division, Austin.

Miller E. K., Blum J. D., and Friedland A. J. (1993) Determination of soil exchangeable-cation loss and weathering rates using Sr isotopes. *Nature* **362,** 438–441.

Mucci A. and Morse J. W. (1990) Chemistry of low-temperature abiotic calcites: Experimental studies on coprecipitation, stability, and fractionation. *Rev. Aquat. Sci.* **3,** 217–254.

Musgrove M. (2000). *Temporal Links Between Climate and Hydrology: Insights From Central Texas Cave Deposits and Groundwater*. Ph.D. dissertation, University of Texas at Austin.

Musgrove M., Banner J. L., Mack L. E., Combs D. M., James E. W., Cheng H., and Edwards R. L. (2001) Geochronology of late Pleistocene and Holocene speleothems from central Texas: Implications for regional paleoclimate. *Geol. Soc. Am. Bull.* **113,** 1532–1543.

Oetting G. C. (1995) *Evolution of Fresh and Saline Groundwaters in the Edwards Aquifer: Geochemical and Sr Isotopic Evidence for Regional Fluid Mixing and Fluid-Rock Interaction*. M.A. thesis, University of Texas at Austin.

Oetting G. C., Banner J. L., and Sharp J. M., Jr. (1996) Geochemical evolution of saline groundwaters in the Edwards aquifer, central Texas: Regional stratigraphic, tectonic, and hydrodynamic controls. *J. Hydrol.* **181,** 251–283.

Ogden A. E. and Collar P. D. (1990) Interpreting calcite, dolomite, and gypsum saturation conditions in the Edwards aquifer, Texas. In *Selected Papers on Hydrogeology from the 28th International Geologic Congress, Vol. 1* (eds. E. S. Simpson and J. M. Sharp, Jr.), pp. 83–96. International Association of Hydrogeologists, Heise, Hannover, Germany.

Oomori T., Kaneshima H., Maezato Y., and Kitano Y. (1987) Distribution coefficient of Mg2+ ions between calcite and solution at 10-50 degrees C. *Mar. Chem.* **20,** 327–336.

Pearson F. J., Jr., Rettman P. L. and Wyerman T. A. (1975) *Environmental Tritium in the Edwards Aquifer, Central Texas, 1963-1971*. U. S. Geological Survey Open File Report 74-362.

Perry K. D., Cahill T. A., Eldred R. A., Dutcher D. D., and Gill T. E. (1997) Long-range transport of North African dust to the eastern United States. *J. Geophys. Res.* **102D,** 11225–11238.

Petta T. J. (1977) Diagenesis and geochemistry of a Glen Rose patch reef complex, Bandera County, Texas. In *Cretaceous Carbonates of Texas & Mexico: Applications to Subsurface Exploration* (eds. D. G. Bebout and R. G. Loucks), pp. 138–167. *Univ. of Texas at Austin, Bureau of Economic Geology, Report of Investigations* **89**.

Plummer L. N. (1977) Defining reactions and mass transfer in part of the Floridan Aquifer. *Water Resour. Res.* **13,** 801–812.

Rabenhorst M. C., Wilding L. P., and Girdner C. L. (1984) Airborne dusts in the Edwards Plateau region of Texas. *Soil Sci. Soc. Am. J.* **48,** 621–627.

Riskind D. H. and Diamond D. D. (1986) Plant communities of the Edwards Plateau of Texas: An overview emphasizing the Balcones Escarpment zone between San Antonio and Austin with special attention to landscape contrasts and natural diversity. In *The Balcones Escarpment—Geology, Hydrology, Ecology and Social Development in Central Texas* (eds. P. L. Abbott and C. M. Woodruff, Jr.), pp. 21–32. Geological Society of America.

Roberts M. S., Smart P. L., and Baker A. (1998) Annual trace element variations in a Holocene speleothem. *Earth Planet. Sci. Lett.* **154,** 237–246.

Rodda P. U., Fisher W. L., Payne W. R. and Schofield D. A. (1966) Limestone and dolomite resources, Lower Cretaceous rocks, Texas. *Univ. of Texas at Austin, Bureau of Economic Geology, Report of Investigations* **56**.

Rose P. R. (1972) Edwards Group, surface and subsurface, central Texas. *University of Texas at Austin, Bureau of Economic Geology, Report of Investigations* **74**.

Sharp J. M., Jr. (1990) Stratigraphic, geomorphic and structural controls of the Edwards aquifer, Texas, U. S. A.. In *Selected Papers on Hydrogeology from the 28th International Geologic Congress, Vol. 1* (eds. E. S. Simpson and J. M. Sharp, Jr.), pp. 67–82. International Association of Hydrogeologists, Heise, Hannover, Germany.

Sharp J. M., Jr. and Banner J. L. (1997) The Edwards aquifer: A resource in conflict. *GSA Today* **7,** 1–9.

Smart P. L. and Friederich H. (1987) Water movement and storage in the unsaturated zone of a maturely karstified aquifer, Mendip Hills, England. In *Proceedings of the Environmental Problems in Karst Terrains and Their Solutions Conference*, pp. 57–87. NWWA, Bowling Green, KY.

Stute M., Schlosser P., Clark J. F., and Broecker W. S. (1992) Paleotemperatures in the southwestern United States derived from noble gases in groundwater. *Science* **256,** 1000–1003.

Suarez D. L. (1996) Beryllium, magnesium, calcium, strontium and barium. In *Methods of Soil Analysis, Part 3: Chemical Methods—SSSA Book Series No. 5*, Soil Science Society of America and American Society of Agronomy.

Toomey R. S., III, Blum M. D., and Smart P. L. (1993) Late Quaternary climates and environments of the Edwards Plateau, Texas. *Global Planet. Change* **7,** 299–320.

Tooth A. F. and Fairchild I. J. (2003) Soil and karst aquifer hydrological controls on the geochemical evolution of speleothem-forming drip waters, Crag Cave, southwest Ireland. *J. Hydrol.* **273,** 51–68.

Trudgill S. T., Laidlaw I. M. S., and Smart P. L. (1980) Soil water residence times and solute uptake on a dolomite bedrock—Preliminary results. *Earth Surf. Proc.* **5,** 91–100.

Trudgill S. T., Pickles A. M., Smettem K. R. J., and Crabtree R. W. (1983) Soil-water residence time and solute uptake. 1. Dye tracing and rainfall events. *J. Hydrol.* **60,** 257–279.

Veni G (1997) Geomorphology, hydrogeology, geochemistry and evolution of the karstic lower Glen Rose Aquifer, south-central Texas. *Texas Speleological Survey Monographs* **1**.

Wigley M. L. (1973) The incongruent solution of dolomite. *Geochim. Cosmochim. Acta* **37,** 1397–1402.

Winograd I. J., Coplen T. B., Landwehr J. M., Riggs A. R., Ludwig K. R., Szabo B. J., Kolesar P. T., and Revesz K. M. (1992) Continuous 500,000-year climate record from vein calcite in Devils Hole, Nevada. *Science* **258,** 255–260.

Selected Abstracts from the 2008 GSA National Meeting

Session: Assessment of Speleothem Paleoenvironment Proxies Using Studies in Modern Karst Systems, Sunday 5 October 2008: 1:30pm, George R. Brown Convention Center, 332AD

2:50-3:05pm

Temporal Variability of Cave-Air CO2 in Central Texas

Brian D. Cowan[1], Michael C. Osborne[2], Jay L. Banner[1]
1) Dept. of Geological Sciences, Jackson School of Geosciences, The University of Texas at Austin, Austin, TX
2) Department of Geological and Environmental Sciences, Stanford University, Stanford, CA

The growth rate and elemental and chemical composition of cave calcite deposits (speleothems) are important proxies for past environmental and hydrologic changes. Understanding the timing and driving mechanisms of calcite growth is therefore important for interpreting such proxies. The deposition of speleothem calcite in two central Texas show caves 130 km apart is known to vary seasonally in response to fluctuations in cave-air CO_2. Calcite deposition is highest in the late fall through spring when cave-air CO_2 is lowest, likely due to density driven ventilation. In the warmer summer months, when cave air becomes stagnant and high CO_2 concentrations develop, calcite deposition decreases to near zero. To determine if this phenomenon is unique to show caves, which, have been modified from their natural state (e.g., enlarged entrances, high numbers of visitors), CO_2 was measured along transects in three wild caves within the central Texas region.

Multiple transects of each cave showed that cave-air CO_2 varies seasonally in all undeveloped caves, with peak concentrations in late August to early October and lower concentrations in December through late March. The timing of seasonal CO_2 fluctuations is consistent in all caves studied. Cave-air CO_2 also shows significant diurnal fluctuations that are well correlated with changes in surface air temperature and barometric pressure. These results indicate that 1) the seasonality of calcite deposition observed in the show caves (as controlled by the concentration of cave-air CO_2) is not due to human alteration of the caves, 2) the concentration of cave-air CO_2 varies significantly on multiple timescales (i.e. daily to seasonally), 3) the seasonal fluctuation of cave-air CO_2 is regional in extent.

3:05-3:20pm

A Global Model for Seasonal Preservation Bias In Speleothem Proxy Records

Eric W. James, *Jay L. Banner*
Dept. of Geological Sciences, Jackson School of Geosciences, The University of Texas at Austin, Austin, TX

CO_2 concentrations in many caves vary seasonally, commonly peaking in summer. These high CO_2 levels suppress cave calcite growth. This seasonal growth rate variability can bias proxy environmental records preserved by speleothems. The bias potential is toward preserving records of cool-season versus warm-season conditions. Cave CO_2 levels represent a balance of inputs, typically from soils, and outputs, typically by exchange with outside air. CO_2 input from soil respiration is controlled by seasonal soil temperature and moisture. Loss of accumulated cave CO_2 is commonly through density-driven exchange (ventilation) with outside air. These density differences are controlled by differences in temperature, relative humidity, and air pressure between cave and surface air, parameters that cycle diurnally and seasonally.

Historical weather data can be used to model cave and surface air densities to predict cave CO_2 accumulation and ventilation. This model predicts first-order geographic controls on speleothem growth. For example, as latitude increases, winter-summer differences in soil temperature and air density increase the magnitude and duration of summer CO_2 build-up. This trend results from the contrast between lower average annual temperatures and comparatively higher summer temperatures with increasing latitude. At low latitudes diurnal temperature (and thus density) variations are greater than seasonal variations and daily ventilation and diffusion control CO_2 levels. Similarly, sites at all latitudes with a moderating maritime influence ventilate more frequently than latitude alone would predict. Thus, the potential for seasonally-biased records is greatest in speleothems from caves at mid to high latitudes and lowest at low latitudes and coastal sites. This first-order model ignores other controls on speleothem growth. Global weather data can be used to map differences between average annual temperature and average high temperatures. Such maps suggest where CO_2 build-up in caves is most likely, which in turn suggests where seasonal preservation biases are most likely.